

# **NMR Structural Determinants of *Lucina pectinata* Hemoglobin I active center moieties**

by

**Brenda Judith Ramos Santana**

A dissertation submitted in partial fulfillment of the requirements for the degree of

**DOCTOR IN PHILOSOPHY**

**in**

**Applied Chemistry  
(Biophysics)**

UNIVERSITY OF PUERTO RICO

MAYAGÜEZ CAMPUS

2013

Approved by:

\_\_\_\_\_  
José Prieto, PhD  
Member, Graduate Committee

\_\_\_\_\_  
Date

\_\_\_\_\_  
Enrique Meléndez, PhD  
Member, Graduate Committee

\_\_\_\_\_  
Date

\_\_\_\_\_  
Carmen Cadilla, PhD  
Member, Graduate Committee

\_\_\_\_\_  
Date

\_\_\_\_\_  
Juan López Garriga, PhD  
President, Graduate Committee

\_\_\_\_\_  
Date

\_\_\_\_\_  
Ana J. Navarro, PhD  
Representative of Graduate Studies

\_\_\_\_\_  
Date

\_\_\_\_\_  
Rene Vieta, PhD  
Chairperson of the Department

\_\_\_\_\_  
Date

## ABSTRACT

The clam *Lucina pectinata* Hemoglobin I (HbI) is a monomeric protein with a prosthetic group, known as heme group, in which the iron atom can either be in the ferrous ( $\text{Fe}^{\text{(II)}}$ ) or the ferric ( $\text{Fe}^{\text{(III)}}$ ) oxidation state. This globin protein is sulfide reactive hemoglobin in its ferric state that binds and transports  $\text{H}_2\text{S}$  to sulfide-oxidizing chemoautotrophic bacteria to maintain a symbiotic relationship. It was discovered that  $\text{H}_2\text{S}$  binding to HbI has a biological function protecting the mollusk from  $\text{H}_2\text{S}$  toxicity as an adaptative process of the invertebrate hemoglobin I from *L. pectinata*. The distal pocket of HbI is characterized by the presence of a GlnE7 and a PheB10. Site-directed mutant of the gene encoding wild-type HbI were made that changed Phe to Tyr at B10 position. The recombinant (rHbI) and rHbI PheB10Tyr mutant proteins were expressed in *Escherichia coli* and purified to homogeneity.  $^1\text{H-NMR}$  studies were conducted on rHbI and rHbI PheB10Tyr mutant to elucidate the structural-functional properties of HbI. The effects of this mutation were evaluated on the ferric cyanide derivative environment to characterize the structural properties of the rHbI and rHbI PheB10Tyr mutant. The results obtained show chemical shifts of TyrB10  $\text{OH}_\eta$  at 31.00 ppm, GlnE7  $\text{N}_{\epsilon 1}\text{H}/\text{N}_{\epsilon 2}\text{H}$  at 10.66/-3.27 ppm, and PheE11  $\text{C}_\delta\text{H}$  at 11.75 ppm, indicating the presence of a crowded, collapsed, and constrained distal pocket. The strong dipolar contacts and inter-residues crosspeaks between GlnE7/6-heme propionate group, GlnE7/TyrB10 and TyrB10/ $\text{CN}^-$  results suggested that a hydrogen bonding network loop between GlnE7, TyrB10, 6-propionate group, and the heme ligand contribute significantly to the modulation of the heme iron electron density as well as the ligand stabilization mechanism. Therefore, the network loop presented here support the fact that the electron withdrawing character of the hydrogen bonding is controlled by the interaction of the propionates and the nearby electronic environments contributing to the modulation of the heme

electron density state. Thus, we hypothesize that in heme proteins with similar electrostatic environment the flexibility of the heme-6-propionate promotes a hydrogen bonding network loop between the 6-propionate, the heme ligand and nearby amino acids, tailoring in this way the electron density in the heme-ligand moiety. Also, a NMR structural model was used to reveal a magnetic field mapping around the heme oxidation-reduction state in presence of H<sub>2</sub>S derivative.

## RESUMEN

La Hemoglobina I (HbI) de la almeja *Lucina pectinata* es una proteína monomérica que contiene en su centro activo un grupo prostético, conocido como grupo hemo, el cual posee un átomo de hierro que puede encontrarse en su estado oxidativo ferroso ( $\text{Fe}^{\text{II}}$ ) o férrico ( $\text{Fe}^{\text{III}}$ ). Esta proteína en su estado férrico es considerada reactiva a sulfuro de hidrógeno ( $\text{H}_2\text{S}$ ) debido a que enlaza y transporta el  $\text{H}_2\text{S}$  a una bacteria quimioautotrófica con la cual vive en una relación simbiótica. Se descubrió que este enlace a  $\text{H}_2\text{S}$  genera una función biológica protectora en el molusco debido a que evita su intoxicación por  $\text{H}_2\text{S}$  como un proceso adaptativo de la hemoglobina invertebrada de *L. pectinata*. El bolsillo distal de HbI está caracterizado por la presencia de GlnE7 y PheB10. Una mutación del código genético que codifica la HbI nativa fue realizada sustituyendo a Phe por Tyr en la posición B10. La proteína recombinada rHbI y el mutante rHbI PheB10Tyr fueron expresados en *Escherichia coli* y purificada para su homogeneidad. Estudios espectroscópicos de  $^1\text{H-NMR}$  fueron realizados en rHbI y el mutante de rHbI PheB10Tyr para dilucidar las propiedades estructurales y funcionales de la HbI. Los efectos de esta mutación se evaluaron utilizando un derivado de cianuro férrico para caracterizar las propiedades estructurales del mutante rHbI PheB10Tyr. Los resultados obtenidos muestran desplazamientos químicos de TyrB10  $\text{OH}_\eta$  en 31.00 ppm, GlnE7  $\text{N}_{\epsilon 1}\text{H}/\text{N}_{\epsilon 2}\text{H}$  en 10.66/-3.27 ppm, y PheE11  $\text{C}_\delta\text{H}$  en 11.75 ppm. Estos resultados indican la presencia de un bolsillo distal que se encuentra colapsado y estrecho. Los contactos dipolares fuertes y las interacciones entre los residuos de GlnE7/grupo propionato-6 del hemo, GlnE7/TyrB10, y TyrB10/ $\text{CN}^-$ , sugieren que existe una red de puentes de hidrógeno entre GlnE7, TyrB10, grupo propionato-6, y el ligando enlazado al hemo. Esto contribuye de manera significativa a la modulación de la densidad de electrones del hierro en el grupo hemo, así como al mecanismo de estabilización del

ligando. Por lo tanto, esta red de puentes de hidrógeno apoya que el carácter de retirar densidad electrónica de los puentes de hidrógeno es controlado por la interacción de los propionatos y el ambiente electrónico cercano modulando la densidad electrónica del grupo hemo. Entonces, se hipotetiza que las hemoproteínas con similar ambiente electrostático con una flexibilidad del grupo propionato-6, promueve una red de puentes de hidrógeno entre el grupo propionato-6, el ligando en el hemo, y amino ácidos cercanos adaptando de esta manera la densidad electrónica en el centro activo ligando-hemo. En adición, un modelo estructural de NMR fue utilizado para trazar un mapa del campo magnético alrededor del estado oxidativo-reductor del grupo hemo en presencia del derivado de H<sub>2</sub>S.

*Copyright © ® Brenda Judith Ramos Santana  
2013*

**To my family for their unconditional love and special support;**

**To my loving mother, Judith Santana Porrata,**

**that encouragement me to follow my dreams,**

**To my strong father, Roberto Ramos Collazo,**

**who gave me strength to keep going, and**

**To my performer sister, Marissa Ramos Santana,**

**that shows me how to get up.**

**With all my heart!!!**

## ACKNOWLEDGEMENTS

I would like to acknowledge the contribution of my graduate committee, Dr. José Prieto, outstanding human being, who believed in me and shared with me his passion for life, Dra. Carmen Cadilla for her contribution and ideas in this research, Dr. Enrique Meléndez for his research orientation, and Dr. Juan López-Garriga, my mentor, friend and dissertation advisor, who supported and believed in my scientific capacity to initiate and complete this research.

This work was supported by funds from the NSF (Grant 0843608) and NIH-NIGMS/MBRS-SCORE 5 S06GM008103-36.

I would like to give special thanks to Dr. Gerd N. La Mar for his motivation on NMR of hemoproteins, Dr. Jeffrey S. De Ropp for allowing me to use the NMR facilities in the University of California at Davis, Dr. Vasyl Bonarenko for his assistance with NMR experiments, Dra. Carmen Vega Olivencia for her special help, and Dra. Laura López for her input in the final edition of the document. A deep appreciation and special thanks to my students, they are my passion and driving force to continue growing as an extraordinary human being.

For that won and that lost, for that known and that ignored, for that harvested of the sowing and for the non grown seed. For that suffered and that enjoyed, for the sweetness and the bitter thing, everything makes us thank you, recognizing the task of receiving it from your hands and to convert it in quiet human. For all that, I worked these years, for you, My Lord., I present it. Thank.....What's impossible when God it is at your side?.... With God all things are possible!!!

# TABLE OF CONTENT

<b>ABSTRACT</b> .....	ii
<b>RESUMEN</b> .....	iv
<b>ACKNOWLEDGEMENTS</b> .....	viii
<b>TABLE OF CONTENT</b> .....	ix
<b>LIST OF TABLES</b> .....	xii
<b>LIST OF FIGURES</b> .....	xiv
<b>LIST OF ABBREVIATION AND SYMBOLS</b> .....	xviii
<b>CHAPTER 1: INTRODUCTION</b> .....	1
1.1 Research justification.....	1
1.2 <i>Phacoides pectinatus</i> : The bivalve mollusk called <i>Lucina pectinata</i> .....	4
1.3 Research Specific Aims.....	16
1.3.1. Characterization of heme prosthetic groups in rHbI and rHbI PheB10Tyr mutant proteins in complexes with CN <sup>-</sup> and H <sub>2</sub> S.....	16
1.3.2. Characterization of distal amino acids from rHbI and rHbI PheB10Tyr mutant proteins heme pocket in complexes with CN <sup>-</sup> and H <sub>2</sub> S.....	16
1.3.3. Determination of NH/OH hydrogen exchange relaxation protons and broad hyperfine shifts for rHbI and rHbI PheB10Tyr mutant proteins complexes.....	16
1.3.4. NMR structural model construction for rHbI PheB10Tyr mutant proteins heme pocket.....	17
<b>CHAPTER 2: METHODOLOGIES</b> .....	18
2.1 Expression, Culture Growth, Purification, and Spectral Properties of the recombinant Hemoglobin I (rHbI) and the rHbI PheB10Tyr single point mutant.....	18
2.1.1. Construction and Cloning.....	18
2.1.2. Small Scale Expression.....	18
2.1.3. Large Scale Expression.....	19
2.1.4. Purification of the Hemoglobins.....	21
2.1.5. Spectral Properties of the hemoglobins.....	23
2.2 Preparation of cyano rHbI and rHbI PheB10Tyr mutant complex.....	24
2.3 Preparation of Hydrogen sulfide rHbI complex.....	27
2.4. Nuclear Magnetic Resonance (NMR) Data Acquisition.....	29
2.4.1. NMR sample preparation.....	29
2.4.2. NMR preliminary data acquisition set up.....	29

2.4.3. One dimensional (1D) Pulse Sequences: <sup>1</sup> H-NMR Experiments.....	32
2.4.3.1. Water Solvent Suppression using Presaturation Pulse Sequence.....	32
2.4.3.2. Variable Temperature Experiments.....	34
2.4.3.3. Water Eliminated Fourier Transformation (WEFT) Experiments.....	34
2.4.3.4. Inversion Recovery Experiment: Non-selective T <sub>1</sub> .....	35
2.4.3.5. 1D Steady-state Nuclear Overhauser Experiments (NOE's)...	35
2.4.4. Two dimensional (2D) Pulse Sequences: <sup>1</sup> H- <sup>1</sup> H NMR Experiments.....	37
2.4.4.1. Nuclear Overhauser Enhancement Spectroscopy (NOESY)....	37
2.4.4.2. Total Correlation Spectroscopy (TOCSY).....	39
2.5. Nuclear Magnetic Resonance (NMR) Data Processing.....	41
2.6. Nuclear Magnetic Resonance (NMR) Protein Structure Determination.....	41
2.6.1. NMR Resonance Assignments: <sup>1</sup> H-Homonuclear Method.....	41
2.6.2. Protein Structure analysis: Magnetic Axes Calculations.....	47
<b>CHAPTER 3: RESULTS</b> .....	49
3.1 Bacterial expression of rHbI and rHbI PheB10Tyr mutant .....	49
3.2 Purification of the rHbI and the rHbI PheB10Tyr mutant .....	55
3.3 Characterization of heme prosthetic group in rHbI and rHbI PheB10Tyr mutant in cyanide complex.....	57
3.3.1. One dimensional (1D) Pulse Sequence: <sup>1</sup> H-NMR Experiments .....	57
3.3.1.1. Water solvent suppression heme group data.....	57
3.3.1.2. Variable Temperature (VT) spectra heme group data.....	61
3.3.1.3. Inversion recovery heme group data: Non-selective T <sub>1</sub> .....	64
3.3.1.4. 1D steady-state nuclear Overhauser (NOE's) heme group data..	67
3.4 Characterization of distal amino acids in rHbI and rHbI PheB10Tyr mutant in cyanide complex.....	72
3.4.1. One dimensional (1D) Pulse Sequence: <sup>1</sup> H-NMR Experiments.....	72
3.4.1.1. Variable Temperature (VT) spectra amino acid data.....	72
3.4.1.2. Water Eliminated Fourier Transform (WEFT) amino acid data .....	74
3.4.1.3. Inversion recovery amino acid data: Non-selective T <sub>1</sub> .....	76
3.4.1.4. 1D steady-state nuclear Overhauser (NOE's) amino acid data...	78
3.4.2. Two dimensional (2D) Pulse Sequences: <sup>1</sup> H- <sup>1</sup> H NMR Experiments .....	81
3.4.2.1. NOESY and TOCSY amino acid data.....	81
3.4.3. Sequences-specific resonance method: CN <sup>-</sup> complex.....	85
3.5 Determination of NH/OH hydrogen exchange relaxation protons and broad hyperfine shifted for the rHbI and rHbI PheB10Tyr CN complex.....	92

3.5.1. Deuterium isotopic labeling ( $^2\text{H}_2\text{O}$ ) data.....	92
3.6 Characterization of rHbI in hydrogen sulfide complex.....	95
3.6.1. rHbIH <sub>2</sub> S complex formation and stabilization analysis data.....	95
3.6.2. One dimensional (1D) Pulse Sequences: $^1\text{H}$ -NMR Experiments.....	100
3.6.2.1. Water Solvent Suppression Data.....	100
3.6.2.2. Variable Temperature (VT) spectra and Deuterium isotopic labeling ( $^2\text{H}_2\text{O}$ ).....	103
3.7 Nuclear Magnetic Resonance structural model construction for rHbI PheB10Tyr mutant in the CN heme pocket.....	107
3.7.1. Nuclear magnetic axes coordinate system.....	107
3.7.2. Hyperfine ( $\delta_{\text{hf}}$ ) and Dipolar ( $\delta_{\text{dip}}$ ) chemical shift validation.....	109
<b>CHAPTER 4: DISCUSSION</b> .....	<b>117</b>
4.1 Recombinant PheB10Tyr mutant <i>Lucina pectinata</i> HbI expression and purification.....	117
4.2 Heme propionate hydrogen bonding network loop in the cyanide moiety.....	118
4.3 Distinctive magnetic field of the H <sub>2</sub> S influences distal structural geometry in hemeproteins.....	124
4.4 H <sub>2</sub> S interactions with ferric rHbI derivative.....	125
<b>CHAPTER 5: CONCLUSIONS AND OUTLOOK</b> .....	<b>127</b>
<b>BIBLIOGRAPHY</b> .....	<b>129</b>

## LIST OF TABLES

Table	Descriptions	Page
1.1	O <sub>2</sub> and H <sub>2</sub> S association and dissociation rate constants of the rHbI and HbI mutants.	9
2.1	Amino acid residues in the wtHbI sequence from <i>Lucina pectinata</i>	44
3.1	Cell growth conditions used to optimize the <i>Escherichia coli</i> expression for the rHbI and rHbI PheB10Tyr mutant proteins	51
3.2	Cell densities and weight, grown in the fermentor for rHbI and rHbI PheB10Tyr mutant proteins	53
3.3	<sup>1</sup> H-NMR chemical shifts of the methyl, vinyl and propionate heme group for rHbICN and rHbICN PheB10Tyr mutant as showed in the Figure 3.5	60
3.4	Longitudinal spin-lattice relaxation time (T <sub>1</sub> ) for strongly relaxed heme group protons of rHbICN PheB10Tyr mutant as showed in the Figure 3.8	66
3.5	<sup>1</sup> H-NMR chemical shifts of the major NOE upon saturation of the downfield 5-CH <sub>3</sub> proton at 27.27 ppm in the rHbICN PheB10Tyr mutant at different temperature	68
3.6	Heme resonance assignments in <i>Lucina pectinata</i> rHbICN and rHbICN PheB10Tyr mutant proteins	70
3.7	<sup>1</sup> H-NMR chemical shifts of the major NOE upon saturation of the TyrB10 OH <sub>η</sub> proton at 31.00 ppm in the rHbICN PheB10Tyr mutant at different temperatures.	79
3.8	<sup>1</sup> H-NMR chemical shifts of the major NOE upon saturation of the GlnE7 N <sub>ε2</sub> H at -3.27 ppm in the rHbICN PheB10Tyr mutant at different temperatures.	80
3.9	Amino acid assignments in the rHbICN and rHbICN PheB10Tyr mutant from <i>Lucina pectinata</i>	87
3.10	Comparison of <sup>1</sup> H-NMR chemical shifts of the B10, E7 and E11 distal amino acid residues in rHbICN PheB10 mutant and wtHbICN from <i>Lucina pectinata</i> .	94

3.11	Chemical shifts contributions for HisF8, GlnE7, TyrB10 and PheE11 distal amino acids in the rHbICN PheB10Tyr mutant	110
3.12	Euler angles and magnetic anisotropies parameters for the cyanide complex in the rHbI PheB10Tyr mutant.	112

---

## LIST OF FIGURES

Figure	Description	Page
1.1	Schematic representation of the living site, physiological functions summary, and gill tissue for the bivalve <i>Lucina pectinata</i> .	6
1.2	Schematic representation of the HbIH <sub>2</sub> S heme pocket from <i>Lucina pectinata</i> in the crystal structure (PDB ID: 1MOH).	8
1.3	Stereo view of the hydrogen bond network in the oxygen bound of the monomer B in the heme pocket of the dimer HbII in <i>Lucina pectinata</i> crystal structure (PDB ID: 3PI2).	11
1.4	The active site of Mb with bound oxygen and after exposure to H <sub>2</sub> S.	14
2.1	Bioreactor used for large scale hemprotein expression.	20
2.2	UV-Vis spectra of ferric rHbI and rHbI PheB10Tyr mutant.	26
2.3	UV-Vis spectrum of rHbIH <sub>2</sub> S complex.	28
2.4	5 mm NMR tube hold by the spinner housing with 3.0 mM of hemeprotein.	31
2.5	Schematic representation of water solvent suppression NMR pulse sequence.	33
2.6	Schematic representation of Steady-state Nuclear Overhauser (NOE's) pulse sequence.	36
2.7	Schematic representation of the NOESY pulse sequence.	38
2.8	Schematic representation of the TOCSY pulse sequence [Bruker Avance, Co; Friebolin, 1998].	40
2.9	Schematic representation of resonance assignment strategy.	43
2.10	Amino acid sequence of wtHbI used as a reference in the resonance assignment method.	46
3.1	Optical density spectrum (OD <sub>600</sub> ) with diverse optimization parameter conditions for the bacterial expression of the rHbI PheB10Tyr mutant	52
3.2	Optical density spectrum (OD <sub>600</sub> ) of the <i>Escherichia coli</i> BLi5 cells using large-scale expression for rHbI PheB10Tyr mutant.	54

3.3	Optical spectra and elution profile of the rHbI PheB10Tyr mutant purification.	56
3.4	600 MHz $^1\text{H}$ -NMR of the paramagnetic shifted regions of rHbICN complex in $^1\text{H}_2\text{O}$ at 25°C and pH 7.00.	59
3.5	Downfield and upfield hyperfine shifted regions of the $^1\text{H}$ -NMR spectra of (A) rHbICN and (B) rHbICN PheB10Tyr mutant in $^1\text{H}_2\text{O}$ at 25°C and pH 7.00.	60
3.6	500 MHz $^1\text{H}$ -NMR temperature dependence spectrum of rHbICN PheB10Tyr in $^1\text{H}_2\text{O}$ at pH 7.00.	62
3.7	Curie plot of propionate group chemical shifts versus reciprocal absolute temperature in $^1\text{H}_2\text{O}$ at pH 7.00.	63
3.8	600 MHz $^1\text{H}$ -NMR inversion-recovery spectra of rHbICN PheB10Tyr mutant in $^1\text{H}_2\text{O}$ at pH 7.0, 25°C.	65
3.9	600 MHz $^1\text{H}$ -NMR steady-state NOE spectrum of the rHbICN PheB10Tyr mutant in $^1\text{H}_2\text{O}$ at pH 7.00, 25 °C.	68
3.10	Schematic representation of the heme pocket structure of rHbI PheB10Tyr with face-on view from the proximal side illustrating the heme pocket dipolar contacts.	71
3.11	500 MHz $^1\text{H}$ -NMR spectra portion of the variable temperature spectral window (10.00 to 13.00 ppm), of the rHbICN PheB10Tyr mutant in $^1\text{H}_2\text{O}$ at pH 7.00.	73
3.12	$^1\text{H}$ -NMR inversion-recovery spectra (WEFT) of rHbICN PheB10Tyr mutant in $^1\text{H}_2\text{O}$ at 25°C and pH 7.00.	75
3.13	600 MHz $^1\text{H}$ -NMR inversion-recovery spectra of rHbICN PheB10Tyr mutant in $^1\text{H}_2\text{O}$ at 25 °C and pH 7.00.	77
3.14	600 MHz $^1\text{H}$ -NMR steady-state NOE spectrum of rHbICN PheB10Tyr mutant in $^1\text{H}_2\text{O}$ at 25 °C and pH 7.00.	79
3.15	600 MHz 2D NOESY slice and steady-state NOE $^1\text{H}$ -NMR spectra of rHbICN PheB10Tyr mutant in $^1\text{H}_2\text{O}$ at 25 °C and pH 7.00 upon saturation of the GlnE7 $\text{N}_{\epsilon 2}\text{H}$ at -3.27 ppm.	80
3.16	600 MHz $^1\text{H}$ - $^1\text{H}$ -NMR NOESY spectrum (80 ms mixing time) rHbICN PheB10Tyr mutant in $^1\text{H}_2\text{O}$ at 25 °C and pH 7.00.	83
3.17	TOCSY spectra (40 ms mixing time) for the single mutant rHbICN PheB10Tyr from <i>L. pectinata</i> in $\text{H}_2\text{O}$ at 25 °C and pH 7.00.	84

3.18	Sequence-specific resonance assignment of E-helix observed in rHbICN PheB10Tyr single mutant protein.	86
3.19	Schematic representation of the heme pocket structure of rHbI PheB10Tyr with face-on view from the proximal side illustrating the dipolar contacts of the conserved amino acid residues.	91
3.20	500 MHz <sup>1</sup> H-NMR spectra of the rHbICN PheB10Tyr at 25°C and pH 7.00.	93
3.21	UV-Vis spectra obtained upon titration of rHbI with the H <sub>2</sub> S buffer solution at pH 6.5.	97
3.22	UV-Vis spectra of rHbIH <sub>2</sub> S during two and half (2½) days after preparation.	98
3.23	UV-Vis spectrum of the rHbIH <sub>2</sub> O derivative.	99
3.24	500 and 600 MHz <sup>1</sup> H-NMR reference spectra of the hyperfine shifted regions of (A) rHbIH <sub>2</sub> S (pH 7.36) and (B) rHbICN (pH 7.00) complexes in <sup>1</sup> H <sub>2</sub> O at 25 °C.	101
3.25	500 MHz <sup>1</sup> H-NMR spectrum of the hyperfine shifted regions of rHbIH <sub>2</sub> S complex in <sup>1</sup> H <sub>2</sub> O at 25 °C and pH 7.36.	102
3.26	500 MHz <sup>1</sup> H-NMR spectra portion of the variable temperature spectral window (5.00 to 20.00 ppm), of rHbIH <sub>2</sub> S in <sup>2</sup> H <sub>2</sub> O at pH 6.50.	104
3.27	500 MHz <sup>1</sup> H-NMR reference spectrum of the hyperfine shifted regions of rHbIH <sub>2</sub> S complex in <sup>2</sup> H <sub>2</sub> O at 25 °C and pH 6.50.	105
3.28	500 and 600 MHz <sup>1</sup> H-NMR downfield region, (15.00 to 95.00 ppm) in <sup>2</sup> H <sub>2</sub> O at 25 °C and pH 6.50 for (A) rHbIH <sub>2</sub> S and (B) rHbIH <sub>2</sub> O PheB10Tyr complexes.	106
3.29	Illustration of the iron-centered reference coordinate system, x',y',z' (R',θ',Ω'), for a porphyrin, the electronic coordinate system, x,y,z where d <sub>xz</sub> , d <sub>yz</sub> are each eigen functions, and the magnetic coordinate system, x*,y*,z* (R,θ*,Ω*), in which χ is diagonal from (A) distal and (B) proximal views.	108
3.30	Plot of the δ <sub>dip</sub> (cal) versus δ <sub>dip</sub> (obs) for 40 amino acids input data set for <i>Lucina pectinata</i> rHbICN PheB10Tyr at 25°C obtained from the optimized magnetic axes.	111

3.31	Plot of the $\delta_{\text{dip}}$ (cal) versus $\delta_{\text{dip}}$ (obs) for GlnE7 and TyrB10 distal residue for <i>Lucina pectinata</i> rHbICN PheB10Tyr at 25°C obtained from the optimized magnetic axes.	115
3.32	Dipolar shifts for residues TyrB10 and GlnE7 with the orientation determined by paramagnetic relaxation, dipolar shifts, and dipolar contacts.	116
4.1	Schematic representation of the distal heme pocket of rHbICN PheB10Tyr mutant showing major NOE dipolar contacts between distal residues (circles) and heme group.	119
4.2	Model of the distal heme pocket of rHbICN PheB10Tyr mutant showing the representation of the TyrB10 mutated residue and GlnE7 as elucidated by NMR spectroscopy.	123
4.3	Stereo diagram of the heme pocket of the A) HbISH <sub>2</sub> and B) HbICN showing the position of the ligand and orientation of distal GlnE7.	126

---

## LIST OF ABBREVIATIONS AND SYMBOLS

%	Percentage
$\alpha$	Alpha
$\alpha$ -meso	Alpha meso
$\tau$	Delay time
$\gamma$	Gamma
$\gamma$ -meso	Gamma meso
$\delta$	Chemical shift, $\delta$ scale
$\delta$	Delta in amino acid side chain
$\delta$	Delta
$\delta$ -meso	Delta meso
$\delta_{\text{con}}$	Contact chemical shift
$\delta_{\text{dia}}$	Diamagnetic chemical shift
$\delta_{\text{dip}}$	Dipolar chemical shift
$\delta_{\text{dip (obs)}}$	Observed dipolar chemical shifts
$\delta_{\text{dip (calc)}}$	Calculated dipolar chemical shifts
$\delta_{\text{hf}}$	Hyperfine chemical shift
$\delta_{\text{rc}}$	Ring current (rc) chemical shift
$\delta_{\text{sec}}$	Secondary structure chemical shift
$\beta$	Beta
$\beta$ -meso	Beta meso
$\mu\text{L}$	Microliters
$\mu\text{s}$	Microseconds
$\Omega$	Omega
$\alpha, \beta, \gamma$	Euler rotation angles
$\Gamma$	Surface concentration
$\varepsilon$	Epsilon
$\Delta\delta$	Chemical shift difference

$\Delta\delta_{\text{obs}}$	Difference observed chemical shift
$\Delta\chi_{\text{ax}}$	Axial magnetic anisotropy
$\Delta\chi_{\text{rh}}$	Rhombic magnetic anisotropy
°	Degrees
$\theta$	Scattering angle
$\nu_{\text{co}}$	Vibrational frequency carbon monoxide
$\nu_{\text{Fe-C}}$	Vibrational frequency iron-carbon
$\rho$	Delocalized spin density
$\chi$	Magnetic anisotropies
$x^*, y^*, z^*$	Magnetic axes
$x', y', z'$	Iron-centered coordinate system
1/s	One per second
Å	Angstrom
AMX + AA'XX'	Spin system
AM(PT)X	Spin system
AQ/acq	Acquisition time
Ala	Alanine
Arg	Arginine
Asn	Asparagine
Asp	Aspartic acid
B-helix	Helix B
BLi5	<i>Escherichia coli</i> cells
C	Celsius
$C\alpha\text{H}$	Proton alpha
$C\gamma\text{H}_3$	Proton gamma
$C\beta\text{H}_3$	Proton beta
$C\delta\text{H}$	Proton delta
$C\epsilon\text{H}$	Proton epsilon
$C\zeta\text{H}$	Proton zeta
$C\eta_2\text{H}$	Proton eta

C-helix	Helix C
cDNA	Complementary deoxyribonucleic acid
CH <sub>3</sub>	Methyl group
CN <sup>-</sup>	Cyanide anion
CO	Carbon monoxide
Co <sup>+2</sup>	Cobalt (II) ion
cos <sup>2</sup>	Cosine
Cys	Cysteine
dB	Decibel
D1 ( <i>t</i> )	Relaxation delay
D8 ( $\Delta$ )	Mixing time
E-helix	Helix E
EM	Exponential multiplication
F-helix	Helix F
Fe <sup>+2</sup>	Ferrous state
Fe <sup>+3</sup>	Ferric state
F/n	Global Error function
FTIR	Fourier transform infrared
FID	Free induction decay
G-helix	Helix G
Gln	Glutamine
Glu	Glutamic acid
Gly	Glycine
H <sub><math>\beta</math>t</sub> / H <sub><math>\beta</math>c</sub>	Vinyl group resonance lines
H <sub>2</sub> S	Hydrogen sulfide
HbI	Recombinant hemoglobin I from <i>Lucina pectinata</i>
HbII	Hemoglobin II from <i>Lucina pectinata</i>
HbIIO <sub>2</sub>	Oxy hemoglobin II
HbII-III	Hemoglobins II-III complex from <i>Lucina pectinata</i>
HbIII	Hemoglobin III from <i>Lucina pectinata</i>

HC	Hemin chloride
His	Histidine
Hz	Hertz
Ile	Isoleucine
IPTG	Isopropyl B-D-1-thiogalactopyranoside
KCl	Potassium chloride
KCN	Potassium cyanide
$K_3Fe(CN)_6$	Potassium ferricyanide
$k_{off}$	Dissociation constant (kinetics)
$k_{on}$	Association constant (kinetics)
L/hr	Liters per hour
<i>L. pectinata</i>	<i>Lucina pectinata</i>
LB	Line broadening
Leu	Leucine
Lys	Lysine
Mb	Myoglobin
Me	Methyl group
Met	Methionine
mL	Mililiters
mM	Milimolar
ms	Millisecond
$N_2$	Nitrogen
$Na_2S_{(s)}$	Sodium sulfide
NMR	Nuclear Magnetic Resonance
NO	Nitric Oxide
NOE	Nuclear Overhauser Enhancement
NOE's	Steady-state nuclear Overhauser spectra
NOESY	Nuclear Overhauser Effect Spectroscopy
$N_pH$	Amino group from the backbone
$^1H-^1H$	Proton-proton Nuclear Magnetic Resonance
$^1H_2O$	Water

$^2\text{H}_2\text{O}$	Hydrogen Isotope deuterium
$^1\text{H}$ NMR	Nuclear magnetic resonance (proton)
1D NMR	One-dimensional Nuclear Magnetic Resonance
2D NMR	Two-dimensional Nuclear Magnetic Resonance
O1	On-resonance
OD	Optical Density
OH	Hydroxyl Group
Oxy, O <sub>2</sub>	Oxygen
pET28(a+)	Vector
pH	Quantitative scale to measure acidity
Phe	Phenylalanine
ppm	Parts per million
Pro	Proline
QSINE	Sine bell window function
R <sub>Fe</sub>	Distant from iron
RF	Radio frequency
RG	Receiver gain
rHbI	Recombinant Hemoglobin I
rHbIH <sub>2</sub> O	Recombinant Metaquo complex
rHbI-H <sub>2</sub> S	Recombinant hemoglobin I hydrogen sulfide complex
RR	Resonance Raman
Ser	Serina
s/n	Signal to noise
sin <sup>2</sup>	Sine
SDS- PAGE	Sodium dodecyl sulfate polyacrylamide gel electrophoresis
T	Temperature, absolute
TB	Terrific Broth
T <sub>1</sub>	Longitudinal spin-lattice relaxation
t <sub>null</sub>	Null time
t <sub>rd</sub>	Relaxation delay
Thr	Threonine

TOCSY	Total Correlation Spectroscopy
trHbs	Truncated Hemoglobins
Tris	2-amino-2-hydroxymethyl-propane-1,3-diol
Trp	Tryptophan
Tyr	Tyrosine
UV	Ultraviolet region
V	Vinyl
Val	Valine
Vis	Visible region
VT	Variable temperature
WEFT	Water Eliminated Fourier Transform
wtHbI	Wild-type hemoglobin I
zg30	Pulse sequence without water presaturation
zgpr	Presaturation pulse sequence

# CHAPTER 1: INTRODUCTION

## 1.1 Research Justification

The hemoproteins are characterized by a heme group in their active centers as instance in globins, cytochromes, and peroxidase proteins [La Mar et al., 2000]. In these proteins, the heme iron serve as: a source or sink of electrons during electron transfer or redox chemistry [Guallar, et al., 2006], oxygen ( $O_2$ ) transport or storage [Weber et al., 2001], and as a gas sensor [Gao et al., 2006]. In essence, peripheral heme side groups, such as vinyl and propionates have been considered as anchors for connecting the heme prosthetic group to the protein matrix [Schneider et al., 2007]. Interestingly, it has been reported that in cytochrome P450 the heme-6 and 7-propionate side chains form hydrogen bonding interactions with the nearby amino acids [Hayashi et al., 2009]. Nevertheless, first: the role of the hydrogen bonding network with the 6 and 7- heme propionate groups is not clear, and second: the role of distal residues in hemeprotein ligand binding, dissociation and stabilization mechanisms remains unclear. Here, the main scope of our study is to elucidate a structural model that will provide an insight about the reactivity of Hemoglobin I (HbI). This goal will be reached understanding the magnetic and electronic structure conformation of the distal amino acid residues in recombinant Hemoglobin I (rHbI) and rHbI PheB10Tyr substitution single point mutation proteins in presence of two ligands such as  $CN^-$  and  $H_2S$ . Thus, the structural analyses of each protein were evaluated using proton nuclear magnetic resonance ( $^1H$ -NMR) spectroscopy.

An intriguing adaptive differentiation between oxygen ( $O_2$ ) and hydrogen sulfide ( $H_2S$ ) ligand is described for the survival of the clam *Lucina pectinata*. *Lucina pectinata* (*L. pectinata*) is one of the most resistant species living in extremely high levels of hydrogen sulfide ( $H_2S$ ) gas [Pietri et al., 2011]. Over the past two decades, it was found that presence of sulfide-reactive

Hemoglobin I (HbI) is responsible for sulfide oxidation; meanwhile, a complex of Hemoglobin II-III (HbII-HbIII) is the oxygen carrier inside the clam [Kraus and Wittenberg, 1990]. Earlier cDNA amino acid sequence studies confirmed that HbI differs from the HbII-HbIII complex by having a phenylalanine (Phe) instead of a tyrosine (Tyr) at the B10 amino acid sequence position [Antommattei-Pérez et al., 1999; Torres-Mercado et al., 2003]. Typically, hemoglobins in vertebrate and invertebrate have amino acids such as PheB10 and HisE7 in the active center. On the basis of physiological functions, the hemoglobins have functional diversity, other than transporting and storing O<sub>2</sub>, including control of nitric oxide (NO) levels in microorganisms, use the NO to control the level of O<sub>2</sub> in nematodes, and binding, transport, and protecting of sulfide in endosymbiont harboring species [Weber et al., 2001]. It is suggested that the identity of the B10 and the E7 residue are very important in regulating the binding and discrimination of ligands, to determine the physiological functions in the proteins [Egawa et al., 2005]. Similar to HbII, TyrB10 and the GlnE7 residues appear in the truncated hemoglobins (trHbs) [Wittenberg et al., 2002; Ouellet et al., 2003]. Some trHbs functions have been suggested to perform an NO detoxification reaction to protect the organisms against NO attack, and other classes of trHbs have physiological function unclear [Lu et al., 2007]. Also, most of the examined trHbs exhibit high O<sub>2</sub> affinities due to unusual slow dissociation rates of the oxygen and the hemoglobin. This slow rate in trHbs has been suggested to be a consequence of a strong hydrogen bonding network between the GlnE7 and TyrB10 with the bound ligand [Ouellet et al., 2002].

A hydrogen bonding network has also been invoked in the stabilization of O<sub>2</sub> in HbII [Peterson et al., 1997]. It has been proposed that this hydrogen bonding network is responsible for the slow oxygen off rate in HbII, similar to the *Ascaris suum* hemoglobin that also has a GlnE7 and TyrB10 on the distal heme pocket [Peterson et al., 1997]. *Ascaris suum* worm uses

endogenously produced NO to detoxify oxygen, which is considered poisonous to the anaerobic mitochondrial oxidation pathway in the worm [Egawa et al., 2005].

On the other hand, the elucidated crystal structure of HbIIO<sub>2</sub> shows a hydrogen bonding network in the heme proximal site between the HisF8 nitrogen proton, and a water molecule, which in turn forms a hydrogen bond with the heme 7-propionate group [Gavira et al., 2008]. It has been suggested that this proximal network modulates the His98 trans-effect affecting the oxygen dissociation rate. Furthermore, NMR studies of the proximal site of the deoxygenated horse heart myoglobin suggest that the replacement of heme-7-propionate with a methyl group slightly weakens the His93-heme iron bond [Hayashi et al., 2002].

High resolution NMR techniques provide an appropriate framework to describe the structural and functional relationship in the hemeprotein. In order to understand the complex structural conformation, it is necessary to explore diverse relevant aspects, such as:

- (a) evaluation of the important role of diatomic ligands in the hemoprotein characterization
- (b) identification of the peripheral heme groups in the heme pocket
- (c) confirmation of the conserved amino acids, such as HisF8 and PheCD1 in the protein
- (d) identification of the spin system of GlnE7, TyrB10 and PheE11 in the distal site of the active center
- (e) identification of the homonuclear dipolar correlations in the active center
- (f) elucidation of the major nuclear Overhauser enhancement (NOE) dipolar contacts between distal residues and heme group
- (g) description of the specific orientation in the space of distal amino acids and the peripheral heme group
- (h) evaluation of the magnetic axes orientation of the heme group

- (i) identification of the possible hydrogen bonding network between distal amino acids, ligand and propionate groups
- (j) evaluation of the electronic and physical properties of the protein-bound heme group
- (k) relation of the structure model with the heme-ligand stabilization mechanism in the protein heme pocket.

Exploring these structural aspects will allow us to understand the electron withdrawing character of the hydrogen bonding network, the electron density state of the heme, and the electrostatic environment in the heme-ligand moiety. A complete NMR structural elucidation of the rHbI PheB10Tyr mutant protein might reveal a tyrosine B10 as a trigger of the heme propionate hydrogen bonding network loop with the glutamine E7 moiety. These structural outcomes provide an excellent contribution to the scientific study of invertebrate hemoglobins, as compared, to similar oxy-heme complexes with analogous heme distal center, where the hydrogen bonding network can modulate the heme O<sub>2</sub> affinity and reactivity with H<sub>2</sub>S. Eventually, these fundamental evidences will be applicable to comparative models between invertebrates and vertebrates hemoglobin to evaluate plausible mechanisms that explain the control of H<sub>2</sub>S or any other ligand (i.e. NO) to protect the hemoproteins from toxicity.

## **1.2 *Phacoides pectinatus*: The bivalve mollusk called *Lucina pectinata***

The invertebrate organism *Phacoides pectinatus*, also known as *Lucina pectinata* (*L. pectinata*), has been used as an ideal model for this research [Frenkiel et al., 1997]. This species lives in extreme environmental conditions with high concentration of hydrogen sulfide (H<sub>2</sub>S) (300-900 μM) on the tropical coastal mud of mangrove swamps of Puerto Rico. This tropical clam has a symbiotic relationship with intracellular, sulfide-oxidizing chemoautotrophic bacteria. *Lucina pectinata* possesses three unique invertebrate hemoglobins concentrated within the

ctenidia gill tissue and adapted to bind oxygen ( $O_2$ ) and hydrogen sulfide ( $H_2S$ ) as ligands [Read, 1962]. These three hemoglobins (HbI, HbII and HbIII), are associated with a cysteine-rich protein. They also have different physical and chemical properties within themselves [Kraus and Wittenberg, 1990]. HbI is a monomeric protein of 142 amino acid residues and a molecular weight of 14,812.80 Da [Antommattei et al., 1999]. It is a sulfide-reactive hemoglobin in the presence of oxygen. HbI is capable to function in its ferric state to transport  $H_2S$  to the symbiotic bacteria, which oxidize sulfide and fix carbon dioxide into nutrients [Kraus and Wittenberg, 1990]. Symbiotic bacteria are the main food source for the mollusks, and they contribute to the survival of mollusks under conditions of high, potentially toxic concentrations of sulfides [Alyakrinskaya, 2003]. It was found that  $H_2S$  binding to the HbI has a biological function protecting the mollusk from  $H_2S$  toxicity as an adaptive process of the invertebrate hemoglobin I from *L. pectinata* [Pietri et al., 2011]. Meanwhile, HbII and HbIII are dimeric proteins, self-associated in a concentration dependent manner, forming a tetramer. HbII and HbIII have 150 and 152 amino acid residues, and a molecular weight of 17,476 Da and 18,068 Da, respectively [Hockenhull-Johnson et al., 1991; 1993]. They have been shown to be oxygen-transporters ( $O_2$ ) proteins that remain oxygenated in the presence of hydrogen sulfide ( $H_2S$ ) [Kraus and Wittenberg, 1990]. Figure 1.1 shows the *L. pectinata* living site, a summary of the hemoglobins physiological functions, and gill tissue in the bivalve.

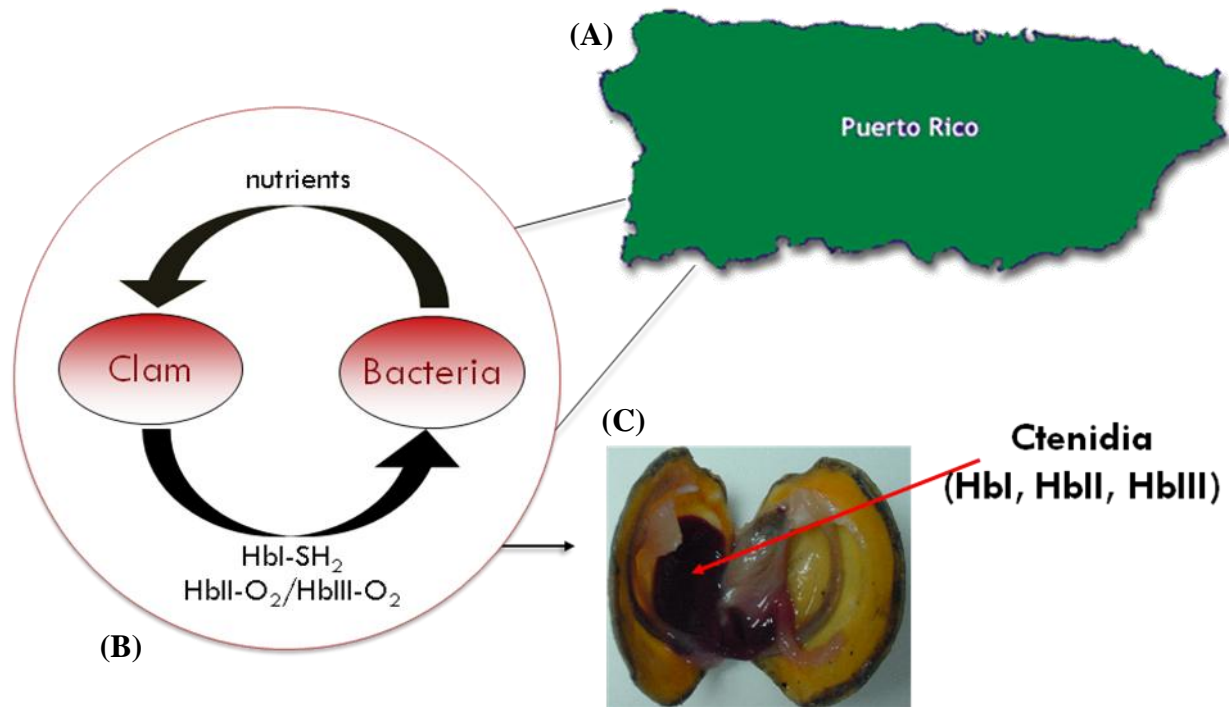


**Figure 1.1: Schematic representation of the living site, physiological functions summary, and gill tissue for the bivalve *Lucina pectinata*. (A) *Lucina pectinata* lives in the tropical coastal mud of mangrove swamps of Puerto Rico. (B) Cycle of the hemoglobins physiological functions where HbI transport H<sub>2</sub>S to the symbiotic bacteria which oxidize sulfide and fix carbon dioxide into nutrients, and HbII and HbII bind O<sub>2</sub> in the presence of H<sub>2</sub>S [Wittenberg et al., 1990]. (C) Ctenidia gill tissue of the *Lucina pectinata* that possesses three unique invertebrate hemoglobins (HbI, HbII, and HbIII) [Read, 1962].**

X-ray structural studies indicate that HbI, HbII and HbIII, as in other myoglobin species, have the highly conserved His96, at a proximal position F8, covalently binding to the 5<sup>th</sup> coordinate position in the heme group [Rizzi et al., 1994]. Similarly, *L. pectinata* hemoglobins are characterized by a distribution of aromatic amino acid residues and a natural replacement of His by Gln at the E7 position, showing an extraordinary structural distal heme pocket [Rizzi et al., 1994, 1996]. Figure 1.2 shows the arrangement of the distal amino acid residues for the HbIH<sub>2</sub>S complex. This crystal structure describes the “Phe cage” composition as follows: PheB10, PheCD1 and PheE11, and the glutamine (Gln) in the E7 position [Rizzi et al., 1996]. Initially, kinetic data was analyzed to understand how the structure and electronic environment of this heme pocket behave in the presence of native ligands such as O<sub>2</sub> and H<sub>2</sub>S. Table 1.1 summarizes the oxygen and hydrogen sulfide dissociation and association rate constants for wtHbI, rHbI and several HbI mutants [Pietri et al., 2009]. The kinetics data of HbI indicate a fast H<sub>2</sub>S association,  $k_{on} = 2.3 \times 10^5 \text{ M}^{-1}\text{s}^{-1}$ , and a slow H<sub>2</sub>S dissociation,  $k_{off} = 0.22 \times 10^{-3} \text{ s}^{-1}$ , showing that the affinity of ferric HbI for H<sub>2</sub>S is 4,000-fold greater than those of ferric HbII, HbIII, and myoglobin [Kraus and Wittenberg, 1990; Pietri et al., 2009]. HbI also exhibits one of the fastest known O<sub>2</sub> association ( $k_{on} = 100\text{-}200 \mu\text{M}^{-1} \text{ s}^{-1}$ ), and dissociation ( $k_{off} = 61 \text{ s}^{-1}$ ) rates [Kraus and Wittenberg, 1990; Pietri et al., 2009]. These data confirmed differences in amino acid composition between HbI, HbII, and HbIII distal heme pocket, illustrating how the distal environment may influence ligand interactions with the heme. It has been shown that the dissociation of the O<sub>2</sub> from the HbI mutants depends strongly on the hydrogen bonding interaction between the E7 residue and the bound ligand [Pietri et al., 2009]. As also shown, the PheB10Tyr mutant decreased O<sub>2</sub> dissociation rate by a factor of 233 suggested a strong H-bond between the bound O<sub>2</sub> and the Tyr amino acid residue at B10 position [Pietri et al., 2009].

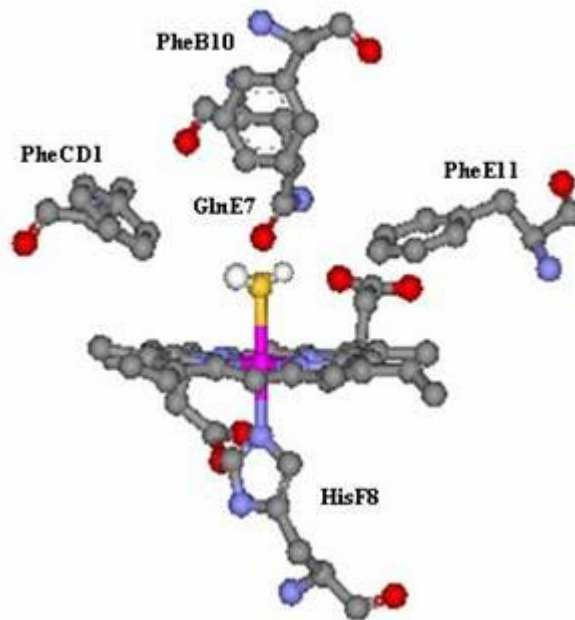


**Figure 1.2:** Schematic representation of the HbIH<sub>2</sub>S heme pocket from *Lucina pectinata* in the crystal structure (PDB ID: 1MOH). The X-ray crystal structure of the sulfide derivative of ferric *L. pectinata* HbI has been determined at 1.9 Å resolution [Rizzi et al., 1996].

**Table 1.1: O<sub>2</sub> and H<sub>2</sub>S association and dissociation rate constants of the rHbI and HbI mutants.**

Protein	O <sub>2</sub>		H <sub>2</sub> S	
	k <sub>on</sub> (10 <sup>6</sup> M <sup>-1</sup> s <sup>-1</sup> )	k <sub>off</sub> (s <sup>-1</sup> )	k <sub>on</sub> (10 <sup>3</sup> M <sup>-1</sup> s <sup>-1</sup> )	k <sub>off</sub> (s <sup>-1</sup> )
wtHbI <sup>a</sup>	100-200	61	27.30 <sup>c</sup>	0.00022
rHbI	190	140 <sup>b</sup>	24.30 <sup>c</sup>	-
ValE7	490	500 <sup>b</sup>	276.78	-
AsnE7	230	375 <sup>b</sup>	39.15	-
HisE7	31	3 <sup>b</sup>	65.80	-
LeuB10	230	300 <sup>b</sup>	61.75	-
ValB10	110	400	<i>nd</i> <sup>d</sup>	-
TyrB10	6.8	0.6 <sup>b</sup>	3.94	-
ValE11	120	325	16.95	-
TyrE11	110	40	11.46	-

<sup>a</sup> data from Kraus and Wittenberg , 1990

<sup>b</sup> data from Pietri et al. 2006

<sup>c</sup> data from Collazo et al. 2004

<sup>d</sup> not determined

The crystal structure obtained for the HbI metaquo form and HbIH<sub>2</sub>S complex by Rizzi and coworkers [Rizzi et al., 1994, 1996], the amino acid sequences for HbII and HbIII reported by Hockenhull-Johnson and coworkers [Hockenhull-Johnson et al., 1991, 1993], and the latest founding by Gavira and coworkers of oxygen-HbII complex [Gavira et al., 2008] reveal and confirm a significant structural alteration at the B10 distal position. Figure 1.3 shows the oxygen-HbII monomer B heme pocket composition with the natural replacement of the Phe by Tyr at B10 position [Gavira et al., 2008].

Elucidation of these structures encouraged comparative solution and crystal structures studies that involved *L. pectinata* Hb's (HbI, HbII and HbIII) and HbI mutants with diverse heme proteins which have chemical similarity in their heme pocket. Nuclear Magnetic Resonance studies elucidated the cavity structure of the sperm whale myoglobin triple mutant: LeuB10Phe/HisE7Gln/ValE11Phe. This system mimics the distal site of HbI from *L. pectinata*, as described in the cyanomet form [Nguyen et al., 1998]. This study was compared with the crystal structure of aquomet *L. pectinata* HbI done by Rizzi and coworkers [Rizzi et al., 1994]. They suggested that a major difference in the distal pocket was that in the aquomet form, the carbonyl of GlnE7 serves as a hydrogen bond acceptor, whereas in the cyanomet form, the amino group acts as a hydrogen bond donor to the ligand [Nguyen et al., 1998]. Nguyen and coworkers suggested three chemical interactions: (a) hydrogen bonding between the sulfide ligand and the GlnE7 side chain carbonyl, (b) hydrophobic pocket interaction by the "Phe cage", and (c) highly favorable electrostatic interactions between the sulfur and the edges of the three aromatic rings [Nguyen et al., 1998]. Resonance Raman (RR) and <sup>1</sup>H-NMR suggested an unusual rocking freedom of the heme group in the hydrogen sulfide-binding HbI from *L. pectinata* that facilitates the binding of the incoming ligand with the heme [Cerdeña-Colón et al., 1998].

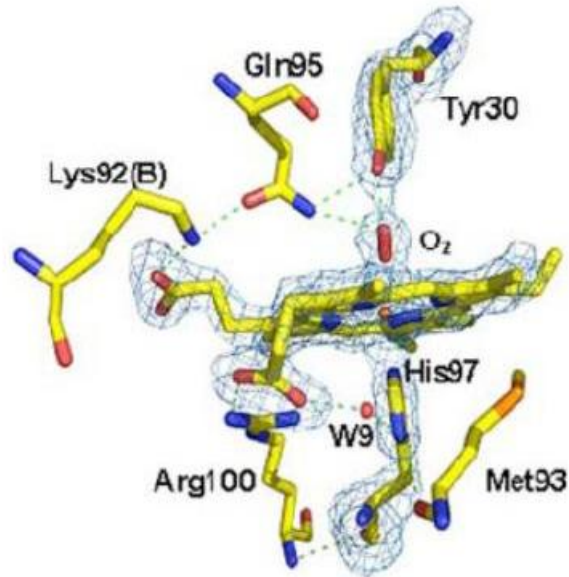


**Figure 1.3:** Stereo view of the hydrogen bond network in the oxygen bound of the monomer B in the heme pocket of the dimer HbII in *Lucina pectinata* crystal structure (PDB ID: 3PI2). Residues at a 5 Å distance cut-off are shown. The omit map (contoured at 3  $\sigma$ ) and bond interactions are shown in blue and green lines, respectively [Gavira et al., 2008].

A  $^1\text{H-NMR}$  model was developed, where the electron withdrawing character of the out-of-plane orientation of the trans-2-vinyl group in the heme contributes to the stability of the  $\text{Fe(III)H}_2\text{S}$  complex [Silfa et al., 1998]. These studies also suggested that not only the distal amino acids contribute to the functional dynamics, but also that the peripheral side groups of the heme are responsible for the heme-ligand stabilization mechanisms. All the above information motivated us to develop a new recombinant protein expression (rHbI) using cDNA and site-directed mutagenesis experiments for the HbI protein from *L. pectinata* [León et al., 2004; Collazo et al., 2004].

Several advances in infrared spectroscopy (FTIR) of the rHbI PheB10Tyr mutant with carbon monoxide in the binding site, indicates that an  $\text{A}_3$  conformer at  $1924\text{ cm}^{-1}$  predominates over the  $\text{A}_0$  conformer at  $1957\text{ cm}^{-1}$ . This fact suggested a closed structure conformation in which the TyrB10 residue is H-bonded to the CO ligand and confirms GlnE7 swings away from the bound ligand [Pietri et al., 2005]. Similarly, Resonance Raman (RR) of rHbICO variants derivative demonstrated a  $\nu_{\text{co}}$  increment from  $1944\text{ cm}^{-1}$  to  $1946\text{ cm}^{-1}$  and  $1963\text{ cm}^{-1}$  upon GlnE7 replacement by Asn and Val, respectively. The substitution of Phe by Tyr at B10 position increased the  $\nu_{\text{Fe-C}}$  mode from  $522\text{ cm}^{-1}$  to  $548\text{ cm}^{-1}$  and decreased the  $\nu_{\text{co}}$  from  $1944\text{ cm}^{-1}$  to  $1926\text{ cm}^{-1}$ , promoting a favorable orientation to form hydrogen bonding with the hemeCO moiety. These results indicated that both GlnE7 and PheB10 are necessary to stabilize the CO ligand [Pietri et al., 2006]. Molecular dynamics studies using deoxy native HbI and various rHbI mutants from *L. pectinata* suggested that GlnE7 and PheB10 are responsible for ligand binding and stability in the HbI heme moiety. Moreover, PheE11 is probably involved in the structural stability and ligand diffusion through the protein [Ramirez et al., 2008]. Based on these studies, single point mutations [León et al., 2004] and the discovery years ago of  $\text{H}_2\text{S}$  as a

neuromodulator and gasotransmitter [Wang et al., 2010] open a new vision about how to define sulfide reactivity with hemeproteins. Kinetics and Resonance Raman results obtained with ferric and ferrous rHbI mutants (E7, B10, and E11) showed diverse factors controlling the reactivity of H<sub>2</sub>S with hemeproteins. Some factors included that the reduction of the heme increased at high H<sub>2</sub>S concentrations and is controlled by the effect of the polarity distal environments surrounding the bound ligand [Pietri et al., 2009]. Also, UV-Vis and Resonance Raman spectroscopy studies suggested that the reaction of H<sub>2</sub>S with Hb and Mb, in the presence of H<sub>2</sub>O<sub>2</sub> or O<sub>2</sub>, results in the formation of the sulfhemoglobin derivative [Román et al., 2010]. However, the formation of the sulfheme derivative requires a HisE7 residue in the heme distal site with adequate orientation to form an active sulfheme complex, and it is observed after heme reduction [Román et al., 2010]. Figure 1.4 shows the active site of Mb with a covalent modification in the β-β double bond of the pyrrole “B” generating the sulfhemoglobin derivative [Román et al., 2010].

Interestingly, Collman and coworkers speculated that H<sub>2</sub>S serve as a source of electrons during periods of hibernation observed in mammals when food supplies are low, affecting the activity of cytochrome C oxidase [Collman et al., 2009]. Meanwhile, Pietri and coworkers discussed direct vertebrate and invertebrate experimental evidence for H<sub>2</sub>S reactivity with hemeproteins and revealed: (i) H<sub>2</sub>S binding to alternate sites such as cysteine, copper, and zinc ions, (ii) H<sub>2</sub>S coordinates to the ferric heme iron without inducing reduction of sulfheme production, and (iii) H<sub>2</sub>S binding to the ferric iron with subsequent reduction of the heme [Pietri et al., 2011]. Furthermore, Guo and coworkers investigated the physiological regulation of H<sub>2</sub>S in both central and peripheral systems. They showed that H<sub>2</sub>S is involved in regulating apoptosis, causes vasorelaxation and inhibits oxidative damage in mitochondria [Guo et al., 2012].

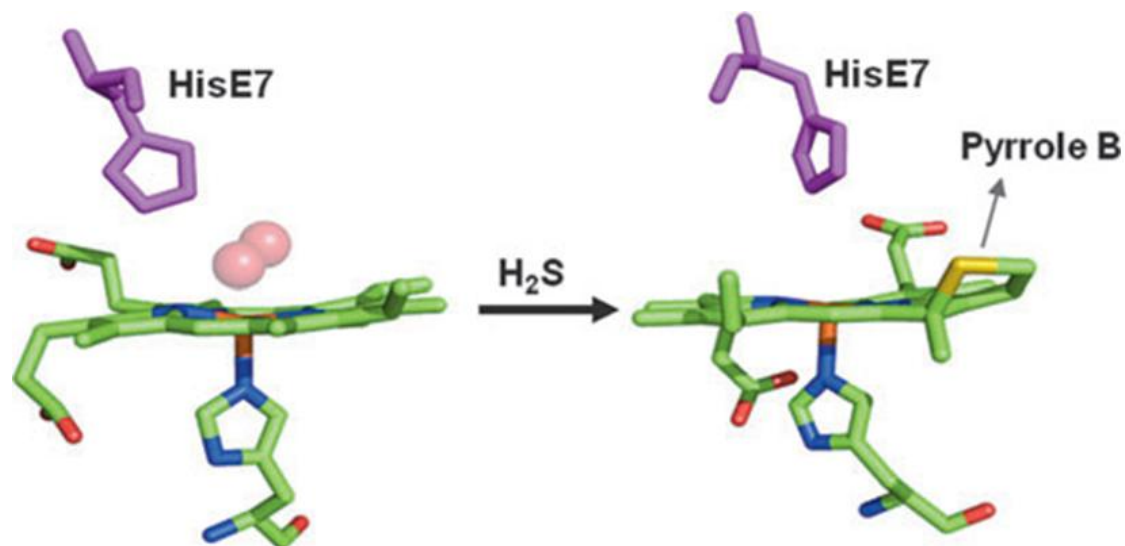


**Figure 1.4: The active site of Mb with bound oxygen (left) and after exposure to H<sub>2</sub>S (right). The final sulfheme product is a modified chlorin-type heme with a sulfur atom incorporated into one of the pyrrole rings. The structures were generated using PDB files 1MBO (left) and 1YMC (right), respectively. In the figure HisE7 refers to the histidine residue at position 7 of helix E, which in human Hb and Mb stabilizes O<sub>2</sub> through hydrogen bonding interactions [Roman et al., 2010; Pietri et al., 2011].**

A subsequent report on vertebrate cells showed that H<sub>2</sub>S has an extremely versatile antioxidant and free radical effect as action of itself [Predmore, 2012]. However, although several different roles of H<sub>2</sub>S have been indicated, the mechanism of H<sub>2</sub>S release remains unknown, and the functionality of specific hemeproteins remains unanswered. As Olson recently stated, the potential of H<sub>2</sub>S in therapeutic treatment is extraordinary, but it is important to understand the real behavior of H<sub>2</sub>S in the blood [Olson, 2013].

Therefore, unresolved structural details could explain the complete hemeproteins functionality, which is responsible for their adaptation capacity to inhabit diverse extreme environments, and analyze the ligand reactivity effects in the heme active center. High resolution Nuclear Magnetic Resonance (NMR) is a powerful spectroscopy technique capable to create a structural functional model for probing intermolecular interactions [Pellecchia, 2005] and structural determinants of reactivity. Solution NMR structural mapping of rHbICN, rHbICN PheB10Tyr mutant and rHbIH<sub>2</sub>S proteins will be a valuable contribution which will answer the following question: What are the constraints related to the heme pocket conformation as consequence of one single point mutation? Which are the distal amino acids orientations in the heme pocket? What is the role of propionate heme groups in the ligand binding process? Which are the interactions that control the stabilization of the bound ligand in the active center? How the reactivity of the ligand affects the heme group oxidative state? How the structure-activity relationship will affect the functionality of the hemeprotein? This research effort primarily could determine a fine structure that provides the structural determinants in hemoglobins.

### 1.3 Research Specific Aims

#### 1.3.1. *Characterization of heme prosthetic groups in rHbI and rHbI PheB10Tyr mutant proteins in complexes with CN and H<sub>2</sub>S.*

To develop <sup>1</sup>H-NMR experiments to determine chemical shifts patterns of the peripheral heme groups which include methyl, meso, vinyl and propionate groups in the rHbI and rHbI PheB10Tyr mutant from the clam *L. pectinata*. A combination of 1D and 2D NMR methods using a water presaturation pulse sequence will be performed to establish experimental parameters such as protein concentration, temperature, optimal pH, and isotopic solvent to obtain the best hyperfine shift signals in the paramagnetic spectrum region. These hyperfine resonance lines will be used as sensors to identify HisF8 invariant residues covalently bonded to the heme group.

#### 1.3.2. *Characterization of distal amino acids from rHbI and rHbI PheB10Tyr mutant proteins heme pocket in complexes with CN and H<sub>2</sub>S.*

To determine the sequential 1D and 2D NOE focused on developing assignments strategies using sequence-specific resonance method through homonuclear scalar spin-spin couplings and homonuclear dipolar correlation [Wüthrich, 1986; Rule and Hitchens, 2006]. Sequential resonance assignments through the intraresidual and interresidue <sup>1</sup>H-<sup>1</sup>H connectivities along the polypeptide backbone could reveal important constrains related to the heme pocket conformation.

#### 1.3.3. *Determination of NH/OH hydrogen exchange relaxation protons and broad hyperfine shifts for rHbI and rHbI PheB10Tyr mutant proteins complexes.*

Comprehensive isotopic experimental methodologies will be designed to confirm side chains of distal amino acids including the conserved HisF8. Detecting NH/OH solvent exchangeable

protons requires special efforts to avoid water resonance through the use of selective pulse or field gradients. The inversion-recovery experiment, commonly called WEFT spectra, will be collected under rapid repetition conditions ( $\sim 8$  to  $12 \text{ s}^{-1}$ ) to resolve very broad lines in the presence of unresolved diamagnetic protons.

#### 1.3.4. NMR structural model construction for rHbI PheB10Tyr mutant proteins heme pocket.

A complete distal heme pocket structural description will be mapped using information contained in the dipolar shifts that include the magnetic anisotropies ( $\chi$ ), geometric factors  $[(3\cos^2\theta-1)R^{-3}, (\sin^2\theta\cos 2\Omega)R^{-3}]$ , and the orientation of the magnetic axes ( $x^*$ ,  $y^*$ ,  $z^*$ ). These analyses involve: (a) the combination of the 1D/2D NMR methods to determine the complete dipolar shifts ( $\delta_{\text{dip}}$ ), (b) conversion of the arbitrary coordinate system into the magnetic coordinate system ( $[x^*, y^*, z^*] = [x', y', z']\Gamma[\alpha, \beta, \gamma]$ ) by the reference iron-centered coordinate system ( $x', y', z'$ ), and (c) determination of the magnetic axes orientation by evaluating and validating the  $\delta_{\text{dip}}$  data sets and minimization of the global error function ( $F/n$ ).

As a summary, this NMR structural model will be used to: (a) identify the structural features in the rHbI and rHbI PheB10Tyr mutant heme moiety, (b) determine the influence of heme peripheral groups such as propionate in the distal region, (c) determine the orientation of rHbI distal amino acids by PheB10Tyr mutation, (d) evaluate contributions from hydrogen bonding network loop to the heme-ligand stabilization dynamic, (e) reveal a magnetic field mapping around the heme oxidation-reduction state, and (f) perform a comparative analysis of hemeproteins with similar electrostatic environment in the heme-ligand moiety. Consequently, it will be possible to establish a correlation between structure-function relationships in rHbI and the rHbI PheB10Tyr mutant proteins from *Lucina pectinata*.

## CHAPTER 2: METHODOLOGIES

### **2.1 Expression, Culture Growth, Purification, and Spectral Properties of the recombinant Hemoglobin I (rHbI) and the rHbI PheB10Tyr single point mutant**

#### *2.1.1 Construction and Cloning*

Recombinant Hemoglobin I (rHbI) and rHbI PheB10Tyr mutant were cloned and expressed in *Escherichia coli* as described previously with slight modifications [León et al., 2004, Ramos et al., 2010]. The gene coding for HbI was obtained and amplified from the total *L. pectinata* gill RNA by RT-PCR [León et al., 2004]. The cDNA of HbI was cloned into the pET28(a+) vector (Novagen) using the *NdeI* and the *XhoI* restriction sites of the vectors polylinker region. The resulting pET-28a(+) vector, containing HbI cDNA, was further transformed into competent BLi5 *E. coli* cells. Recombinant colonies of transformed cells were selected in media containing kanamycin (70 µg/mL) and chloramphenicol (30 µg/mL) (Sigma, St. Louis, MO) and stored as frozen stocks in sterilized glycerol (Sigma, St. Louis, MO) at -80 °C. These frozen stocks were then used for cell growth and rHbI expression. Similarly, the rHbI PheB10Tyr mutant was obtained by introducing single amino acid substitutions into the HbI coding region, using the Quick Change Site-directed mutagenesis kit (Stratagene, La Jolla, CA), and cloned into the pET28(a+) vector.

#### *2.1.2 Small Scale Expression*

The expression of rHbI was first performed in Fernbach flasks. First, 50 mL of TB (Sigma, St. Louis, MO) was inoculated with a frozen stock of the *E. coli* cells transformed with the rHbI plasmid, and incubated overnight on a shaker at 125 rpm with 70 µg/mL kanamycin and 30 µg/mL chloramphenicol antibiotics at 37 °C. This overnight culture was then used to inoculate

50 mL of fresh terrific broth (TB) medium with the corresponding antibiotics. The new culture was grown and induced with 1 mM IPTG during the mid-log phase at an OD<sub>600</sub> of 1.5 to 2.0, followed by supplementation with 1.0 % w/v glucose and 30.0 µg/mL hemin chloride (Sigma, St.Louis, MO). To determine the optimal conditions for the expression, different glucose concentrations were examined. Three experiments at different glucose concentrations were carried out first by adding 1.0 %w/v glucose during the beginning of the log phase (optical density, OD<sub>600</sub> of ~1.0), second adding 0.5 %w/v glucose at the beginning of the log phase (optical density, OD<sub>600</sub> of ~1.0) and adding 0.5 %w/v glucose later in this stage (OD<sub>600</sub> between 1.5 and 2), and third adding 1.0 %w/v glucose during mid-log phase (OD<sub>600</sub> between 1.5 and 2). The best glucose concentration was then used in the large scale expression. In all cases, the cells were harvested in the stationary phase by centrifugation at 4,000 rpm for 20 min at 4 °C and stored until further protein purification.

### *2.1.3 Large Scale Expression*

The growth of the transformed *E. coli* cells to high culture densities was performed using a 5 Liter BioFlo 110 Modular Benchtop Fermentator (New Brunswick, Edison, NJ) as illustrated in the Figure 2.1. The protocol was tested and optimized for the *E. coli* cells transformed with HbI cDNA, applying the best expression conditions obtained in the small scale experiments. Prior to the fermentation process, a flask containing 50 mL of Luria–Bertani medium (Sigma, St. Louis, MO) was inoculated with a frozen stock of rHbI and incubated overnight with 70 µg/mL kanamycin and 30 µg/mL chloramphenicol at 37 °C on a shaker at 125 rpm. This preculture was then used to inoculate a 2.5 L flask containing 500 mL of fresh LB medium and grown overnight under similar conditions.



**Figure 2.1: Bioreactor used for large scale hemprotein expression. The growth of the transformed *E. coli* cells to high culture densities was performed using a 5 Liter BioFlo 110 Modular Benchtop Fermentator (New Brunswick, Edison, NJ). A total of 5 L of TB media was supplemented with 30  $\mu\text{g}/\text{mL}$  of chloramphenicol, 70  $\mu\text{g}/\text{mL}$  of kanamycin, and 100  $\mu\text{L}/\text{L}$  of antifoam agent (Sigma, St. Louis, MO). The protein expression was induced by adding 1 mM of IPTG in the mid-log phase ( $\text{OD}_{600}$ , of 1.5–2.0) along with 1 %w/v glucose and 30  $\mu\text{g}/\text{mL}$  hemin chloride. The temperature was maintained at 37 °C before induction and at 30 °C after the addition of IPTG. The culture pH was controlled at 7.0 throughout the process using 1.5 M  $\text{KH}_2\text{PO}_4$  and 30%  $\text{NH}_4\text{OH}$  (Sigma, St. Louis, MO). Oxygen supply was maintained a concentration of  $\text{dO}_2$  at 35 % with an agitation cascade of 300-700 rpm. [León et al., 2004; Ramos et al., 2010].**

The fermentation process was initiated by adding this second overnight culture to 4.5 L of TB media supplemented with 30 µg/mL of chloramphenicol, 70 µg/mL of kanamycin, and 100 µL/L of antifoam agent (Sigma, St. Louis, MO). Recombinant protein expression was induced by adding 1 mM of IPTG in the mid-log phase (OD<sub>600</sub>, of 1.5–2.0) along with 1 % w/v glucose and 30 µg/mL hemin chloride. The temperature was maintained at 37 °C before induction and at 30 °C after the addition of IPTG. The culture pH was controlled at 7.0 throughout the process using 1.5 M KH<sub>2</sub>PO<sub>4</sub> and 30% NH<sub>4</sub>OH (Sigma, St. Louis, MO). To increase the population of transformed *E. coli* cells, oxygen supply was maintained a concentration of dO<sub>2</sub> at 35 % with an agitation cascade of 300-700 rpm. The amount of protein achieved under this condition was 135 mg/L protein concentration. This optimized fermentation protocol was then applied to the rHbI PheB10Tyr mutant. Similar to the small scale expression, the cells were harvested in the stationary phase by centrifugation for 20 min at 4 °C and stored until further protein purification.

#### *2.1.4 Purification of the Hemoglobins*

The cells containing either rHbI or the rHbI PheB10Tyr mutant were lysed and purified by metal affinity chromatography on Co<sup>+2</sup> affinity columns (TALON, Clontech), desalting purification and size exclusion chromatography. Initially, the bacterial pellets, obtained by centrifugation, were weighed and resuspended in 2.6 mL of buffer/per g of bacteria (58 mM Na<sub>2</sub>HPO<sub>4</sub>, 17 mM NaH<sub>2</sub>PO<sub>4</sub>, and 68 mM NaCl, pH 7.5). One milligram of lysozyme (Sigma, St. Louis, MO) per gram of bacteria and one tablet of protease inhibitor cocktail (Roche Applied Science) per 50 mL of buffer were then added to the resuspended cells. The mixture was incubated on ice for 1 h, sonicated and homogenized for 1 min several times until a liquefied solution was obtained. To separate the soluble proteins from the bacterial pellets the mixture was centrifuged at 4 °C, 15,000 rpm for 1 h. To purify the proteins, first, a His-tagged affinity

chromatography method was used. As a first step, a metal affinity resin column was packed with 10 mL of cobalt resin (BD TALON™ Resins, Clontech, Palo Alto, CA) and equilibrated with 10 bed volume (BV) of the equilibrating buffer (50 mM NaH<sub>2</sub>PO<sub>4</sub>, 300 mM NaCl, pH 7.0) at a gravity flow. Approximately, 20 mL of the soluble proteins were loaded into the column. The column was shaken for 20 min at room temperature. The BD Talon resins are durable, cobalt-based Immobilized Metal Affinity Chromatography (IMAC) resins designated to purify recombinant polyhistidine-tagged proteins. Unbound proteins were eluted first with two column volume (CV) of the equilibrating buffer. Subsequently, the resin was washed with 10 CV of buffer containing 50 mM NaH<sub>2</sub>PO<sub>4</sub>, 300 mM NaCl, and 10 mM imidazole at pH 7.0, to remove weakly bound and unwanted proteins. The desired protein was then eluted with 10 CV of 50 mM NaH<sub>2</sub>PO<sub>4</sub>, 300 mM NaCl, and 150 mM imidazole at pH 7.0 and collected in a 10.0 mL FALCON tubes. To eliminate the excess of imidazole, an AMICON ultra-filtration cell with an YM-10 membrane was employed. The proteins were stored in phosphate buffer, pH 7.0, at -80 °C until further purification.

The second purification process was performed using a FPLC Hi-Trap desalting column (AKTA FPLC system, GE Healthcare, Piscataway, NJ). The column was packed with 10 mL of size exclusion matrix Sephadex G-25 supefine resin (GE Healthcare, Piscataway, NJ) and equilibrated with 10 bed volume (BV) of the equilibrating buffer (50 mM NaH<sub>2</sub>PO<sub>4</sub>, 300 mM NaCl, pH 7.0) at a flow rate of 5.0 mL/min. Approximately, 20 mL of the soluble proteins (maximum concentration of 70 mg/mL of protein) were loaded into the column. The sample should be filtered immediately before loading the column to remove any particulate material. Subsequently, the desired protein was then eluted using the elution profile with 10 CV of 50 mM

NaH<sub>2</sub>PO<sub>4</sub>, and 300 mM NaCl, and automatically collected in a fraction collector. To concentrate the sample, an AMICON ultra-filtration cell with an YM-10 membrane was employed. The proteins were stored in phosphate buffer, pH 7.0, at -80 °C until further purification.

The last purification process was performed using a FPLC HiLoad 26/60 Superdex 200 prep grade column with 26 x 60 cm dimension. (AKTA FPLC system, GE Healthcare, Piscataway, NJ). The column was equilibrated and eluted a pH 7.5 with 0.5 mM EDTA and 50 mM sodium phosphate buffer at a flow rate of 4.4 ml/min under 0.5 mPa of pressure. Approximately, 5 mL of the filtrated soluble proteins was loaded into the column. The eluted fractions were automatically collected in a Frac-950 (Amersham Pharmacia Biotech) fraction collector. The FPLC instrument has a UV-Vis lamp that monitored the presence of proteins in each fraction at 280 nm. To concentrate the sample, an AMICON ultra-filtration cell with an YM-10 membrane was employed. The proteins were stored in phosphate buffer, pH 7.0, at -50 °C until further characterization. During all the purification process, aliquots of each step were stored for sodium dodecyl sulfate polyacrylamide gel electrophoresis (SDS-PAGE on 10 % acrylamide gel) analysis, to verify the purity and integrity of the proteins.

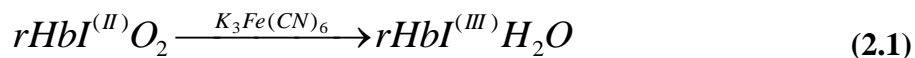
### *2.1.5 Spectral Properties of the hemoglobins*

The spectral properties of the purified rHbI and rHbI PheB10Tyr were evaluated by analyzing their UV-Vis spectra using Shimadzu 2101 PC spectrometer. The active ferrous oxy form of rHbI and rHbI PheB10Tyr mutant was initially obtained by exposing the proteins samples to an O<sub>2</sub> atmosphere. The oxy-rHbI and oxy-rHbI PheB10Tyr mutant were monitored at 414 nm, the maximum absorption in the static, UV-Vis spectra of the rHbIO<sub>2</sub> and rHbIO<sub>2</sub> PheB10Tyr mutant complexes. The samples were concentrated to 2.50-3.0mM protein concentration using an AMICON ultra-filtration cell with an YM-10 membrane. Protein

concentrations were estimated measuring their optical absorption spectra and stored at  $-50\text{ }^{\circ}\text{C}$  until further characterization.

## 2.2 Preparation of cyano rHbI and rHbI PheB10Tyr mutant complex

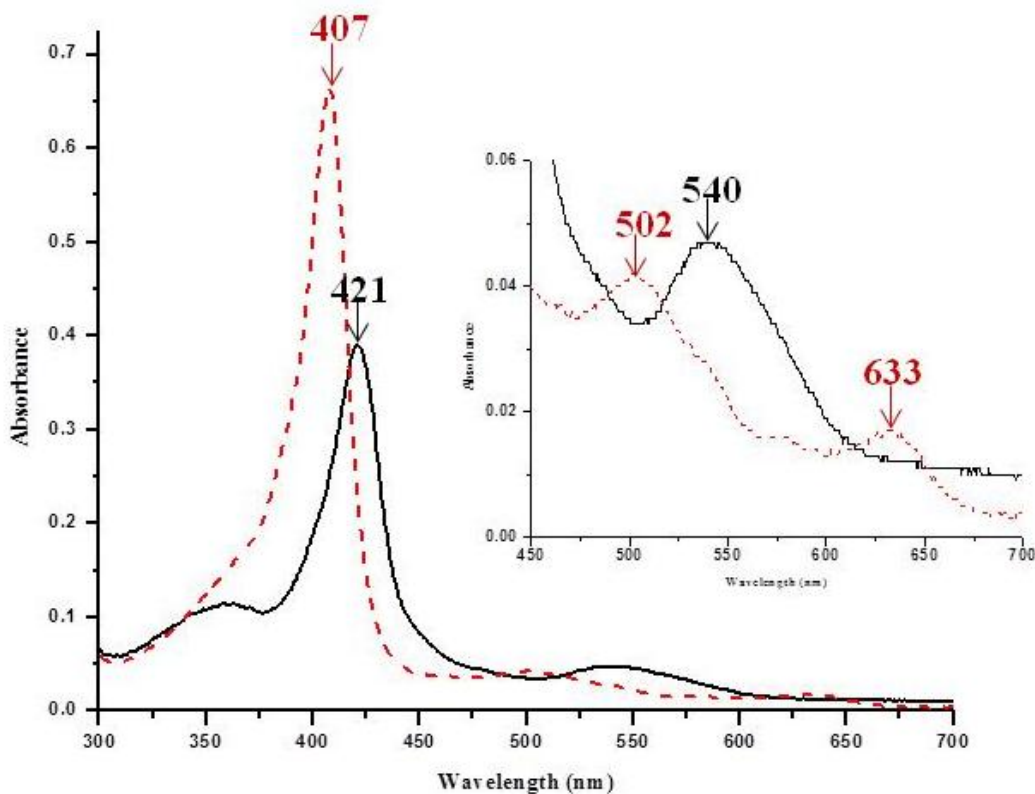
Purified rHbI and rHbI PheB10Tyr mutant proteins were mostly found as the ferrous oxy-hemoglobins complex. These ferrous oxy-rHbI and oxy-rHbI PheB10Tyr variant were oxidized slowly to ferric hemoglobin by titration with 1:1 oxidation reaction to obtain the metaquo-rHbI derivative [Kraus and Wittenberg, 1990]. A 10 % excess of a potassium ferricyanide ( $\text{K}_3\text{Fe}(\text{CN})_6$ ) solution was titrated against 2.50 to 3.00 mM concentrated oxy-rHbI and oxy-rHbI PheB10Tyr mutant solution at pH 7.0. The protein complex oxidation (heme  $\text{Fe}^{\text{II}}$  to heme  $\text{Fe}^{\text{III}}$ ) was monitored using Ultraviolet-Visible (UV-Vis) spectroscopy (Shimadzu UV-2101 PC spectrometer).



The potassium ferricyanide titration was performed until the UV-Vis spectrum of the sample showed a characteristic Soret band at 407 nm and two Q bands at 502 and 633 nm [Kraus and Wittenberg, 1990]. These wavelengths are characteristic of the ferric metaquo rHbI and rHbI PheB10Tyr complexes. After hemoglobin oxidation titration, excess oxidant was removed using a Centricon centrifugal filter device equipped with an YM-10 membrane (AMICON).

Cyanide rHbI and rHbI PheB10Tyr variant complexes were obtained by titration of ferric hemoglobin I (2.50 to 3.00 mM) with a 50 mM potassium chloride (KCl)/20 mM potassium cyanide (KCN) solutions prepared with  $^1\text{H}_2\text{O}$ (90 %)/ $^2\text{H}_2\text{O}$ (10 %) and  $^2\text{H}_2\text{O}$ (100 %) at pH 7.0. The cyanide optical spectra are characteristic by a Soret maximum absorption and Q bands at 421 and 540 nm, respectively [Kraus and Wittenberg, 1990]. According to this, Figure 2.2 shows the formation of the cyanide derivative from the metaquo hemoglobin complex, observing

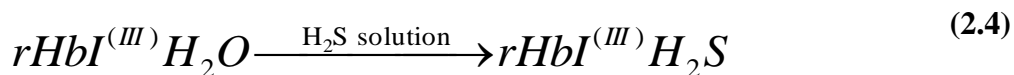
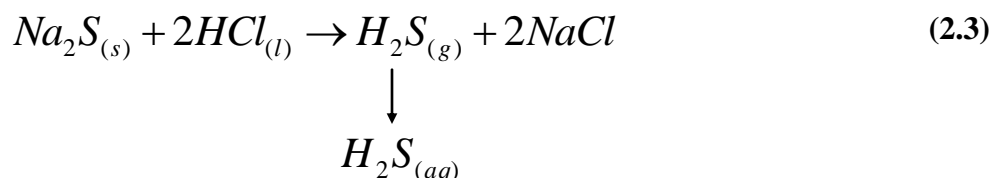
changes in their UV-Vis Soret band (from 407 to 421 nm) and the Q bands (from 502 and 633 nm to 540 nm). After the rHbICN and rHbICN PheB10Tyr protein variant complex formation, excess cyanide was removed using Centricon centrifugal filter device equipped with an YM-10 membrane (AMICON).



**Figure 2.2:** UV-Vis spectra of ferric rHbI and rHbI PheB10Tyr mutant. The spectra show the formation of the cyanide derivative (black solid line (—)) from metaquo complex (red dash line (----)) observing changes in their absorption maxima at 407 to 421 nm and the Q bands at 502 and 633 nm to 540 nm. To obtain the cyanide derivative of the proteins, the metaquo form (2.50 to 3.00 mM) was titrated with a 50 mM KCl/20 mM KCN solutions prepared with 90 %  $^1\text{H}_2\text{O}$ /10 %  $^2\text{H}_2\text{O}$  and 100 %  $^2\text{H}_2\text{O}$  at pH 7.0.

### 2.3 Preparation of Hydrogen sulfide rHbI complex.

Prior to complex preparation, the oxidized protein and hydrogen sulfide solutions were degassed and purged with nitrogen (N<sub>2</sub>) to eliminate oxygen from the sample atmosphere. The sulfide solutions were prepared by adding sodium sulfide (Na<sub>2</sub>S<sub>(s)</sub>) salt in <sup>1</sup>H<sub>2</sub>O(90%)/<sup>2</sup>H<sub>2</sub>O(10%) and <sup>2</sup>H<sub>2</sub>O(100%) at pH 7.0. Hydrogen sulfide complexes were prepared by adding 10 mM of the sodium sulfide solution to the deoxygenated oxidized protein with a concentration of 2.50 to 3.0 mM [Pietri et al., 2009]. Typically, a 3 to 10 fold molar excess of H<sub>2</sub>S was needed to form the complex. Protein concentration was determined using the Beer-Lambert law using the mean extinction coefficients reported for HbI complexes [Kraus and Wittenberg, 1990]. Figure 2.3 shows the hydrogen sulfide optical spectra with characteristic Soret maximum absorption and Q bands at 426 and 544 nm, and 574 nm, respectively [Kraus and Wittenberg, 1990]. According to this, H<sub>2</sub>S derivative formation from metaquo hemoglobin complex was monitored by observing changes in UV-Vis Soret band (from 407 to 426nm) and Q bands (from 502 and 633 nm to 540 nm).



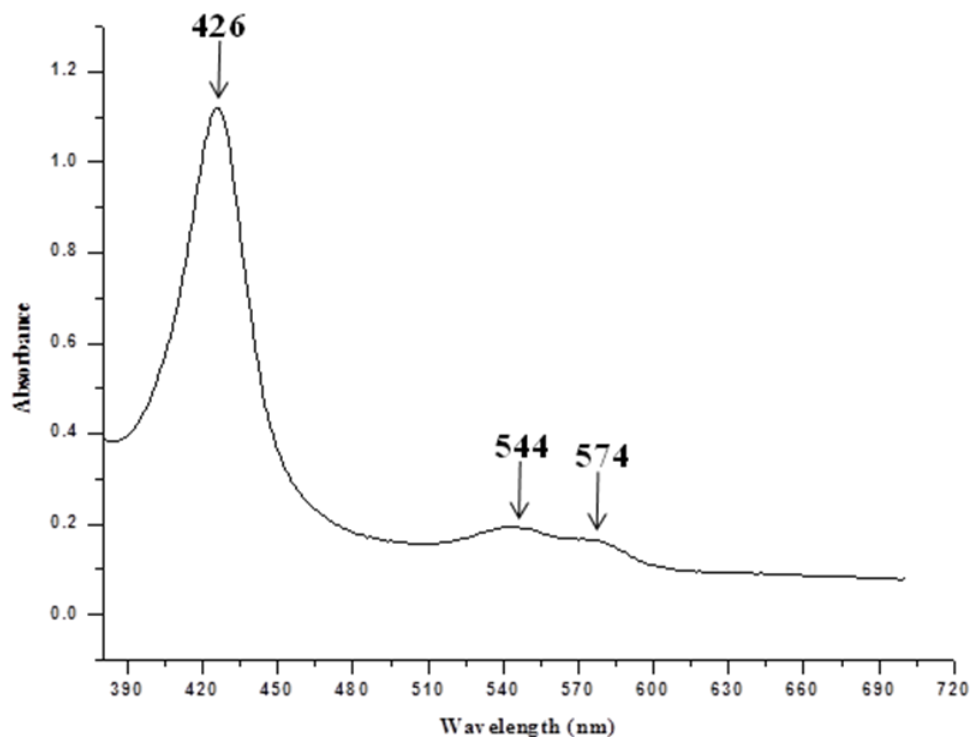


**Figure 2.3: UV-Vis spectrum of rHbIH<sub>2</sub>S complex. The spectra show the absorption maxima at 426 nm and the Q bands at 544 and 574 nm for rHbIH<sub>2</sub>S complex. To obtain the hydrogen sulfide derivative of the protein, the deoxygenated metaquo form (2.50 to 3.0 mM) was titrated with a 10 mM of the sodium sulfide solutions prepared with 90 % <sup>1</sup>H<sub>2</sub>O/10 % <sup>2</sup>H<sub>2</sub>O and 100 % <sup>2</sup>H<sub>2</sub>O at pH 7.0.**

## 2.4 Nuclear Magnetic Resonance (NMR) Data Acquisition

### 2.4.1 NMR sample preparation

In order to acquire high resolution data in NMR spectroscopy, a careful preparation of the protein sample is needed. Homogeneity of the magnetic field needs to be conserved by preparing a filtrated, concentrated, and homogeneous protein sample solution without air bubbles. rHbI and rHbI PheB10Tyr mutant proteins were concentrated using an YM-10 membrane Centricon centrifugal filter (AMICON, Millipore Co.) and degassed with N<sub>2</sub> to remove dioxygen (O<sub>2</sub>). Final concentrations of monomeric rHbI and single PheB10Tyr mutant samples were obtained at 3.0 mM using <sup>1</sup>H<sub>2</sub>O (90 %)/<sup>2</sup>H<sub>2</sub>O (10 %) and <sup>2</sup>H<sub>2</sub>O (100 %) solution at pH 7.0. It was important to decrease by 25 % the ionic strength from the solution and increase 30 % of the sample concentration. A volume of 500 µl of the rHbI and rHbI PheB10Tyr mutant complexes were transferred under argon atmosphere to high quality 5 mm NMR tubes.

### 2.4.2 NMR preliminary data acquisition set-up

NMR spectra of rHbI and rHbI PheB10Tyr variant derivatives were collected on a Bruker Avance-500 and 600 MHz spectrometer equipped with a 5 mm multinuclear gradient probe (i.e. QXI-<sup>1</sup>H-<sup>13</sup>C/<sup>15</sup>N/<sup>31</sup>P-D-Z gradient and TXI <sup>1</sup>H-<sup>13</sup>C/<sup>15</sup>N-D-XYZ-GRD ZX) and a cryoprobe (cryocooling unit Z49290 2mTFL ethylene glycol), respectively . Figure 2.4 illustrate the NMR tube containing the sample in the spinner housing to adjust the NMR tube position with the depth gauge. The sample was inserted in the transfer tube at the center of the magnet. A preliminary set-up was performed using the following basic steps: (i) sample temperature was equilibrated in the probe, (ii) lock the spectrum on the deuterium line and adjusted to lock frequency, power of the lock transmitter, and gain of the lock receiver, (iii) shim was attuned shimming the coils to

ensure homogeneity of the magnetic field, (iv) tune and match the probe for  $^1\text{H}$  nucleus, and (v) calibrated the acquisition parameter of the pulse sequences.

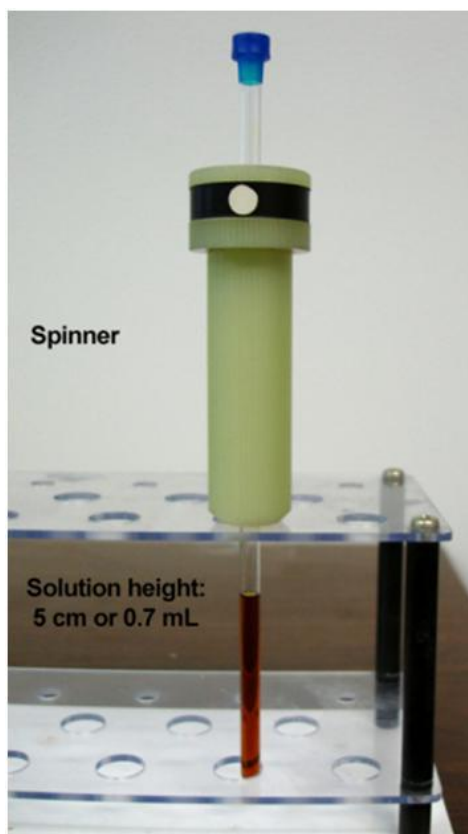


**Figure 2.4: 5 mm NMR tube hold by the spinner housing with 3.0 mM of hemoprotein. Each tube was prepared with 500  $\mu\text{l}$  of 3.0 mM of protein using 90 %  $^1\text{H}_2\text{O}$ /10 %  $^2\text{H}_2\text{O}$  and 100 %  $^2\text{H}_2\text{O}$  solution at pH 7.0 under argon atmosphere.**

### 2.4.3 One dimensional (1D) Pulse Sequences: $^1\text{H}$ -NMR Experiments

#### 2.4.3.1 Water Solvent Suppression using Presaturation Pulse Sequence

$^1\text{H}$  reference spectra (pulprog = zg30) were successfully achieved by using a delay time of  $1.0\text{ s}^{-1}$  for 128 scans and 4096 data points with a spectral width of 30,030 Hz. The  $90^\circ$  pulse length of the pulse sequence was calibrated through the calibration of the  $360^\circ$  pulse length [Keifer, 1998]. It was necessary to attenuate the intensity of the solvent line as the rHbI and rHbI PheB10tyr mutant protein spectra were acquired in  $\text{H}_2\text{O}$ . Water solvent suppression was performed by direct saturation with a low power radio frequency (RF) field in the relaxation delay ( $t_{\text{rd}}$ ) period using presaturation pulse sequence (pulprog = zgpr). Figure 2.5 illustrates a schematic representation of the water solvent suppression pulse sequence. The transmitter was placed on-resonance (O1) at the same frequency as the water reference resonance line at 4.70 ppm which allows elimination of any residual solvent signal. A receiver gain (RG) setting was required to improve the signal to noise (s/n) ratio where the intensity of the signal went from  $\frac{1}{2}$  to  $\frac{2}{3}$  of the range of the digitizer [Rule and Hitchens, 2006]. Isotopic experiments were performed using the same water solvent suppression pulse sequence previously described using the hydrogen isotope deuterium ( $^2\text{H}_2\text{O}$ ) as a solvent.

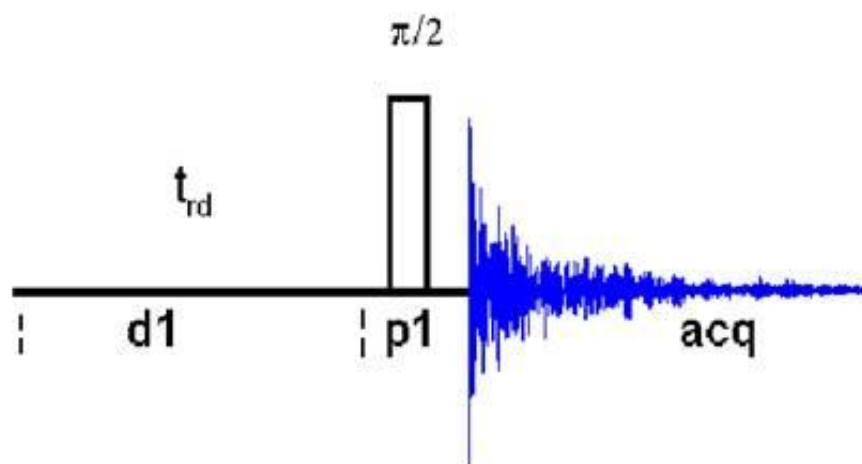


**Figure 2.5: Schematic representation of water solvent suppression NMR pulse sequence [Bruker Avance, Co]. The transmitter was placed on-resonance (O1) at the same frequency as the water reference resonance line at 4.70 ppm which allows elimination of any residual solvent signal.**

### 2.4.3.2 Variable Temperature Experiments

Variable temperature experiments of rHbI and rHbI PheB10Tyr protein complexes were performed to determine the temperature dependence of heme peripheral groups and to detect resonance lines in the NMR spectra. These experiments were achieved using a cryogenic cooling unit of ethylene glycol with an air flow of 670 L/hr. Sample temperature was measured by the instrument using a thermocouple that was placed outside of the sample. The real temperature of the sample was determined by measuring the chemical shift difference ( $\Delta\delta$ ) between the hydroxyl and ethyl resonances in ethylene-glycol [Rule and Hitchens, 2006]. The following formula was used for setting the VT experiments:

$$T = 403.0 - 29.53\Delta\delta - 23.87[\Delta\delta]^2 \quad (2.5)$$

where T is the temperature in Kelvin units. The variable temperature (VT) experiments were collected over the range of 281 K to 303 K (8-30 °C) at pH 7.0 using a  $^1\text{H}$  water suppression pulse sequence (pulprog = zgpr), with a delay time of 1.0 s<sup>-1</sup> for 128 scans, 4096 data points, and a spectral width of 35,000 Hz (21.5 ppm).

### 2.4.3.3 Water Eliminated Fourier Transform (WEFT) Experiments

Water Eliminated Fourier Transformation commonly known as WEFT is a modification of the classic inversion-recovery experiment for the measurement of spin-lattice relaxation ( $T_1$ ) times [Emerson and La Mar, 1990]. The principal advantage of this technique is that it provides one of the best chances for observing solute signals that lie very close to the water frequency [Freeman, 1987]. The WEFT spectra were collected using a 10 s<sup>-1</sup> delay time, a range between 20 ms to 80 ms mixing period, and 58.6 ms acquisition time. The WEFT spectra collections were repeated at temperature of 18 °C, 25 °C, and 33 °C.

#### 2.4.3.4 *Inversion Recovery Experiment: Non-selective $T_1$*

Nonselective  $T_1$  values were collected by using a standard inversion recovery pulse sequence,  $t-90^\circ_x-240^\circ_y-90^\circ_x-\tau-90^\circ_\phi$ -Acq, where the delay time ( $\tau$ ) was set at two different ranges, one between 1 ms to 400 ms, and the other between 0.5 ms to 100 ms with increment of 5 and 10 ms each one [Emerson and La Mar, 1990]. The 8192 block size and 34,965 Hz spectral window gave an acquisition time of 117 ms. This acquisition time allowed optimal detection of the rapid relaxation signals throughout the spectral window. The spectra were recorded at temperature of 18 °C, 25 °C, and 33 °C. Signals intensities were analyzed with a single exponential return to equilibrium.

#### 2.4.3.5 *1D Steady-state Nuclear Overhauser Effect Experiments (NOE's)*

Steady-state nuclear Overhauser Effect spectra (NOE's) were recorded by applying 200 ms of irradiation time at 1.5 s<sup>-1</sup> repetition rate and a decoupler on-resonance to saturate signal at 16,336.80 Hz (27.27 ppm-5-methyl), 18,619.22 Hz (31.00 ppm-TyrB10 OH<sub>η</sub>) and -1,994.02 Hz (-3.00 ppm-GlnE7 NH<sub>ε2</sub>). In addition, spectra were collected with a decouple off-resonance at 14,031 Hz to provide a reference. The NOE spectra were acquired at 18 °C, 25 °C, and 33 °C temperatures. The 4096 block size and 34,965 Hz spectral window gave an acquisition time of 58.0 ms. Figure 2.6 illustrates a schematic representation of the NOE pulse sequence, showing the presaturation on-resonance region to saturate specific signals of the protein and the off-resonance region for reference.

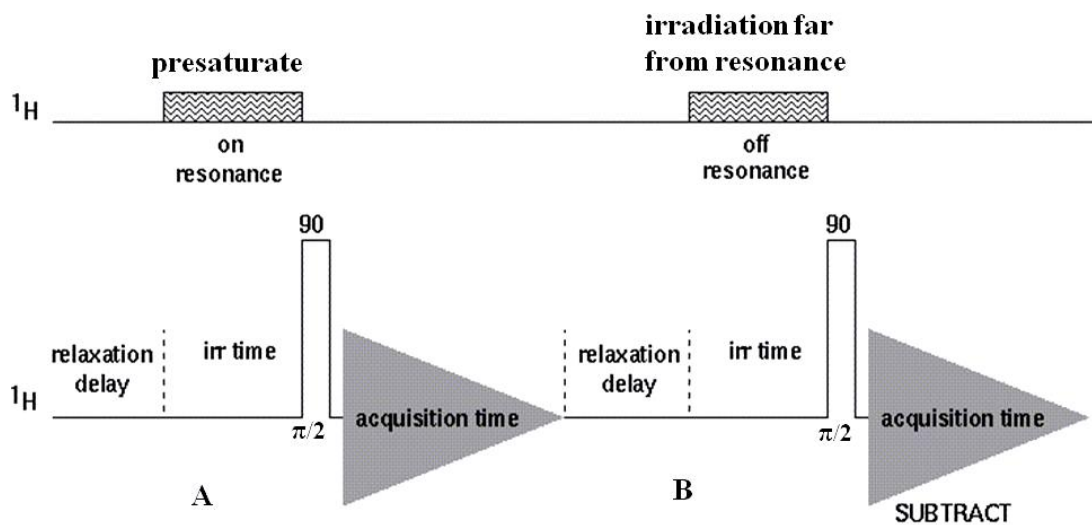


**Figure 2.6: Schematic representation of Steady-state Nuclear Overhauser (NOE's) pulse sequence [Bruker Avance, Co]. It is illustrated the presaturation on-resonance region to saturate specific signals of the protein and the off-resonance region for reference.**

## 2.4.4 Two dimensional (2D) Pulse Sequences: $^1\text{H}$ - $^1\text{H}$ NMR Experiments

### 2.4.4.1 Nuclear Overhauser Enhancement Spectroscopy (NOESY)

NOESY spectra were collected with an 11.70  $\mu\text{s}$   $90^\circ$  pulse over a spectral window of 20,325 Hz using 2048 complex points and a block size of 512 with 128 scans for each block. The length of the mixing time was 80 ms at 33  $^\circ\text{C}$ . Water solvent suppression was achieved using a presaturation pulse sequence, as described previously, by a decoupler power at 44.00 dB during the relaxation delay and mixing time. To determine the time for 1 per second (1/s) relaxation delay, the following equation was used:

$$D1 = 1 - AQ - D8 \quad (2.6)$$

where  $D1$  ( $t$ ) is the relaxation delay,  $AQ$  is the acquisition time and the  $D8$  ( $\Delta$ ) is the mixing time. Figure 2.7 illustrate the classic NOESY pulse sequence,  $t$ - $90^\circ_x$ - $t_1$ - $90^\circ_x$ - $\Delta$ - $90^\circ_x$ -Acq. The total acquisition time to obtain the NOESY spectra was 19 h. This two dimensional technique gave evidence for spatial proximity for nuclei.

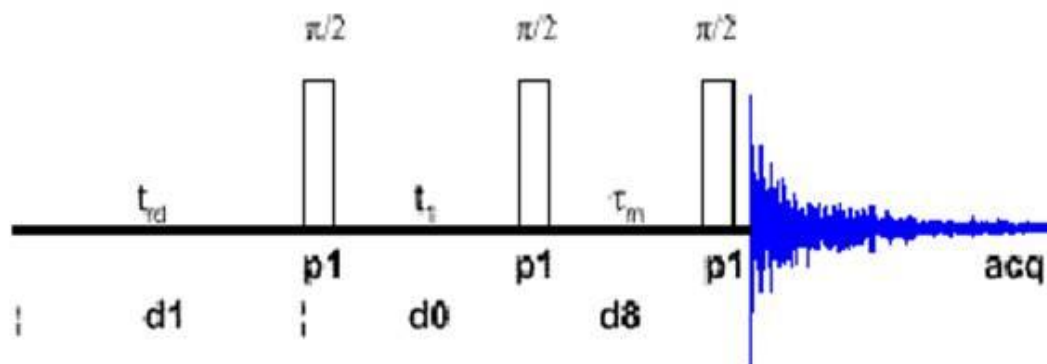


**Figure 2.7:** Schematic representation of the NOESY pulse sequence [Bruker Avance, Co; Friebohn, 1998]. Water solvent suppression was achieved using a presaturation pulse sequence by a decoupler power at 44.00 dB during the relaxation delay ( $t_{rd}$ ) at 1/s and mixing time at 80 ms in a temperature at 33 °C.

#### 2.4.4.2 Total Correlation Spectroscopy (TOCSY)

Figure 2.8 illustrate the TOCSY pulse sequence as described by the following sequence:  $t$ -90°- $t_1$ -spin-lock-Acq. This experiment was performed using 40 ms during the spin lock time,  $1 \text{ s}^{-1}$  for the delay time, and 13.34  $\mu\text{sec}$  RF pulse length. A matrix of 2048 x 512 (F2 x F1) over an 8,503 Hz spectral window was attained in an acquisition time of 121 ms. The total acquisition time to obtain the TOCSY spectra was 32 h. A total of 128 dummy scans per  $t_1$  were used for each free induction decay (FID). TOCSY experiments required a temperature of decrease at less 3 °C of the target temperature (25 °C), due to the heat generated from the spin lock. As previously described, water solvent suppression for the TOCSY experiment was achieved using a presaturation pulse sequence by a decoupler power at 50.00 dB during the relaxation delay and spin lock. To determine the time for 1 per second (1/s) relaxation delay, the following equation was used:

$$D1 = 1 - AQ - \text{spin lock (mixing time)} \quad (2.7)$$

where D1 ( $t$ ) is the relaxation delay and AQ is the acquisition time. This two dimensional technique allowed to identify all the protons belonging to a common coupled spin system.

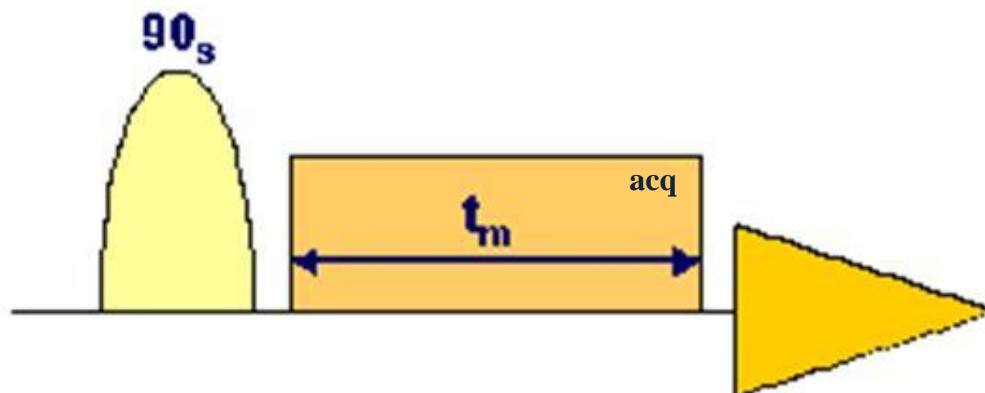


**Figure 2.8:** Schematic representation of the TOCSY pulse sequence [Bruker Avance, Co; Friebolin, 1998]. Water solvent suppression for the TOCSY experiment was achieved using a presaturation pulse sequence by a decoupler power at 50.00 dB during the relaxation delay at 1/s, spin lock time at 40 ms and RF pulse length at 13.34  $\mu$ sec.

## 2.5 Nuclear Magnetic Resonance (NMR) Data Processing

All spectra were calibrated for solvent reference after each data acquisition (i.e. water peak at 4.70 ppm). NMR data were processed using two software: Xwin-NMR Plot Version 3.1 (Bruker BioSpin, Germany) and MestRe-C Version 3.17 (Universidad de Santiago de Compostela, Spain). The 1D processing parameters included the application of exponential multiplication (EM) and line broadening (LB) as a window function for the modification of the FID [Rule and Hitchens, 2006]. Line broadening (LB) should be in a range between 1.00 to 5.00 Hz. The 2D processing parameters included sine bell window function (QSINE) with a SSB6 and States-TPPI method [Emerson and La Mar, 1990].

## 2.6 Nuclear Magnetic Resonance (NMR) Protein Structure Determination

### 2.6.1 NMR Resonance Assignments: <sup>1</sup>H-Homonuclear Method

NMR resonance assignments were performed following traditional assignment strategies for proteins with slight modifications [Hus et al., 2002; Rule and Hitchens, 2006]. Figure 2.9 illustrate the resonance assignment strategy overview according to Rule and Hitchens [Rule and Hitchens, 2006]. Initially, resonances within a spin-system were assigned to atoms with spin on the same amino acid residue using Fischer notation (i.e.  $\alpha$ ,  $\beta$ ,  $\gamma$ ,  $\delta$ ,  $\epsilon$ ). Usually, resonance frequencies are divided into two groups: main-chain atoms or backbone atoms (i.e.  $H_N$ ,  $H_\alpha$ ) and side-chain atoms (i.e.  $H_\beta$ ,  $H_\gamma$ ,  $H_\delta$ ,  $H_\epsilon$ ). The <sup>1</sup>H-homonuclear resonance assignment was based in the sequence-specific resonance method using the conservative amino acid HisF8 which is covalently bonded to the heme group as start point. Next, the spin system was organized by a matrix with amino acid type in the horizontal axis and chain atoms in the vertical axis. Furthermore, sequential NOE connectivity's of assigned spin systems were identified from the

adjacent and distant side-chain protein residues. Finally, the connected segment of spin-systems was related with the segment of primary sequence. All resonance frequencies associated with the spin-system of each residue on the rHbI and rHbI PheB10Tyr mutant amino acid sequence were collected through the data acquired by scalar spin-spin couplings and space-dipolar couplings. Resonance assignments involved the identification of the total number and sequence position of each amino acid found in the  $\alpha$ -helix of the protein. Table 2.1 details the amino acid residues in the wtHbI sequence from *L. pectinata*. Figure 2.10 shows the amino acid sequence of the wtHbI used as a reference in the resonance assignment method [Antommattei-Pérez et al., 1999].

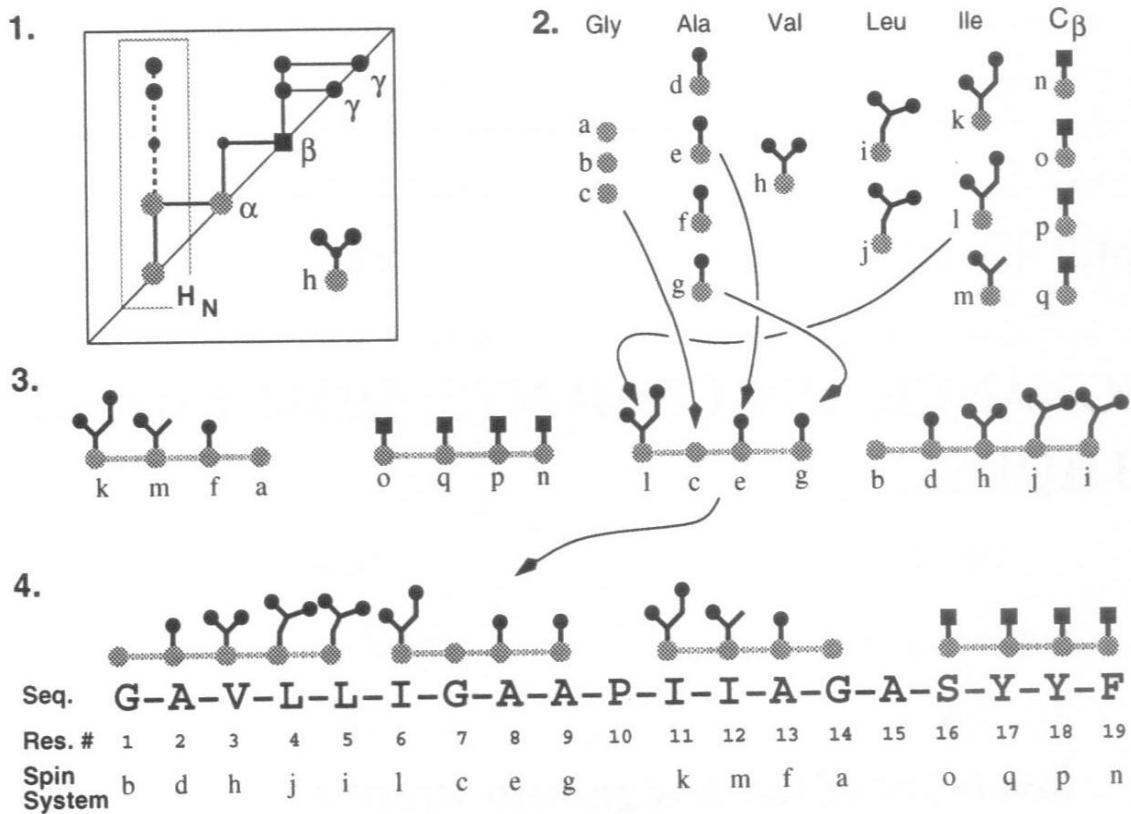


Figure 2.9: Schematic representation of resonance assignment strategy [Rule and Hitchens, 2006].

**Table 2.1: Amino acid residues in the wtHbI sequence from *Lucina pectinata*<sup>a</sup>**

<b>Amino Acid</b>	<b>Position Sequence (helix)</b>	<b>Total Number</b>
Gly (G)	22(B3), 25(B6), 45, 49, 53(D2), 70(E13), 83, 87, 100, 104(G3), 115(G14), 121(H2), 122(H3), 125(H6), 132(H13), 136(H17)	16
Ala (A)	4(A2), 5(A3), 15(A13), 17(A15), 19, 20(B1), 24(B5), 31(B12), 35(B16), 41(C6), 50, 51, 62(E5), 63(E6), 65(E8), 82, 84, 93(F5), 94(F6), 98(F10), 103(G2), 108(G7), 109(G8), 114(G13), 126(H7), 129(H10), 131(H12), 133(H14)	28
Val (V)	10(A8), 39(C4), 55(D4), 72(E15), 76(E19), 112(G11), 130(H11)	7
Leu (L)	2, 32(B13), 46, 71(E14), 79, 85, 106(G5), 113(G12), 134(H15)	9
Ile (I)	101, 138(H19)	2
Pro (P)	26(B7), 59(E2), 140(H21)	3
Phe (F)	28(B9), 29(B10), 33(B14), 40(C5), 43, 47, 68(E11), 92(F4), 110(G9), 116(G15)	10
Trp (W)	14(A12), 21(B2), 75(E18), 127(H8)	4
Tyr (Y)	120(G19)	1
Met (M)	30(B11), 61(E4), 117(G16), 135(H16), 137(H18), 142(H23)	6
Cys (C)	89(F1)	1
Ser (S)	1, 3(A1), 12(A10), 13(A11), 18(A16), 44, 67(E10), 73(E16), 102(G1), 119(G18)	10
Thr (T)	23(B4), 54(D3), 58(E1), 91(F3), 128(H9)	5
Asn (N)	9(A7), 57(D6), 74(E17), 78, 81, 95(F7), 141(H22)	7
Gln (Q)	6(A4), 64(E7), 66(E9), 88, 105(G4)	5
His (H)	36(C1), 96(F8)	2

**Table 2.1 (Continued)**

<b>Amino Acid</b>	<b>Position Sequence (helix)</b>	<b>Total Number</b>
Lys (K)	7(A5), 11(A9), 16(A14), 42(C7), 48, 52(D1), 56(D5), 69(E12), 90(F2), 97(F9), 111(G10), 118(G17)	12
Arg (R)	99, 139(H20)	2
Asp (D)	8(A6), 34(B15), 37(C2), 38(C3), 77(E20), 80, 123(H4)	7
Glu (E)	27(B8), 60(E3), 86, 107(G6), 124(H5)	5

<sup>a</sup> [Antommattei-Pérez et al., 1999]

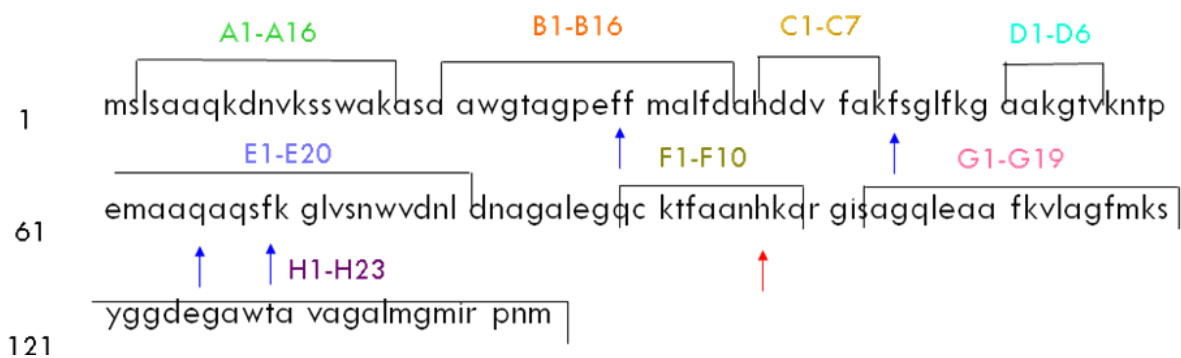


**Figure 2.10:** Amino acid sequence of wtHbI used as a reference in the resonance assignment method [Antommattei-Pérez et al., 1999]. Blue arrows identify the amino acid in the distal site of the heme pocket: PheB10, PheCD1, GlnE7 and PheE11. Red arrow identifies the conserved His96 at proximal position F8. Each segment of the helix was identified.

## 2.6.2 Protein Structure analysis: Magnetic Axes Calculations

A silicon graphics Xenon computer with the Insight II program was used for protein structure analysis. Experimentally, the protein structural analysis involved resonance assignments dipolar shifts to determine magnetic axes in the protein. Magnetic axes orientation and paramagnetic susceptibility tensor anisotropies were determined by a least-squares search using the reference iron-centered coordinate system ( $x'$ ,  $y'$ ,  $z'$ ) to (0, 0, 0), and the X-ray derived heme symmetry crystal coordinates of a ligation state as Fe(III)CN [PDB: 1BOB; Bolognesi et al., 1999]. Magnetic axes calculation was performed using a computer program designed by Emerson [Emerson, 1988]. Correlation between observed ( $\delta_{dip,obs}$ ) and calculated ( $\delta_{dip,calc}$ ) dipolar shifts was approached to define the orientation of the distal amino acids residues and structural perturbations due to the PheB10Tyr single point variant in the heme moiety [La Mar et al., 2000]. Calculations of dipolar shifts were carried out minimizing the following normalized error functions:

$$F / n = \sum |\delta_{dip}(obs) - \delta_{dip}(calc)F(\alpha, \beta, \gamma)|^2 \quad (2.8)$$

where Euler rotation angles ( $\alpha, \beta, \gamma$ ), convert the arbitrary coordinate system into the magnetic coordinate system ( $[x^*, y^*, z^*] = [x', y', z']\Gamma[\alpha, \beta, \gamma]$ ), using as input the experimental dipolar shifts for the structurally conserved proximal side of the heme. Observed ( $\delta_{dip,obs}$ ) and calculated ( $\delta_{dip,calc}$ ) dipolar shifts were expressed as:

$$\delta_{dip}(obs) = \delta_{ref}(obs) - \delta_{ref}(dia) \quad (2.9)$$

$$\delta_{dip}(cal) = -\frac{1}{3N} \left[ \Delta\chi_{ax}(3\cos^2\theta' - 1)r^{-3} + \frac{3}{2}\Delta\chi_{rh}\sin^2\theta'\cos 2\Omega'r^{-3} \right] \quad (2.10)$$

where  $\Delta\chi_{ax}$  is the axial magnetic anisotropy and  $\Delta\chi_{rh}$  is the rhombic magnetic anisotropy.

The axial magnetic anisotropy was calculated by

$$\Delta\chi_{ax} = \chi_{zz} - \frac{1}{2}(\chi_{xx} + \chi_{yy}) \quad (2.11)$$

where  $\chi$  is the diagonal paramagnetic susceptibility tensor. The rhombic magnetic anisotropy is calculated by

$$\Delta\chi_{rh} = \chi_{xx} - \chi_{yy} \quad (2.12)$$

Since the observed chemical shift is a contribution between diamagnetic and dipolar shifts, NMR experimental data was estimated and corroborated for an arbitrary nucleus (iron nucleus) using:

$$\delta_{ref}(obs) = \delta_{ref}(dia) + \delta_{hf} \quad (2.13)$$

where diamagnetic shifts were determined by:

$$\delta_{ref}(dia) = \delta_{sec} + \delta_{rc} \quad (2.14)$$

where  $\delta_{sec}$  is the secondary structure chemical shift [Wishart et al.,1992] and  $\delta_{rc}$  is the ring current (rc) chemical shift calculated from rc program in the UNIX shell system.

and where hyperfine shifts were determined by:

$$\delta_{hf} = \delta_{con} + \delta_{dip(calc)} \quad (2.15)$$

where  $\delta_{con}$  is the contact chemical shift calculated from:

$$\delta_{con} = \delta_{ref(obs)} - \delta_{ref(dia)} - \delta_{dip(calc)} \quad (2.16)$$

## CHAPTER 3: RESULTS

### 3.1 Bacterial expression of rHbI and rHbI PheB10Tyr mutant

Bacterial expression of the recombinant hemoglobin I (rHbI) and the rHbI PheB10Tyr mutant proteins was produced under the optimal expression conditions by evaluating the percentage of glucose in diverse OD<sub>600</sub> time. Table 3.1 and Figure 3.1 details the cell growth conditions used for the bacterial expression of rHbI PheB10Tyr mutant. The main modification in the methodology was the glucose concentrations during the expression procedure. A 50 mL of fresh terrific broth (TB) medium culture was grown and induced with 1 mM IPTG during the mid-log phase at an OD<sub>600</sub> of 1.5 to 2.0, followed by supplementation with 1.0 % w/v glucose and 30.0 µg/mL hemin chloride. To determine the optimal conditions for the expression, different glucose concentrations were examined. Three experiments at different glucose concentrations were carried out first by adding 1.0 % w/v glucose during the beginning of the log phase (optical density, OD<sub>600</sub> of ~1.0), second adding 0.5 % w/v glucose at the beginning of the log phase (optical density, OD<sub>600</sub> of ~1.0) and adding 0.5 % w/v glucose later in this stage (OD<sub>600</sub> between 1.5 and 2), and third adding 1.0 % w/v glucose during mid-log phase (OD<sub>600</sub> between 1.5 and 2). Figure 3.1 shows comparative results of the optical density (OD<sub>600</sub>) measurements during optimization of bacterial growth of the rHbI PheB10Tyr mutant protein in small culture volumes. Inspection of the Figure 3.1 clearly demonstrated that the highest yield was obtained when the culture was induced in the mid-log phase at an OD<sub>600</sub> of 1.5-2.0 with 1.0 % w/v of glucose. These conditions were used to perform a large scale bacterial expression in a fermentation process obtained approximately 135 mg/mL for the BLi5 cells as illustrated in the Figure 3.2. Table 3.2 summarizes the cell densities and weight, grown in the fermentation for rHbI and rHbI PheB10Tyr mutant proteins. In general, the results show the possibility of

expressing high level of rHbI and rHbI PheB10Tyr by inducing the BLi5 cells in the mid-log phase at OD<sub>600</sub> of 1.5-2.0 with 1 mM IPTG and 1.0 %w/v of glucose, decrease the temperature from 37 to 30 °C, and maintained a concentration of dO<sub>2</sub> at 35 % at 350 rpm.

**Table 3.1: Cell growth conditions used to optimize the *Escherichia coli* expression for the rHbI and rHbI PheB10Tyr mutant proteins**

<b>Conditions<sup>a</sup></b>	<b>A</b>	<b>B</b>	<b>C</b>	<b>D</b>
<b>TB (mL)</b>	50.0	50.0	50.0	50.0
<b>HC<sup>b</sup> (μL)<sup>b</sup></b>	0.0	15.0	15.0	15.0
<b>IPTG (μL)<sup>c</sup></b>	0.0	25.0	25.0	25.0
<b>Glucose (% w/v)</b>	0.0	1.0 (log-phase) <sup>d</sup>	0.5 (log-phase) <sup>d</sup> 0.5 (mid-log phase) <sup>d</sup>	1.0 (mid-log phase) <sup>d</sup>

<sup>a</sup> Constant temperature at 37°C and 135 rpm agitation.

<sup>b</sup> 30.0 μg/mL of the Hemin Chloride (HC)

<sup>c</sup> 1 mM of the Isopropyl β-D-1-thiogalactopyranoside (IPTG)

<sup>d</sup> OD<sub>600</sub> at 1.0 to log-phase and OD<sub>600</sub> at 1.5-2.0 to mid-log phase

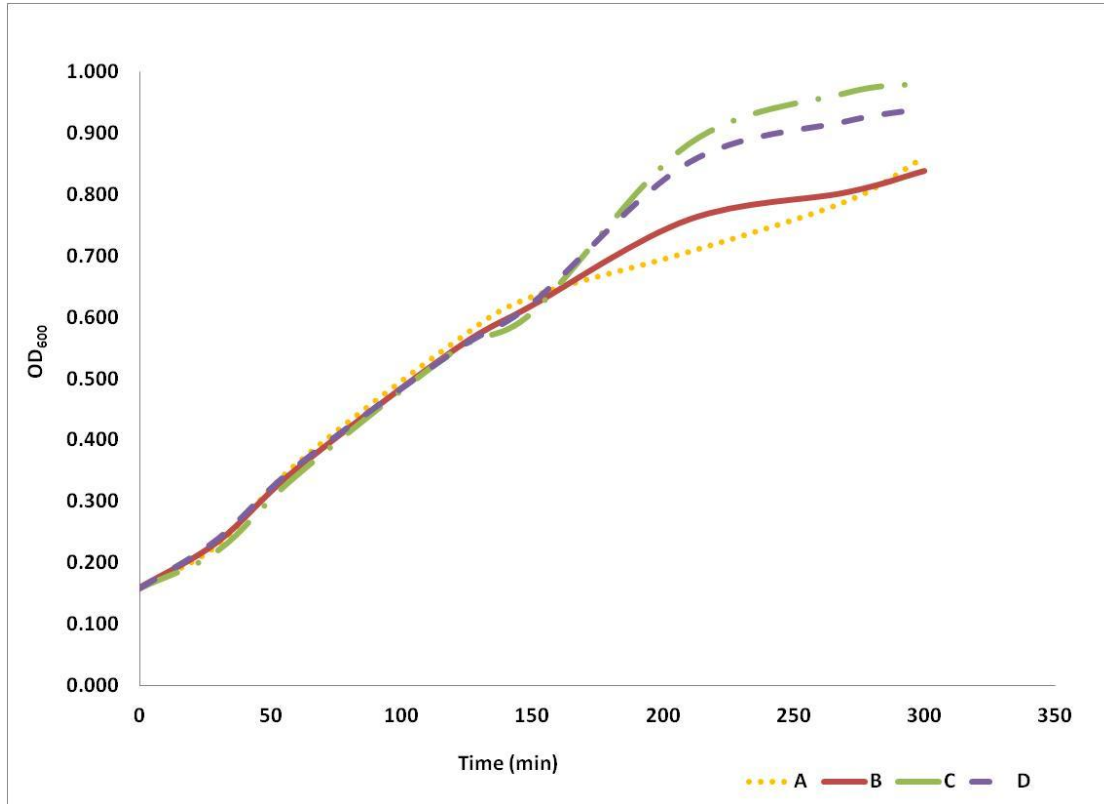


**Figure 3.1: Optical density spectrum (OD<sub>600</sub>) with diverse optimization parameter conditions for the bacterial expression of the rHbI PheB10Tyr mutant as described in Table 3.1. Optical spectra at 0 % glucose (yellow line A), 1% (log-phase) glucose (red line B), 0.5 % (log-phase) / 0.5 % (mid-log phase) glucose (green line dot line C), and 1% (mid-log phase) glucose (blue line-line D).**

**Table 3.2: Cell densities and weight, grown in the fermentation for rHbI and rHbI PheB10Tyr mutant proteins**

<b>Protein</b>	<b>OD<sub>600</sub></b>	<b>Cell wet weight (g)</b>
rHbI	20	115
rHbI PheB10Tyr	16	114

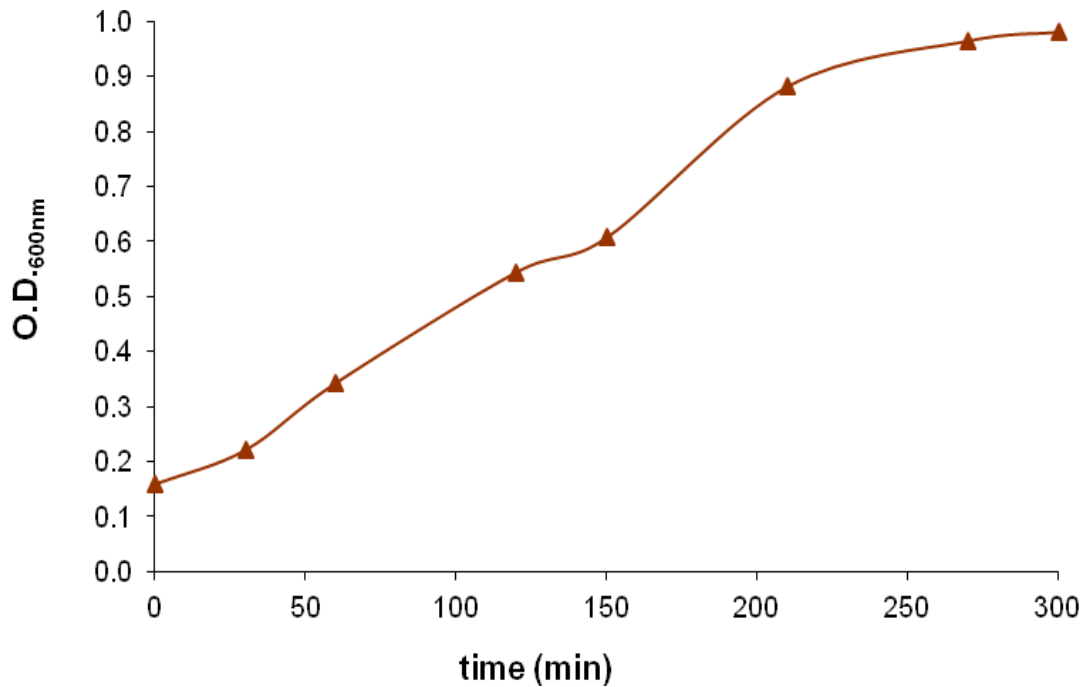


**Figure 3.2: Optical density spectrum ( $OD_{600}$ ) of the *Escherichia coli* BLi5 cells using large-scale expression for rHbI PheB10Tyr mutant. To obtain optimal expression induction of the BLi5 cells in the mid-log phase at  $OD_{600}$  of 1.5-2.0 with 1 mM IPTG and 1.0 %w/v of glucose, decrease the temperature from 37 to 30 °C, and maintained a concentration of  $dO_2$  at 35 % at 350 rpm was achieved.**

### **3.2 Purification of the rHbI and the rHbI PheB10Tyr mutant**

High resolution of Nuclear Magnetic Resonance (NMR) data was obtained improving the quality of our sample protein preparation. The sample quality was improved to avoid contamination of the crude cell during the lysate procedure and decreasing salts concentration. The generation of ion currents during radio-frequency (RF) pulses should be avoided decreasing the ionic strength ( $< 0.2$  M salts) in the sample. Figure 3.3 (A) shows UV-Vis spectrum results of the rHbI PheB10Tyr mutant after desalting procedure that removes imidazole and salt residues in the protein sample. The UV-Vis spectrum shows a characteristic metaquo ( $\text{HbIH}_2\text{O}$ ) Soret band at 407 nm. Figure 3.3 (B) shows a UV-Vis chromatogram of the size exclusion chromatography purification process for rHbI PheB10Tyr mutant. The elution profile clearly presents an intense single peak at 250 ml that evidences a purified protein after three purification processes, a former cobalt ( $\text{Co}^{+2}$ ) affinity chromatography, Hi-trap desalting, and a final size exclusion fast performance liquid chromatography. The same purification process was performed for the rHbI samples protein. After each purification process a UV-Vis spectrum was obtained to verify and confirm the integrity of the samples.

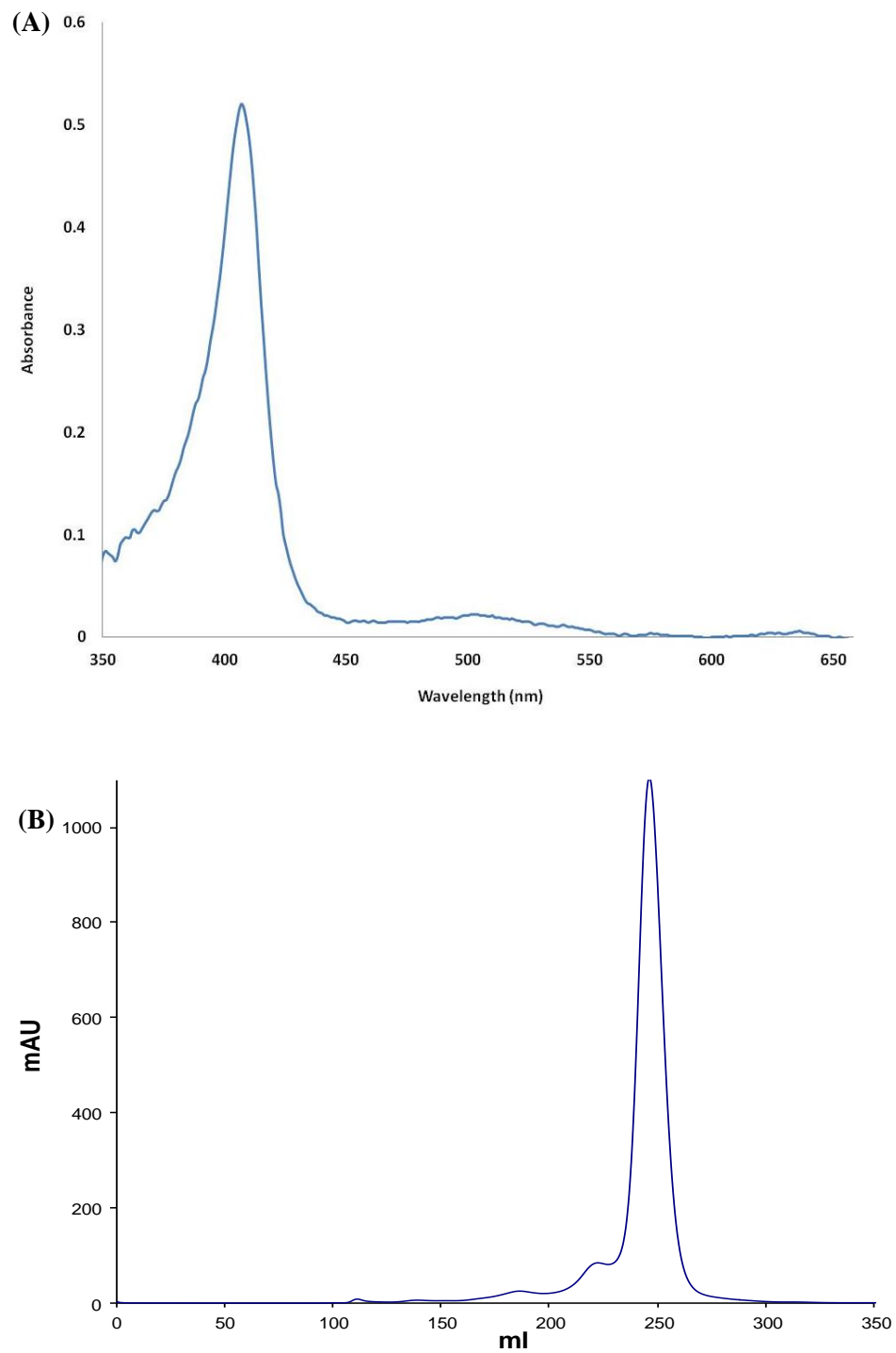


**Figure 3.3: Optical spectra of the rHbI PheB10Tyr mutant purification: (A) UV-Vis spectrum after desalting procedure and (B) Elution profile chromatogram after size exclusion chromatography.**

The following Nuclear Magnetic Resonance (NMR) results show a structural characterization of the heme group and distal site of *Lucina pectinata* Hemoglobin I (rHbICN, rHbICN PheB10Tyr and rHbIH<sub>2</sub>S) moieties.

### **3.3 Characterization of heme prosthetic group in rHbI and rHbI PheB10Tyr mutant cyanide complex**

This NMR spectroscopic characterization contributes to understanding how relevant is the B10 position in the amino acids sequence of invertebrate hemoglobin from *L. pectinata* and others hemoproteins for their environmental adaptation.

#### *3.3.1 One dimensional (1D) Pulse Sequences: <sup>1</sup>H-NMR Experiments*

##### *3.3.1.1 Water solvent suppression heme group data*

Figure 3.4 (A) shows a <sup>1</sup>H-NMR reference spectrum of the rHbICN in <sup>1</sup>H<sub>2</sub>O at 25 °C and pH 7.00. An intense diamagnetic envelope between 10.00 to -1.00 ppm from the outside protons in the globin is observed. The <sup>1</sup>H-NMR resonance lines of the heme-bound CN in the rHbI were observed in the downfield region (10.00 to 26.00 ppm) and upfield region (-1.00 to -8.00 ppm). These resonance lines were assigned to the degree possible, as limited by diamagnetic spectral congestion and paramagnetic relaxation for the hemeprotein. However, this spectrum clearly shows an effective suppression of the diamagnetic envelope. The pattern of heme chemical shifts is similar to that observed in wild-type hemoglobin I (wtHbI) (not shown) [Nguyen et al., 1998; Ramos-Santana, 2003]. This result indicate that the rHbI conserve the nature of the porphyrin in the heme pocket similar to wtHbI. Figure 3.4 (B) shows an expansion of the downfield region illustrating the resonance lines assigned to methyls, vinyl and propionate protons from the heme, 5-CH<sub>3</sub>, 1-CH<sub>3</sub>, 6-H<sub>α</sub>', 2-H<sub>α</sub> at 24.97, 17.54, 17.25, and 17.07 ppm,

respectively. Figure 3.4 (C) shows an expansion of the upfield region illustrating the 2-vinyl group resonance lines assigned to 2-H<sub>βt</sub> and 2-H<sub>βc</sub> at -5.62 and -7.39 ppm, respectively.

A comparative analysis of the rHbICN and rHbICN PheB10Tyr mutant <sup>1</sup>H-NMR spectra were performed to elucidate the structural difference between them. Figure 3.5 (A-B) shows the downfield and upfield hyperfine shifted portions of the <sup>1</sup>H-NMR spectra of (A) rHbI and (B) rHbI PheB10Tyr mutant in cyanide derivative. The heme resonance lines in the mutant shifts slightly downfield comparative to the rHbI resonance lines with an increase of resolution and high intensity of the signals. These heme hyperfine shifts patterns have been reported for hemoproteins active in both diamagnetic and paramagnetic region, specifically in six coordinated heme complexes with low spin, Fe(III) oxidation, and ½ spin state configuration [La Mar et al., 2000]. The pattern of heme chemical shifts observed here is similar to that observed for wild-type *Lucina pectinata* HbICN and rHbICN with some significant differences in the propionate and vinyl regions [Nguyen et al., 1998; Cerda-Colón et al., 1998; Ramos-Santana et al., 2012]. Table 3.3 shows an overview of the chemical shifts ( $\delta_{\text{obs}}$ ) assigned to the heme protons including difference observed ( $\Delta_{\delta_{\text{obs}}}$ ) between rHbICN and rHbICN PheB10Tyr mutant. The main difference between the rHbICN PheB10Tyr and the rHbICN spectra is that for the former the 6-H<sub>α</sub>' propionate peak appears as a downfield peak at 19.90 ppm, while for the latter this is a upfield peak present at 17.25 ppm. Likewise, the 2-H<sub>α</sub> vinyl peak for rHbICN PheB10Tyr appears very downfield shifted at 19.40 ppm while for rHbICN this is an upfield peak present at 17.07 ppm. These results indicated that the heme environment between rHbICN and rHbICN PheB10Tyr mutant were affected for the single substitution of Phe by Tyr at the B10 position.

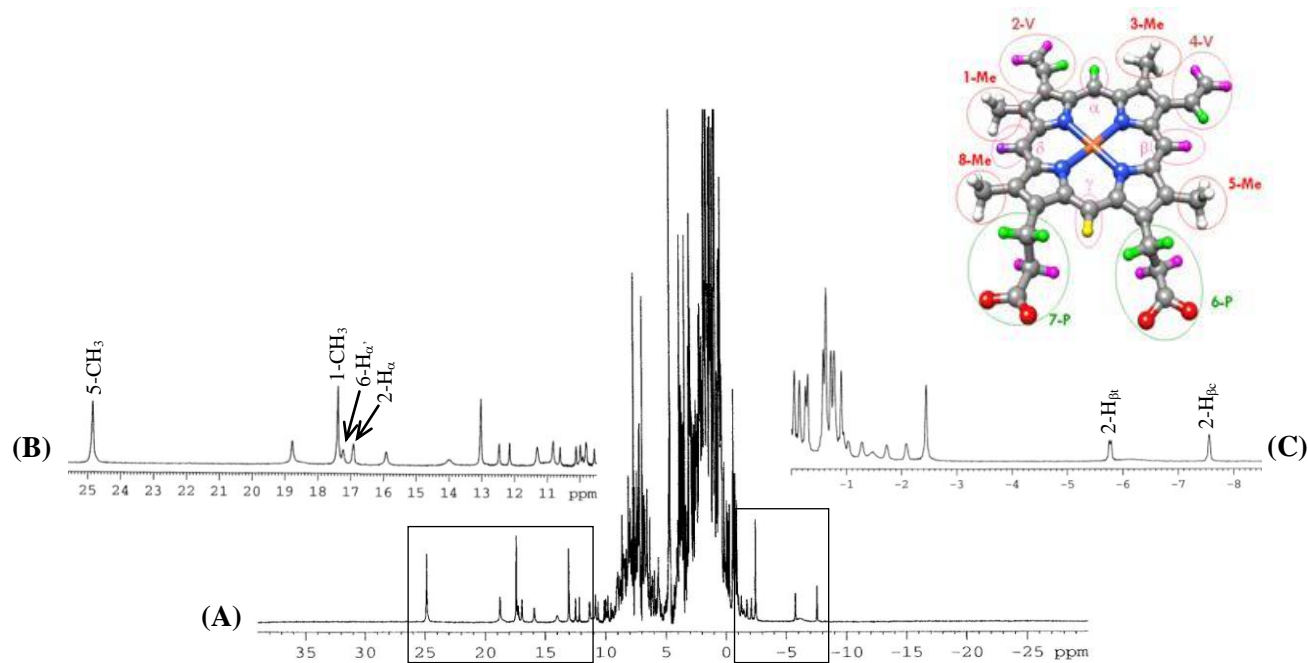


**Figure 3.4:** 600 MHz  $^1\text{H}$ -NMR of the paramagnetic shifted regions of rHbICN complex in  $^1\text{H}_2\text{O}$  at 25°C and pH 7.00: (A) reference spectrum, (B) downfield region (10.00 to 26.00 ppm) and (C) upfield region (-1.00 to -8.00ppm). The heme signals were labeled in Fisher Notation (i.e. 1- $\text{CH}_3$ , 6 $\text{H}_a$ ). Inset illustrated a schematic representation of the heme group.

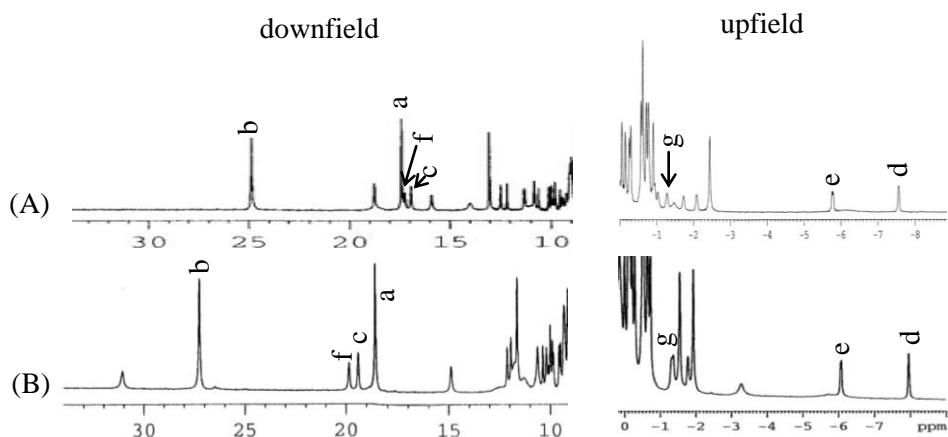


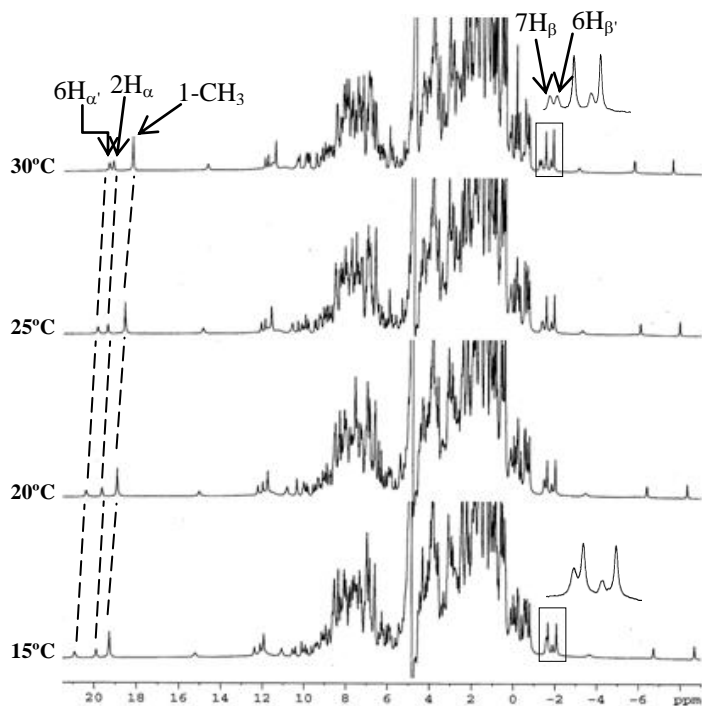
**Figure 3.5:** Downfield (left) and upfield (right) hyperfine shifted regions of the  $^1\text{H}$ -NMR spectra of (A) rHbICN and (B) rHbICN PheB10Tyr mutant in  $^1\text{H}_2\text{O}$  at  $25^\circ\text{C}$  and pH 7.00. The heme signals were labeled with alphabetic letters according to table 3.2.

**Table 3.3:**  $^1\text{H}$ -NMR chemical shifts of the methyl, vinyl and propionate heme group for rHbICN and rHbICN PheB10Tyr mutant as showed in the Figure 3.5

Peak label	Heme protons	$\delta_{\text{obs}}$ (ppm)		$\Delta\delta_{\text{obs}}$ (ppm)
		rHbICN	rHbICN PheB10Tyr	$\delta_{\text{obs, rHbI}} - \delta_{\text{obs, rHbI mutant}}$
a	1- $\text{CH}_3$	17.54	18.60	1.06
b	5- $\text{CH}_3$	24.97	27.27	2.30
c	2- $\text{H}_\alpha$	17.07	19.40	2.33
d	2- $\text{H}_{\beta\text{c}}$	-7.39	-7.99	0.60
e	2- $\text{H}_{\beta\text{r}}$	-5.62	-6.10	0.48
f	6- $\text{H}_{\alpha'}$	17.25	19.90	2.65
g	6- $\text{H}_{\beta'}$	-1.20	-1.40	0.20

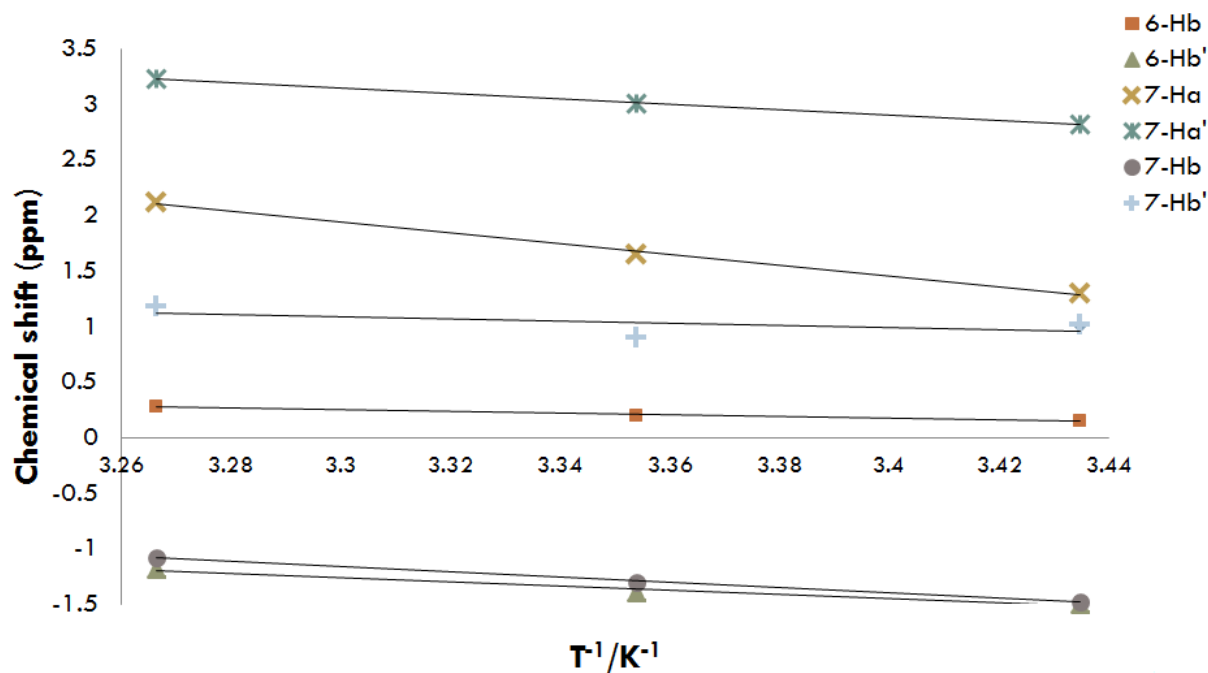
### 3.3.1.2 Variable Temperature (VT) spectra heme group data

Figure 3.6 show a  $^1\text{H-NMR}$  spectra of rHbICN PheB10Tyr mutant as a function of temperature in the range from 15 °C to 30 °C with increments of 5 °C between each spectrum. This variable temperature study facilitated the assignment of the hyperfine shifted resonances, as illustrated on the insets, under the diamagnetic envelope. The protons in the heme groups (methyl, propionate, and vinyl) are strongly dependent of temperature. The resonance lines from the 6- $\text{H}_\alpha$ , 2- $\text{H}_\alpha$ , and 1- $\text{CH}_3$  observed in the downfield region increase resolution depending on low temperature. This behavior confirms the assignment of these heme protons at 19.90, 19.40, and 18.60 ppm, respectively. Furthermore, new manifold signals appear at higher temperature whose overlapping signals were exposed dramatically. The overlapping signals observed in the upfield region at 15 °C was splitting when the temperature increased was to 30 °C for the two high resolution resonance lines that are assigned to 7- $\text{H}_\beta$  and 6- $\text{H}_\beta$  at -1.30 and -1.40 ppm, respectively. As previously reported by Emerson and La Mar, the 6 and 7 propionate groups split and shift in different direction, such as, 6-H move to right and 7-H move to left in the upfield region compared with paramagnetic systems of several hemoproteins with standard Mb fold [Emerson et al., 1990, La Mar, 2000]. Figure 3.7 illustrated a Curie plot for the 6 and 7-propionate groups in the heme pocket of the rHbI PheB10Tyr mutant protein. This Curie relaxation behavior as observed is indicative that the low-spin ferrohemo protein strongly depends on the His/ $\text{CN}^-$  axial ligand interaction and the electron distribution of the iron in the heme pocket [La Mar, 2000]. The results are improved in the  $^1\text{H-NMR}$  spectra quality through large magnetic anisotropy reflecting resolved and narrower resonances lines.



**Figure 3.6: 500 MHz <sup>1</sup>H-NMR temperature dependence spectrum of rHbICN PheB10Tyr in <sup>1</sup>H<sub>2</sub>O at pH 7.00. The variable temperature spectrum was observed in the range of 15-30 °C with increments of 5 °C between each one. The overlapping signals are resolved for the propionate groups are illustrated in the upfield region, 0.00 to -4.00 ppm, at the temperature increase due to Curie relaxation. Labeled signals include heme signals in Fisher Notation (i.e. 6H<sub>α'</sub>)**

**$^1\text{H}$  shift versus reciprocal of absolute temperature for heme propionates groups**



**Figure 3.7:** Curie plot of propionate group chemical shifts versus reciprocal absolute temperature in  $^1\text{H}_2\text{O}$  at pH 7.00. Simulated temperature dependence, based on result obtained in variable temperature experiments, for six heme propionate group of the rHbI PheB10Tyr mutant protein. The shifts used are typical for heme with  $\phi \sim 0^\circ$ , 0.15 ppm (6-Hb), -1.50 ppm (6-Hb'), 1.30 ppm (7-Ha), 2.82 ppm (7-Ha'), -1.48 ppm (7-Hb), 1.02 ppm (7-Hb') at 18 °C, 0.20 ppm (6-Hb), -1.40 ppm (6-Hb'), 1.65 ppm (7-Ha), 3.00 ppm (7-Ha'), -1.30 ppm (7-Hb), 0.90 ppm (7-Hb') at 25 °C, and 0.28 ppm (6-Hb), -1.18 ppm (6-Hb'), 2.11 ppm (7-Ha), 3.23 ppm (7-Ha'), -1.08 ppm (7-Hb), 1.18 ppm (7-Hb') at 33 °C.

### 3.3.1.3 Inversion recovery heme group data : Non-selective $T_1$

Figure 3.8 shows the rHbICN PheB10Tyr inversion recovery spectra with a delay time ( $\tau$ ) set at 1ms to 400 ms. Reference spectrum with residual solvent presaturation collected with a repetition rate of  $1.0 \text{ s}^{-1}$  was used to show relative enhanced intensities for faster relaxing signals. The inversion recovery spectrum was collected under rapid pulsing conditions to selectively suppress slowly relaxing signals. Estimates of the nonselective paramagnetic relaxation times ( $T_1$ ) for resolved peaks have been determined by the following equation:

$$T_1 = \frac{t_{null}}{\ln 2} \quad (3.1)$$

Table 3.4 lists the values for the relaxed heme group protons of rHbICN PheB10Tyr at 25 °C and pH 7.0. The propionates 7- $H_\beta$  and 6- $H_\beta$  heme protons were determined at 30 °C. Analysis of paramagnetic  $T_1$  over 500 ms based on observed NOE's and/or NOESY crosspeaks. The long  $T_1$ s observed for rHbICN PheB10Tyr heme protons are similar to the same protoporphyrin systems in heme proteins model complexes. The resonances signals from 8- $\text{CH}_3$ , 3- $\text{CH}_3$ ,  $\alpha$ -meso,  $\beta$ -meso,  $\gamma$ -meso, and  $\delta$ -meso remain unassigned at this point where these peaks for Mb models are located inside in the upfield and downfield diamagnetic envelope.

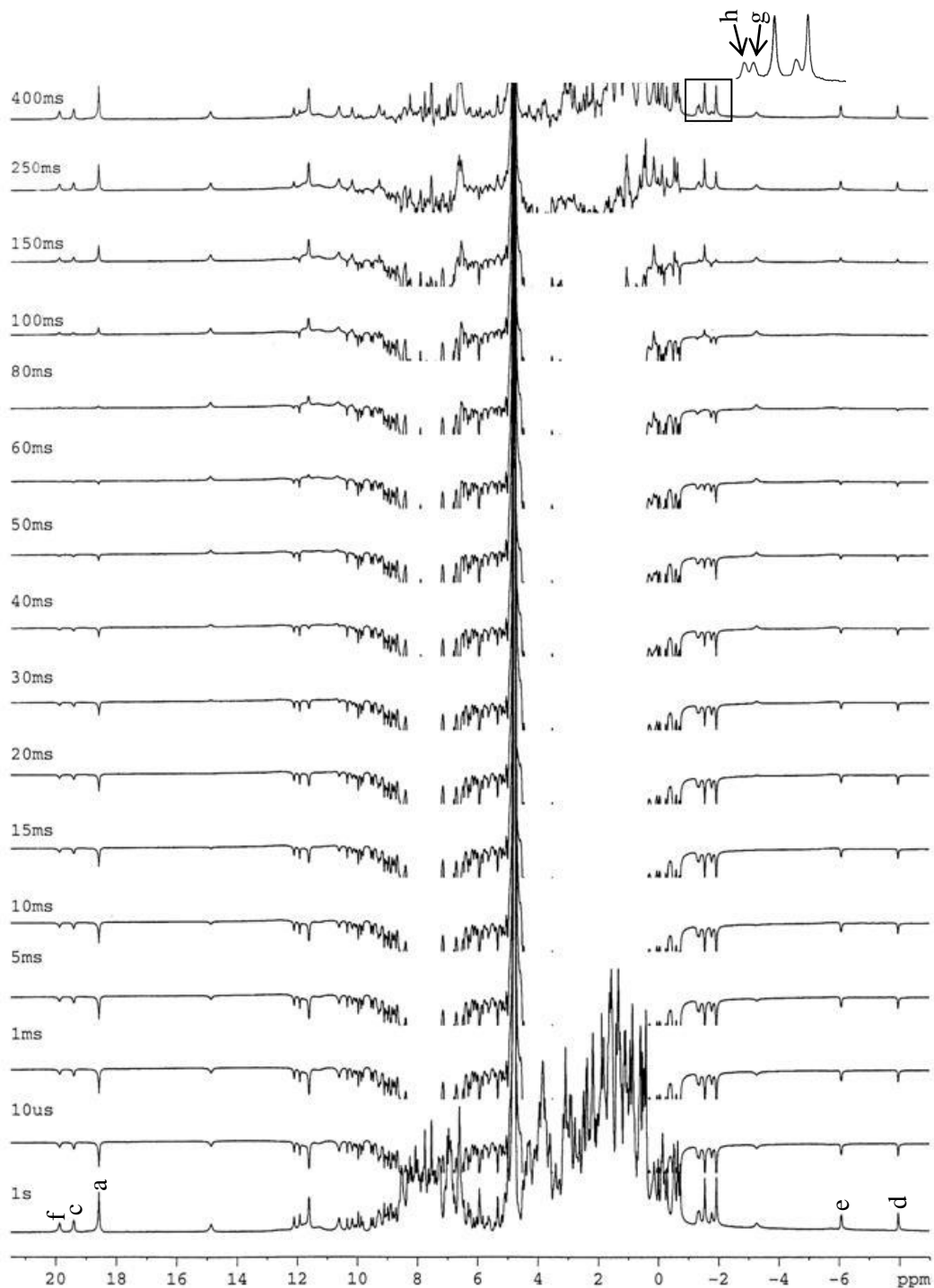


**Figure 3.8: 600MHz <sup>1</sup>H-NMR inversion-recovery spectra of rHbICN PheB10Tyr mutant in <sup>1</sup>H<sub>2</sub>O at pH 7.00, 25°C. The delay time (τ) was set at a different fixed value for each spectrum among 1ms to 400ms, as shown at the left-hand side of the spectrum. Labeled in the spectrum are relevant resonances from heme protons as peaks label listed in the table 3.3. Inset shows the propionate group signals at 30°C.**

**Table 3.4: Longitudinal spin-lattice relaxation time ( $T_1$ ) for strongly relaxed heme group protons of rHbICN PheB10Tyr mutant as showed in the Figure 3.8**

Peak label	Heme protons	$T_1$ (ms)
a	1-CH <sub>3</sub>	86.6
b	5-CH <sub>3</sub>	43.3
c	2-H <sub><math>\alpha</math></sub>	86.6
d	2-H <sub><math>\beta</math>c</sub>	144.3
e	2-H <sub><math>\beta</math><math>\tau</math></sub>	115.4
f	6-H <sub><math>\alpha'</math></sub>	115.4
g <sup>‡</sup>	6-H <sub><math>\beta'</math></sub>	180
h <sup>‡</sup>	7-H <sub><math>\beta</math></sub>	*

<sup>‡</sup> Determined at 30°C.

\* Not Calculated

### 3.3.1.4 1D steady-state nuclear Overhauser (NOE's) heme group data

The 1D NOE studies have been used to detect internal dipolar and mobility interaction in resolved heme protons. Figure 3.9 shows the steady-state NOEs to heme protons upon complete saturation of proton 5-CH<sub>3</sub> at 27.27 ppm. The saturation process affects the delocalized spin density ( $\rho$ ) of the 5-methyl engendering the NOE respect to the distance from the nucleus in paramagnetic hemoproteins [La Mar et al., 2000]. Also, the NOE pattern is strongly dependent of the T<sub>1</sub>. However, the steady-state NOE yields a time-independence of the relaxation to the proton that is saturated, but demands the determination of T<sub>1</sub> from others proton to detect the dipolar contact between them. Previously, the T<sub>1</sub> measures for the heme group were described after analysis of the inversion recovery data. The strong <sup>1</sup>H-<sup>1</sup>H dipolar NOE observed with the 5-methyl proton are 6-H<sub>α'</sub> at 19.90 ppm, 6-H<sub>β</sub> at 0.20 ppm, 6-H<sub>β'</sub> at -1.40 ppm, and β-meso at 2.50 ppm. Moreover, moderate NOEs were observed at 7.23 ppm and 5.56 ppm assigned to 6-H<sub>α</sub> and 4-vinyl H<sub>α</sub>, respectively. On the conserved globin fold, the 5-CH<sub>3</sub> group as well as the γ-meso protons are considered a probe to determine the heme orientation in the heme cavity [Xia et al., 1999]. The strong NOE detected at 6.60 ppm is characteristic of the <sup>1</sup>H-<sup>1</sup>H dipolar contact between the 5-CH<sub>3</sub> and the conserved PheCD1<sub>δ</sub> amino acid residue. This NOE defined the close proximity ( $R < 7.0\text{\AA}$ ) of the 5-CH<sub>3</sub> heme group to the PheCD1 amino acid residue located in the coil of the secondary structure moiety. Table 3.5 summarizes the majors NOE's upon saturation of the 5-CH<sub>3</sub> at 25 °C and 33 °C temperature. Meanwhile, the γ-meso assigned at 5.15 ppm have NOE's with 6-H<sub>α</sub> at 7.50 ppm, 6-H<sub>α'</sub> at 19.09 ppm, 6-H<sub>β</sub> at 0.28 ppm, 6-H<sub>β'</sub> at -1.18 ppm, and 7-H<sub>β</sub> at -1.08 ppm. These NOE's provides evidence about the unambiguously assigned resonance lines from the propionate groups in the heme pocket.

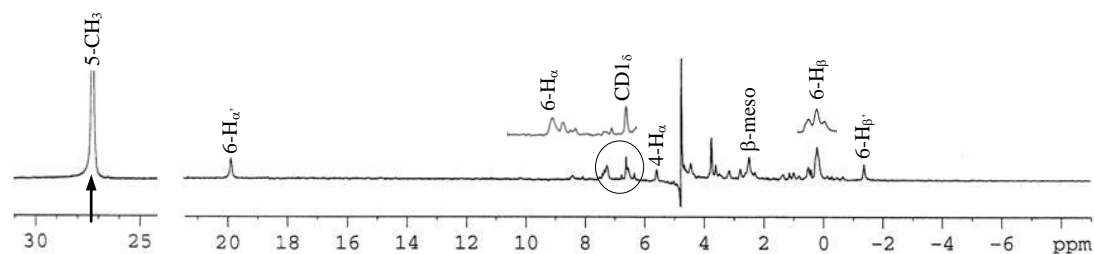


**Figure 3.9:** 600 MHz  $^1\text{H}$ -NMR steady-state NOE spectrum of the rHbICN PheB10Tyr mutant in  $^1\text{H}_2\text{O}$  at pH 7.00, 25 °C. The insert illustrates the position of the on-resonance saturation in 5- $\text{CH}_3$  proton at 27.27 ppm, as indicated with an arrow. The majors NOE with the 5- $\text{CH}_3$  proton were labeled in the spectrum with Fisher notation. The expanded windows show three resolved NOE after resolution enhancement at 33 °C.

**Table 3.5:**  $^1\text{H}$ -NMR chemical shifts of the major NOE upon saturation of the downfield 5- $\text{CH}_3$  proton at 27.27 ppm in the rHbICN PheB10Tyr mutant at different temperature.

Protons	$\delta_{\text{obs}}$ , ppm		Strengthen
	25°C	33°C	
6- $\text{H}_{\alpha'}$	19.90	19.09	Strong
6- $\text{H}_{\alpha}$	7.23	7.50	Moderate
CD1 $_{\delta}$	6.60	6.63	Strong
4- $\text{H}_{\alpha}$	5.56	5.91	Moderate
$\beta$ -meso	2.50	†	Strong
6- $\text{H}_{\beta}$	0.20	0.28	Strong
6- $\text{H}_{\beta'}$	-1.40	-1.18	Strong

† not assigned at 33°C.

Previous, NMR based approaches have been developed to characterize the heme group in the rHbI and rHbI PheB10Tyr single point mutation in the cyanide complex from the invertebrate *Lucina pectinata*. A direct approach was used as a main technique to detect and assign the hyperfine-shifted resonance lines in the  $^1\text{H}$ -NMR spectra. A summary of the heme assignments, chemical shifts at 18°C, 25°C, and 33°C and  $T_1$  values are listed in Table 3.6. Figure 3.10 show a schematic representation of the heme pocket structure of rHbI PheB10Tyr with face-on view from the proximal side illustrating the heme pocket dipolar contacts. The heme substituents are labeled Me (methyl), V (vinyl), and P (propionate). The solid, dashed and dashed-dots arrows represent strong, moderate and weak residue-heme dipolar contacts, respectively.

**Table 3.6: Heme resonance assignments in *Lucina pectinata* rHb1CN and rHb1CN PheB10Tyr mutant proteins**

rHb1CN PheB10Tyr					rHb1CN	
Heme Protons	$\delta_{\text{obs}}$ , ppm				Major NOEs	$\delta_{\text{obs}}$ , ppm ( $T_1$ , ms)
	18 °C	25 °C	33 °C	$T_1$ , ms		25 °C
1-Me	19.08	18.60	18.05	86.6	2-V, E14, E15, E11 $_{\alpha}$	17.54 (146)
3-Me	6.36	6.38	‡	‡	G5, G8 $_{\beta}$	5.64
5-Me	28.14	27.27	26.32	43.3	6-P, 4-H $_{\alpha}$ , CD1 $_{\delta}$	24.97 (96)
8-Me	‡	7.72	8.05	‡	7-H $_{\beta}$ , $\delta$ -meso-H, E14 $_{\alpha}$ , E11 $_{\alpha}$	8.25
2-H $_{\alpha}$	19.76	19.40	19.05	86.6	1-Me, G8	17.07 (138)
2-H $_{\beta c}$	‡	-7.99	‡	144.3	1-Me, 2-H $_{\beta t}$	-7.39 (137)
2-H $^{\beta t}$	‡	-6.10	‡	115.4	1-Me, 2-H $_{\beta c}$	-5.62 (120)
4-H $_{\alpha}$	‡	5.56	5.91	‡	5-Me	5.76
4-H $_{\beta c}$	‡	-0.66	-0.51	‡	$\beta$ -meso-H	-0.96
4-H $_{\beta t}$	‡	-0.47	-0.32	‡	$\beta$ -meso-H	-0.71
6-H $_{\alpha}$	‡	7.23	7.50	‡	5-Me, $\gamma$ -meso	5.70
6-H $_{\alpha'}$	20.60	19.90	19.09	115.4	5-Me, 6-H $_{\beta'}$ , $\gamma$ -meso	17.25 (167)
6-H $_{\beta}$	0.15	0.20	0.28	‡	5-Me, 6-H $_{\beta'}$ , E7 $_{\epsilon}$	0.13
6-H $_{\beta'}$	-1.50	-1.40	-1.18	180	5-Me, 6-H $_{\beta}$ , E7 $_{\epsilon}$	-1.2 (173)
7-H $_{\alpha}$	1.30	1.65	2.11	‡	7-H $_{\beta}$	0.94
7-H $_{\alpha'}$	2.82	3.00	3.23	‡	7-H $_{\beta}$	2.08
7-H $_{\beta}$	-1.48	-1.30	-1.08	‡	8-Me, 6-H $_{\beta'}$ , 6-H $_{\alpha}$	-1.65 (260)
7-H $_{\beta'}$	1.02	0.90	1.18	‡	7-H $_{\beta}$	0.80
$\alpha$ -meso-H	‡	2.10	2.39	‡	2-H $_{\alpha}$	2.51
$\beta$ -meso-H	‡	2.50	‡	‡	4-V	1.68
$\gamma$ -meso-H	4.57	4.85	5.15	‡	E7 $_{\epsilon}$	4.26
$\delta$ -meso-H	‡	3.98	4.25	‡	1-Me, 8-Me	3.25

‡ not assigned to the temperature.

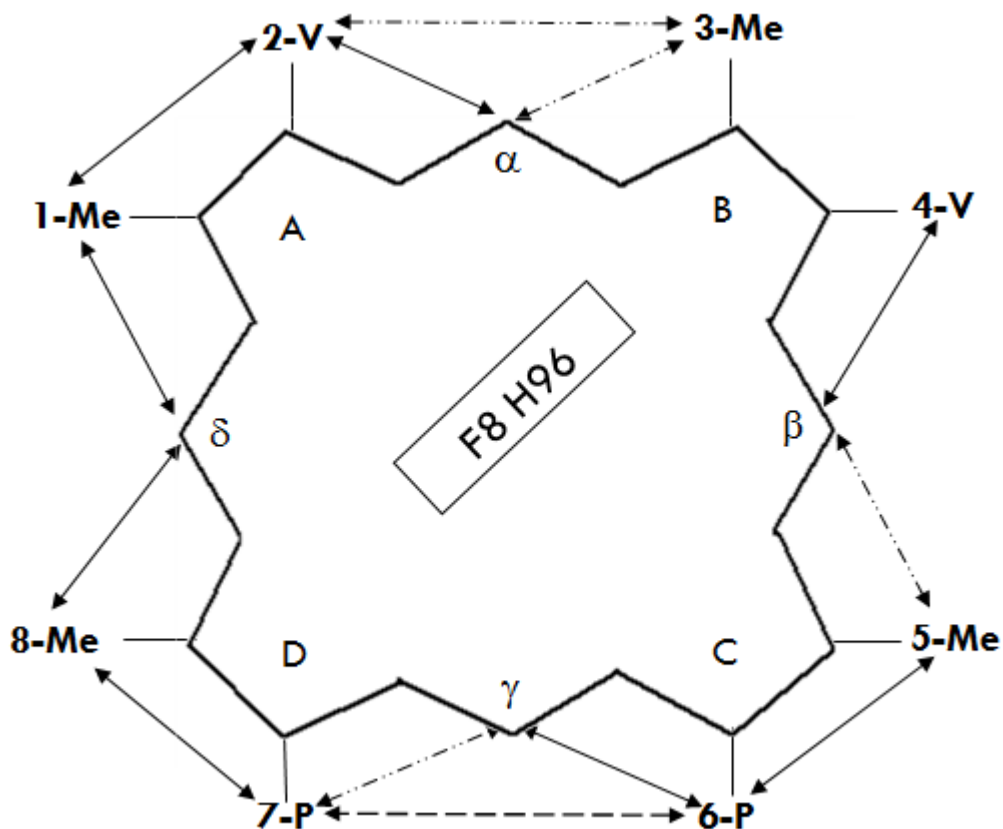


Figure 3.10: Schematic representation of the heme pocket structure of rHbI PheB10Tyr with face-on view from the proximal side illustrating the heme pocket dipolar contacts. The heme substituents are labeled Me (methyl), V (vinyl), and P (propionate). The solid ( $\longleftrightarrow$ ), dashed ( $\leftarrow\rightarrow$ ), and dashed-dots ( $\leftarrow\cdots\rightarrow$ ) arrows represent strong, moderate and weak residue-heme dipolar contacts, respectively.

### **3.4 Characterization of distal amino acids in rHbI and rHbI PheB10Tyr mutant cyanide complex**

#### *3.4.1 One dimensional (1D) Pulse Sequences: <sup>1</sup>H-NMR Experiments*

##### *3.4.1.1 Variable Temperature (VT) spectra amino acid data*

The variable temperature studies allowed detection of overlapping signals under the diamagnetic and paramagnetic envelope. Figure 3.11 shows a <sup>1</sup>H-NMR spectral window from 10.00 ppm to 13.00 ppm for the rHbICN PheB10Tyr mutant in <sup>1</sup>H<sub>2</sub>O at pH 7.00. The first NMR approach to start the amino acid sequence is assignment to assign the proton from the proximal HisF8 conserved in hemoprotein globins. Usually, the HisF8 protons are found in the paramagnetic region between 10.00 ppm to 15.00 ppm. New broadbands with low intensity resonance lines are detected exhibiting significant proton chemical shifts as the temperature is increase from 15 °C to 30 °C. The chemical shifts are observed in the spectra at 11.78, 11.53, 11.30, 10.35, and 10.25 ppm. These resonance signals are characterized using WEFT, NOE, NH/OH exchangeable proton, NOESY and TOCSY data as described in the following sections.

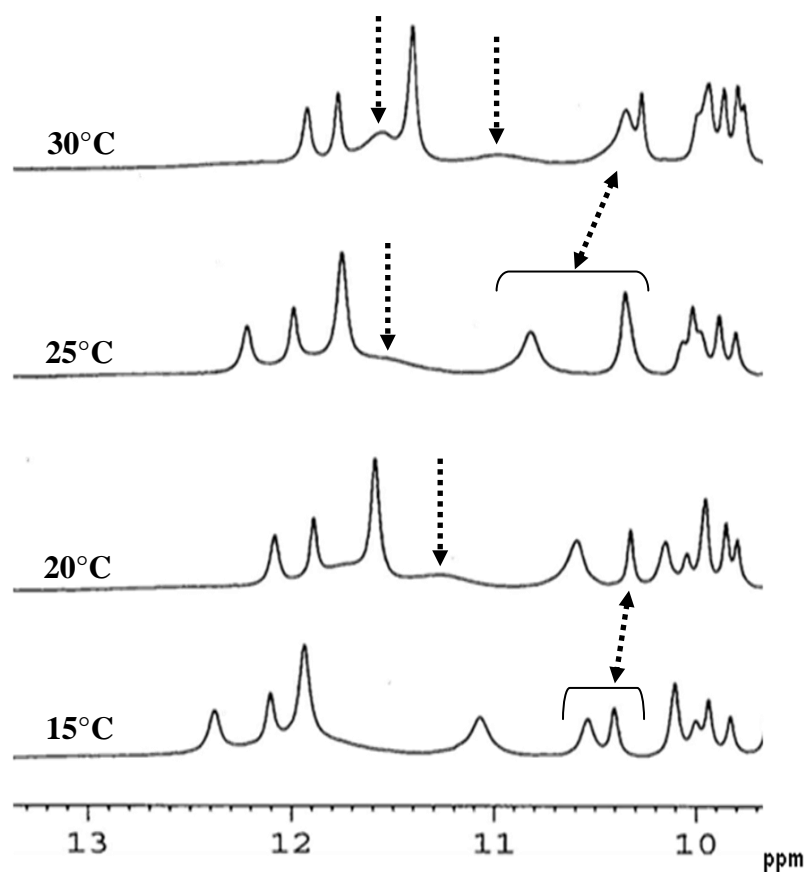


**Figure 3.11:** 500 MHz  $^1\text{H}$ -NMR spectra portion of the variable temperature spectral window (10.00 to 13.00 ppm), of the rHbICN PheB10Tyr mutant in  $^1\text{H}_2\text{O}$  at pH 7.00. The temperature dependence spectra were observed in the range of 15-30 °C with 5 °C increments between each spectrum. Arrows indicate the overlapping signals in the spectra.

### 3.4.1.2 Water Eliminated Fourier Transform (WEFT) amino acid data

Figure 3.12 shows a  $^1\text{H}$ -NMR inversion-recovery spectra called WEFT of rHb1CN PheB10Tyr mutant in  $^1\text{H}_2\text{O}$  at pH 7.00 and 25 °C. The delay time ( $\tau$ ) between the composite 180 ° and 90 ° pulses were (A) 20 ms, (B) 40 ms, (C) 60 ms, and (D) 80 ms. The spectra reveal the presence of multiple moderately relaxed signals with  $T_{1s}$  approximately at 20ms to 60ms. Clear visualization of several broadest and stronger resonances lines are assigned to the proximal histidine (HisF8) and distal glutamine (GlnE7) side chains protons. The hyperfine-chemical shifts for HisF8 were assigned to  $N_{\delta 1}\text{H}$ ,  $N_{\rho}\text{H}$ , and  $C_{\epsilon 1}\text{H}$  at 14.86, 12.10, and -5.86 ppm, respectively. Meanwhile, the hyperfine-chemical shifts for GlnE7 were assigned to  $N_{\epsilon 1}\text{H}$  at 10.66 ppm and  $N_{\epsilon 2}\text{H}$  at -3.27 ppm. These proximal and distal residues were identified in the spectrum by red and blue arrows, respectively.

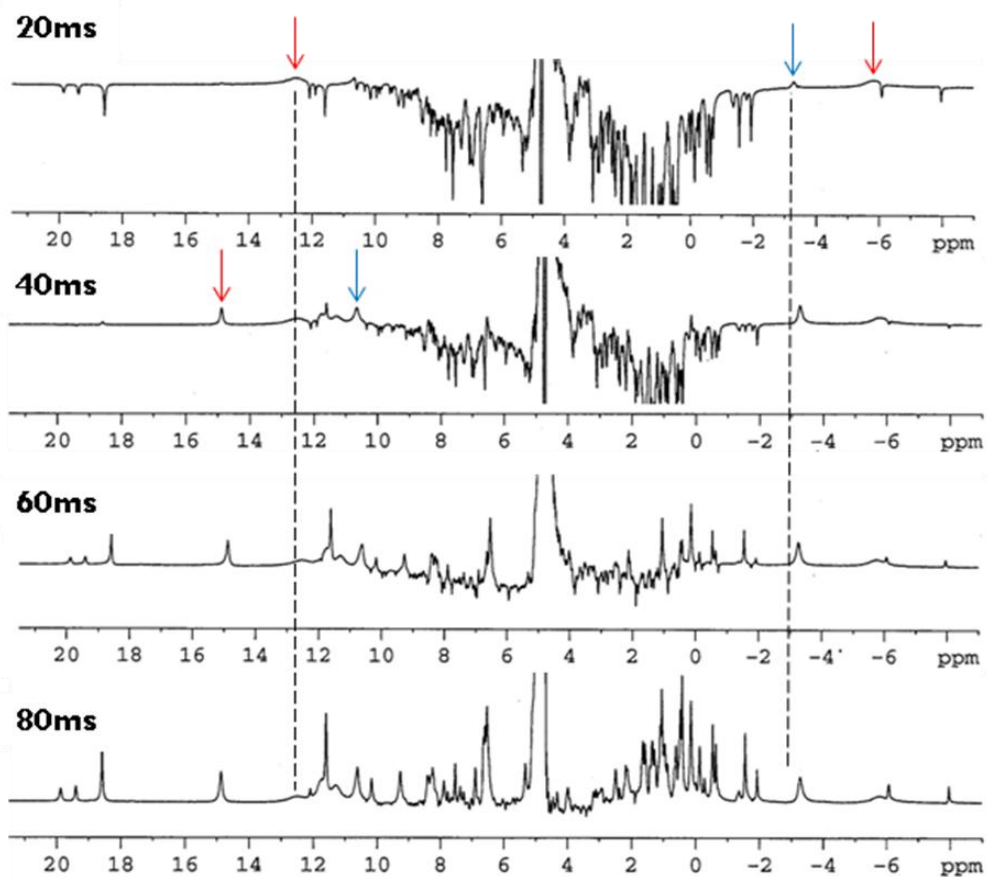


**Figure 3.12:**  $^1\text{H}$ -NMR inversion-recovery spectra (WEFT) of rHbICN PheB10Tyr mutant in  $^1\text{H}_2\text{O}$  at  $25^\circ\text{C}$  and pH 7.00. The proximal and distal residues resonances signals were identified with red and blue arrows, respectively.

### 3.4.1.3 Inversion recovery amino acid data: Non-selective $T_1$

Figure 3.13 shows the rHbICN PheB10Tyr inversion recovery spectra with a delay time ( $\tau$ ) set at 0.5 ms to 100 ms to detect the nuclei with rapid nuclear relaxation behavior ( $< 100$  ms) as NH and OH protons. Reference spectrum collected with a repetition rate of two per second ( $2.0 \text{ s}^{-1}$ ) with a carrier at 30.00 ppm. The inversion recovery spectrum was collected under slow pulsing conditions to selectively eliminate rapid relaxing signals. Estimates of the nonselective paramagnetic relaxation times ( $T_1$ ) for resolved peaks have been determined by the equation 3.1 as described for the heme prosthetic group relaxation times ( $T_1$ ).

The strongly relaxed amino acids protons from residues with distances from the iron at  $R_{\text{Fe}} < 6.0 \text{ \AA}$  have long relaxation time ( $T_1$ ) values for TyrB10  $\text{OH}_\eta$  and HisF8  $\text{N}_{\delta 1}\text{H}$ . The  $T_1$  value for the resonance signal from the GlnE7  $\text{N}_{\epsilon 1}\text{H}$  is observed (not shown). Amino acids closet to the iron ( $R_{\text{Fe}} < 3.4 \text{ \AA}$ ) have short  $T_1$ s ( $\sim 4.0$  ms). It is important to remember that the proton further from the iron ( $R_{\text{Fe}} > 7.0 \text{ \AA}$ ) will not be dominated by paramagnetic effects [Emerson et al., 1990]. Analysis of paramagnetic  $T_1$  over 100 ms for amino acids residues are based on observed 1D NOE, 2D NOESY, and/or 2D TOCSY cross-peaks. The internal motion of the distal amino acid residues is monitored by nuclear spin relaxation measurements ( $T_1$ s) as described. It turns out that protein mobility in solution is non-uniform, with large structural determinants responsible of the protein orientation and dynamics. The nuclear spin relaxation factor suggests a correlation between the side chains of the amino acid and the functional aspects of the rHbI from *Lucina pectinata* as confirmed at the end.

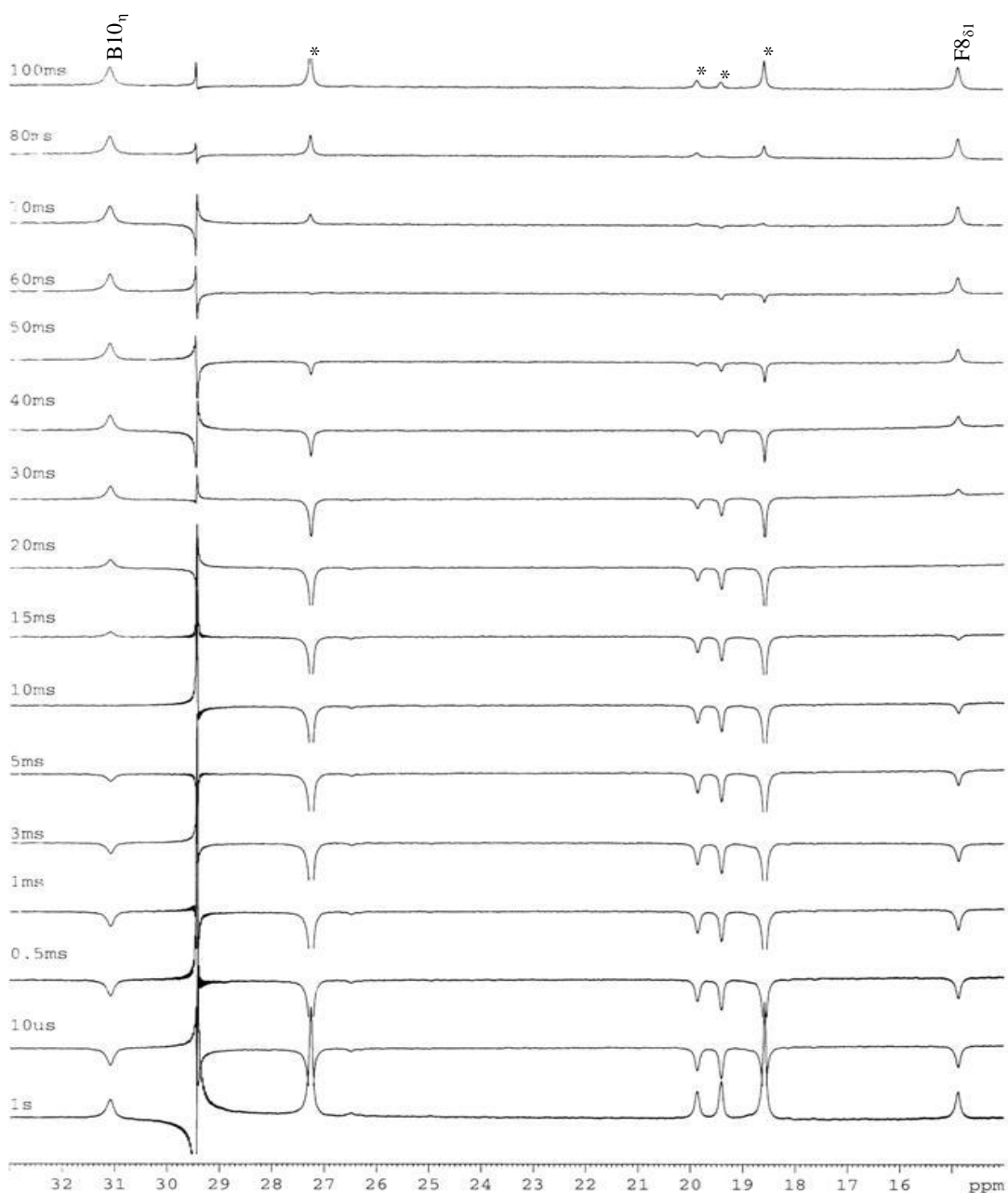


**Figure 3.13: 600 MHz  $^1\text{H}$ -NMR inversion-recovery spectra of rHbICN PheB10Tyr mutant in  $^1\text{H}_2\text{O}$  at 25 °C and pH 7.00. The delay time ( $\tau$ ) was set at a different fixed value for each spectrum among 0.5 to 100 ms, as shown at the left-hand side of the spectrum. The relaxation time was two per second (2/s) with a carrier at 30.00 ppm. Labeled in the spectrum are relevant resonances from amino acids protons as peaks label using helix sequence position. The asterisks represent resonance lines from heme groups as described in previous sections.**

#### 3.4.1.4 1D steady-state nuclear Overhauser (NOE's) amino acid data

The 1D NOE studies have been used to detect internal dipolar interaction and structural orientation in resolved amino acid residues in the distal heme pocket. Figure 3.14 shows the 1D steady-state NOEs upon complete saturation of proton TyrB10 OH<sub>η</sub> at 31.00 ppm. The saturation process affects the delocalized spin density ( $\rho$ ) of the TyrB10 OH<sub>η</sub> engendering the NOE respect to the distance from the nucleus. Also, the NOE pattern is strongly dependent on the amino acids spin-relaxation time ( $T_1$ ). Previously, the  $T_1$  measures for amino acid residues were described after analysis of the inversion recovery data. The strong  $^1\text{H}$ - $^1\text{H}$  dipolar NOEs observed with the TyrB10 OH<sub>η</sub> proton are TyrB10 C<sub>ε</sub>H at 11.60 ppm, TyrB10 C<sub>δ</sub>H at 8.24 ppm, PheE11 C<sub>β2</sub>H at 7.36 ppm, GlnE7 C<sub>γ1</sub>H at 6.46 ppm, AlaE8 C<sub>α</sub>H at 6.25 ppm, and PheE11 C<sub>β1</sub>H at 5.33 ppm. Moreover, a moderate NOE was observed at 4.31 ppm assigned to GlnE7 C<sub>γ2</sub>H. The intensity of each NOE's is in accordance with to the cross peaks observed in the 2D NOESY map. Table 3.7 summaries the majors NOE's upon saturation of the TyrB10 OH<sub>η</sub> at 25 °C and 33 °C temperature. Significantly, no NOE to GlnE7N<sub>ε1</sub>H and GlnE7N<sub>ε2</sub>H were observed in the spectrum, showing strong decoupling among these protons. Figure 3.15 shows the 1D steady-state NOEs upon complete saturation of proton GlnE7 N<sub>ε2</sub>H at -3.27 ppm. The saturation process affects the delocalized spin density ( $\rho$ ) of the GlnE7 N<sub>ε2</sub>H engendering the NOE respect to the distance from the nucleus. The strong  $^1\text{H}$ - $^1\text{H}$  dipolar NOEs observed with the GlnE7 N<sub>ε2</sub>H proton are GlnE7 N<sub>ε1</sub>H at 10.66 ppm, GlnE7 C<sub>γ1</sub>H at 6.46 ppm, GlnE7 C<sub>β1</sub>H at 2.90 ppm, and 6-H<sub>β</sub>' at -1.40 ppm. Moreover, moderate NOEs were observed at 4.31, 5.15 (30 °C), and 0.20 ppm assigned to GlnE7 C<sub>γ2</sub>H,  $\gamma$ -meso and 6-H<sub>β</sub>, respectively. The intensity of each NOE is in according to the cross peaks observed in the 2D NOESY map. Table 3.8 summaries the majors NOE's upon saturation of the GlnE7 N<sub>ε2</sub>H at 25 °C and 33 °C temperature.

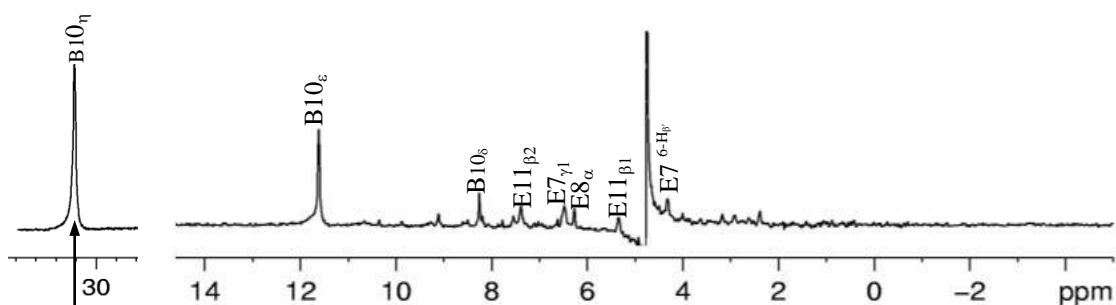


**Figure 3.14: 600 MHz  $^1\text{H}$ -NMR steady-state NOE spectrum of rHbICN PheB10Tyr mutant in  $^1\text{H}_2\text{O}$  at 25 °C and pH 7.00. Insert illustrates the position of the on-resonance saturation in the TyrB10  $\text{OH}_\eta$  proton at 31.00 ppm, as indicated with an arrow. The major NOE's with the TyrB10  $\text{OH}_\eta$  proton were labeled in the spectrum using the helix sequence position.**

**Table 3.7:  $^1\text{H}$ -NMR chemical shifts of the major NOE upon saturation of the TyrB10  $\text{OH}_\eta$  proton at 31.00 ppm in the rHbICN PheB10Tyr mutant at different temperatures.**

Residues	Peak label	$\delta_{\text{obs}}$ , ppm		Strength
		(25°C)	(33°C)	
TyrB10	B10 $_\epsilon$	11.60	11.38	Strong
TyrB10	B10 $_\delta$	8.24	8.17	Strong
PheE11	E11 $_{\beta 2}$	7.36	7.20	Strong
GlnE7	E11 $_{\gamma 1}$	6.46	6.26	Strong
AlaE8	E8 $_\alpha$	6.25	6.20	Strong
PheE11	E11 $_{\beta 1}$	5.33	5.25	Strong
GlnE7	E11 $_{\gamma 2}$	4.31	4.18	Moderate

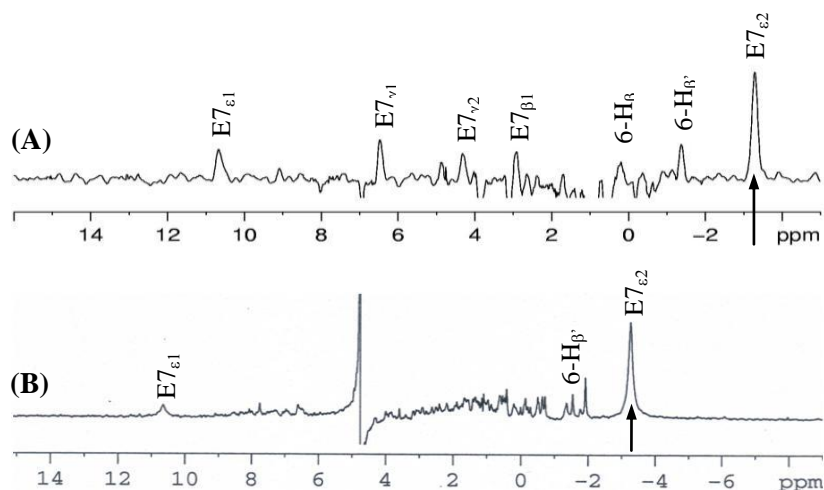


**Figure 3.15:** 600 MHz  $^1\text{H}$ -NMR of rHbICN PheB10Tyr mutant in  $^1\text{H}_2\text{O}$  at 25 °C and pH 7.0: (A) 2D NOESY slice and (B) steady-state NOE spectra showed the NOE's to GlnE7  $\text{N}_{\epsilon 2}\text{H}$  at -3.27 ppm. The position of the on-resonance saturation is indicated with an arrow. The majors NOEs with the GlnE7  $\text{N}_{\epsilon 2}\text{H}$  proton were identified in the spectra using the helix sequence position.

**Table 3.8:**  $^1\text{H}$ -NMR chemical shifts of the major NOE upon saturation of the GlnE7  $\text{N}_{\epsilon 2}\text{H}$  at -3.27 ppm in the rHbICN PheB10Tyr mutant at different temperatures.

Residues	Peak label	$\delta_{\text{obs}}$ , ppm		Strength
		(25°C)	(33°C)	
GlnE7	$\text{E7}_{\epsilon 1}$	10.66	10.35	Strong
GlnE7	$\text{E7}_{\gamma 1}$	6.46	6.26	Strong
GlnE7	$\text{E7}_{\gamma 2}$	4.31	4.18	Moderate
GlnE7	$\text{E7}_{\beta 1}$	2.90	2.88	Strong
-----	$\gamma$ -meso	‡	5.15	Moderate
-----	$6\text{-H}_{\beta}$	0.20	0.28	Moderate
-----	$6\text{-H}_{\beta}'$	-1.40	-1.18	Strong

‡ not assigned at 25°C.

### 3.4.2 Two dimensional (2D) Pulse Sequences: $^1\text{H-NMR}$ Experiments

#### 3.4.2.1 NOESY and TOCSY amino acid data

Several strong NOESY cross peaks are exhibited in the dipolar map of the rHbICN PheB10Tyr mutant. Figure 3.16 shows the NOESY map for the rHbICN PheB10Tyr mutant in  $^1\text{H}_2\text{O}$  at 25 °C and pH 7.00. The NOESY map reveals cross peaks between the low-field hyperfine-shifted resonances at 6.00 to 12.50 ppm and the diamagnetic window from 13.00 to 2.00 ppm. This diagonal portion of the NOESY map showed in part A is combined with the up-field of -3.00 ppm in the right portion part B of the Figure 3.16. The peaks were identify using the one letter standard labeling according to the amino acid sequences. The NOESY cross peaks pattern are observed between the distal amino acids TyrB10 (Y29), GlnE7 (Q64), and PheE11 (F68). The assignment of individual residues are considered using both NOESY and TOCSY data, first confirming earlier assignments and then extending them to unassigned protons. The NOESY map exhibit the dipolar contacts between the intra-residual amino acids allowing develop the sequential spin system by the sequence-specific resonance method. The portion A shows the dipolar chemical shifts for the TyrB10 (Y29) side chain protons at 8.22 and 11.60 ppm assigned to  $\text{C}_\delta\text{H}$  at and  $\text{C}_\epsilon\text{H}$ , respectively. Similarly, dipolar chemical shifts for the PheE11 (F68) side chain protons were observed at 9.09 ppm and  $\text{N}_\beta\text{H}$  at 6.52 ppm and  $\text{C}_\zeta\text{H}$  at 7.53 ppm. The portion B shows 2D NOE slice at -3.00 ppm assigned to GlnE7 (Q64)  $\text{N}_{\epsilon 2}\text{H}$  including dipolar contacts with 10.66, 6.46, 4.31, and 2.90 ppm cross-peaks assigned to GlnE7 (Q64)  $\text{N}_{\epsilon 1}\text{H}$ ,  $\text{C}_{\gamma 1}\text{H}$ ,  $\text{C}_{\gamma 2}\text{H}$ , and  $\text{C}_{\beta 1}\text{H}$ , respectively. All NOESY cross peaks outside the small portion within 9.00 to -1.4 ppm shifts were first observed in 1D NOE spectra by saturating the resolved resonance whose better resolution allows clear visualization of the dipolar contacts as previously described for TyrB10  $\text{OH}_\eta$  at 31.00 ppm and GlnE7  $\text{N}_{\epsilon 2}\text{H}$  at -3.00 ppm.

Figure 3.17 illustrates a TOCSY spectrum showing the scalar correlation for the TyrB10, GlnE7, and PheE11 spin systems in the rHbICN PheB10Tyr mutant from *Lucina pectinata*. The scalar coupling correlation observed in the TOCSY spectra are hyperfine-shifted resonances between 6.70 to 8.80 ppm and 2.70 to 11.80 ppm spectral window. The portion A in the TOCSY spectrum show the diamagnetic window at 2.70 to 5.40 ppm, where the  $N_p$ H backbone,  $\alpha$ , and  $\beta$  protons for the amino acid residues are found. The chemical shifts for the TyrB10 (Y29) AMX + AA'XX' spin system were assigned to  $N_p$ H at 8.54 ppm,  $C_\alpha$ H at 4.30 ppm, and the  $C_{\beta 2}$ H at 3.63 ppm. The chemical shifts for the GlnE7 (Q64) AM(PT)X spin system were assigned to  $N_p$ H at 8.59 ppm,  $C_\alpha$ H at 3.98 ppm,  $C_{\beta 1}$ H at 2.90 ppm, and  $C_{\beta 2}$ H at 2.60 ppm. The chemical shifts for the PheE11 (F68) AMX + AMM'XX' spin system were assigned to  $C_\alpha$ H at 3.18 ppm,  $C_{\beta 1}$ H at 5.33 ppm, and the  $C_{\beta 2}$ H at 7.36 ppm. The portion B and C in the spectra detect TOCSY fragments from the PheE11 and TyrB10 confirming connectivity in the inter-residue aromatic rings with strong hyperfine shifts. The inter-residue scalar coupling aromatic ring protons for the TyrB10 (Y29) were assigned to  $C_\delta$ H at 8.22 ppm and  $C_\epsilon$ H at 11.60 ppm. PheE11 (F68) inter-residue scalar coupling aromatic ring protons were assigned to  $C_\epsilon$ H at 6.52 ppm and  $C_\zeta$ H at 7.53 ppm.

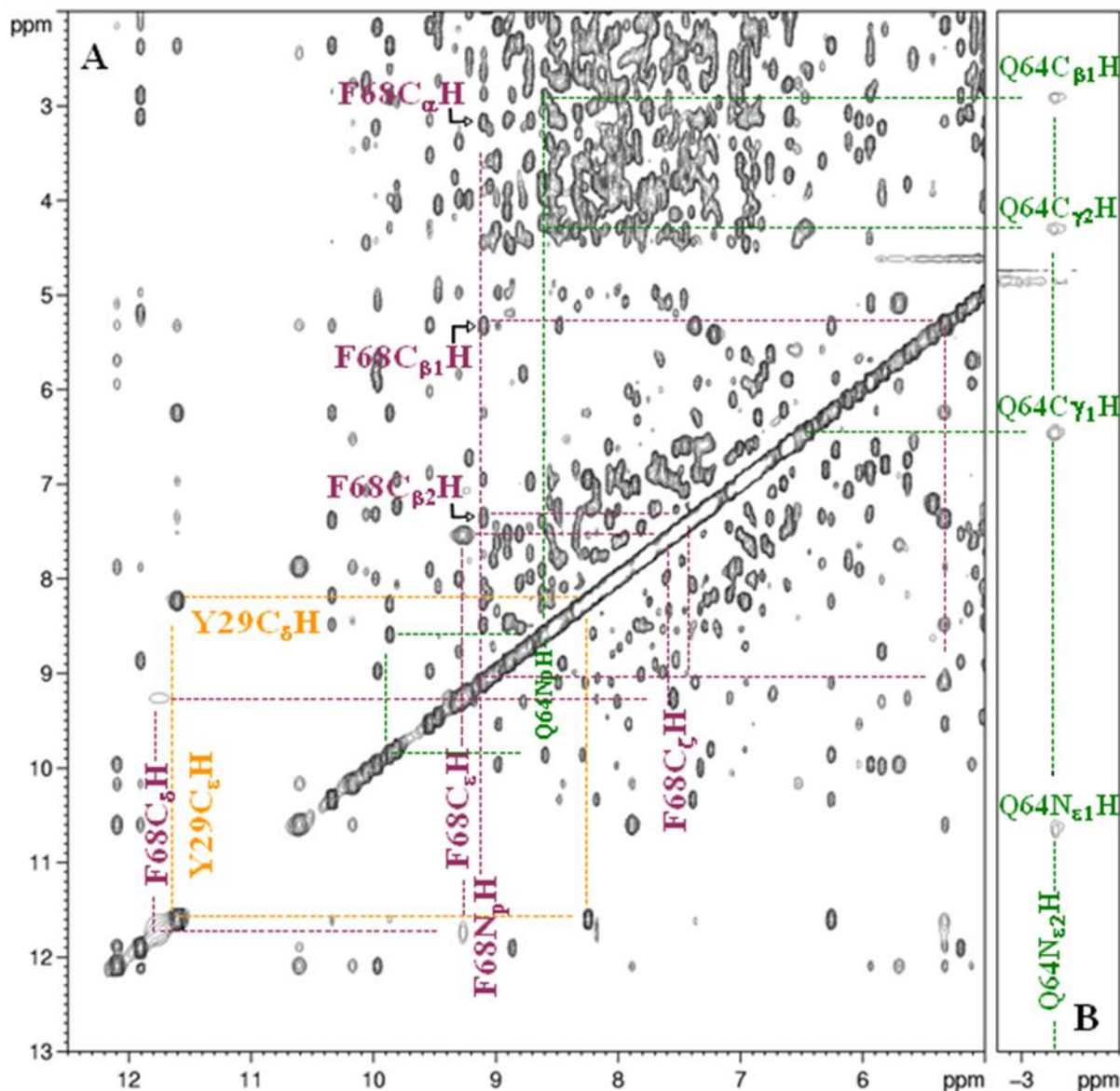


**Figure 3.16:** 600 MHz  $^1\text{H}$ - $^1\text{H}$ -NMR NOESY spectrum (80 ms mixing time) rHbICN PheB10Tyr mutant in  $^1\text{H}_2\text{O}$  at 25 °C and pH 7.00. (A) Correlations cross-peaks in the spectra give the resonance positions of proton signals for TyrB10 (Y29) and PheE11 (F68) distal amino acids residues. (B) Dipolar contacts observed in GlnE7 (Q64) distal amino acid residue. The assigned resolved signals are labeled by the one-letter code for the residue and sequence position. [Ramos et al., 2012]

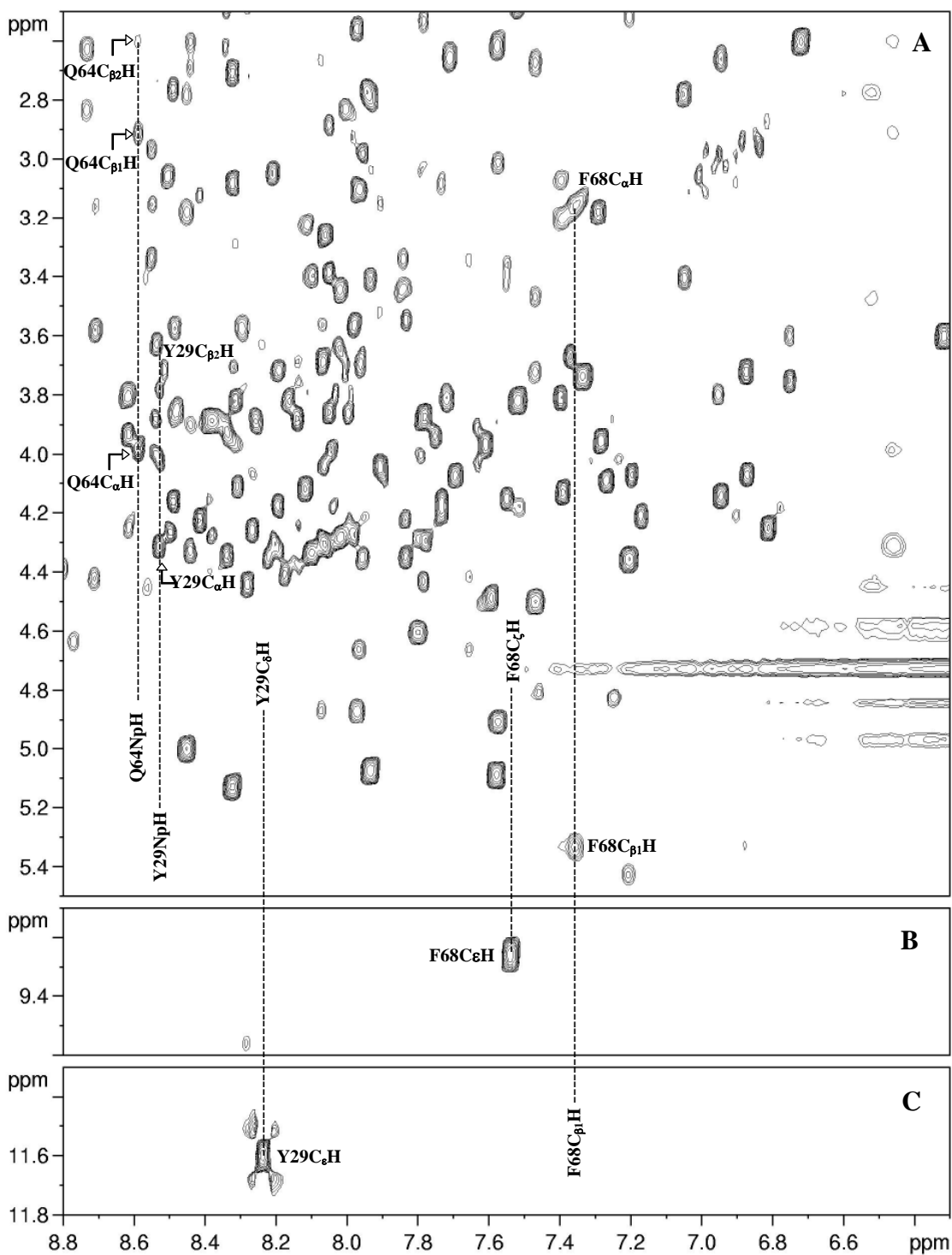


**Figure 3.17:** A, B, and C portions of the TOCSY (40 ms mixing time) spectra for the single mutant rHbICN PheB10Tyr from *L. pectinata* in H<sub>2</sub>O at 25 °C and pH 7.00, showing the scalar correlation for TyrB10 (Y29), GlnE7 (Q64), and PheE11 (F68) spin systems. The assigned resolved signals are labeled by the one-letter code for the residue and sequence position. [Ramos et al., 2012]

### 3.4.3 Sequence-specific resonance method: CN complex

The 1D and 2D NMR analysis described above allowed probing intermolecular interactions between amino acids residues by the sequence-specific resonance method. This method uses the amino acids coding sequence of the rHbI single mutant constructed where PheB10 was mutated to TyrB10 as described by León and coworker [León et al., 2004]. Figure 3.18 shows the sequence-specific resonance assignment of the E-helix for rHbICN PheB10Tyr single mutant. This assignment strategy satisfies interactive resonance assignments among residues side chains that reveal intermolecular and intramolecular interactions in the amino acids sequence. Each helix from the rHbI sequence was analyzed analog to the E-helix. It was elucidated the TrpB2 and TyrB10 from B-helix, ValC4 from C-helix, PheCD1 from the coil, GlnE7, AlaE8, GlnE9, SerE10, PheE11, LysE12, GlyE13, LeuE14, and ValE15 from E-helix, PheF4, AlaF5, AlaF6, AsnF7, HisF8, LysF9, and AlaF10 from F-helix, and LeuG5 and AlaG8 from G-helix.

Previous sections detailed NMR results that have been developed to characterize the amino acid residues in the rHbI and rHbI PheB10Tyr single point mutation in the cyanide complex from the invertebrate *Lucina pectinata*. A sequence specific resonance approach was used as a main technique to assign the hyperfine-shifted backbone and side chain resonance lines from the amino acids in the  $^1\text{H}$ -NMR spectra. A summary of the amino acid side chain protons chemical shifts assignments, at 18 °C, 25 °C, and 33 °C are listed in Table 3.9. Figure 3.19 show a schematic representation of the heme pocket structure of rHbI PheB10Tyr with face-on view from the proximal side illustrating the dipolar contacts of the conserved amino acid residues. The distal amino acid residues are labeled helix and one-letter code, C4 (V39), CD1 (F43), E14 (L71), E15 (V72), G8 (A109), and G5 (L106). The solid, dashed and dashed-dots arrows represent strong, moderate and weak interresidue and residue-heme dipolar contacts, respectively.

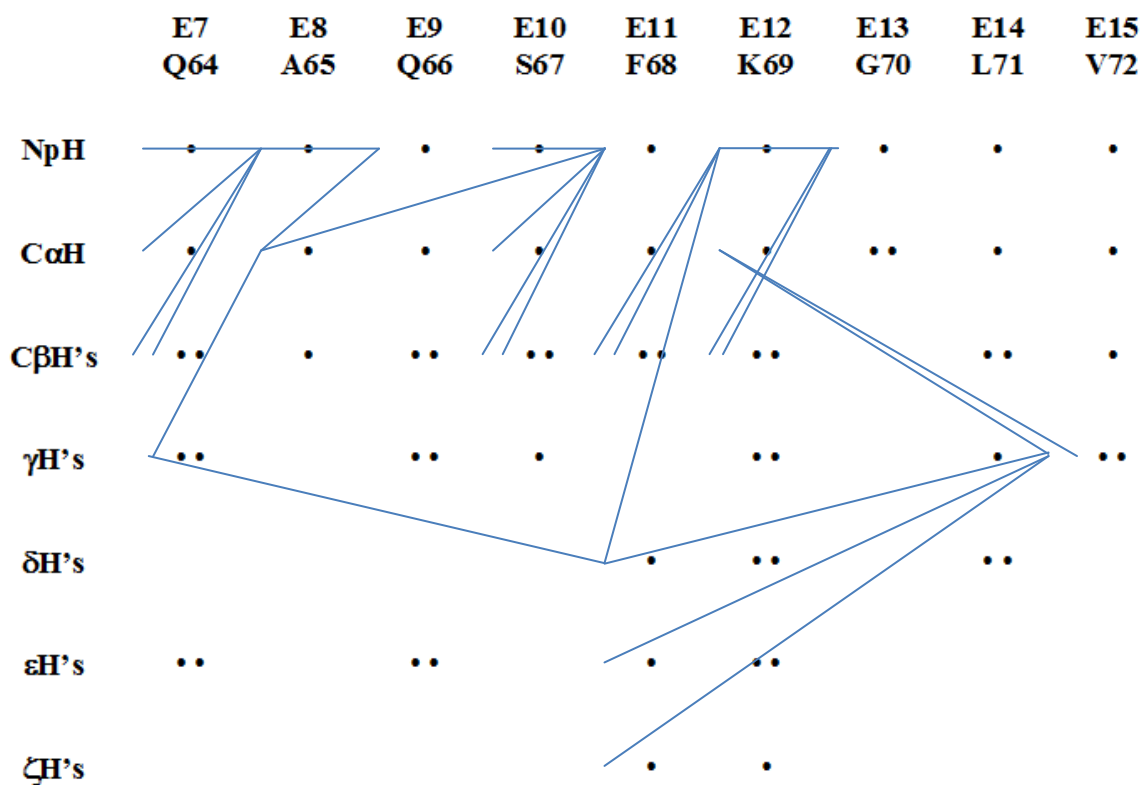


**Figure 3.18:** Sequence-specific resonance assignment of E-helix observed in rHbICN PheB10Tyr mutant protein. Lines represent observed intermolecular and intramolecular residue interactions between the backbone and side chains in the amino acid sequence.

**Table 3.9: Amino acid assignments in the rHbICN and rHbICN PheB10Tyr mutant from *Lucina pectinata***

Residue	rHbICN PheB10Tyr			Major NOEs	rHbICN	
	Protons	$\delta_{\text{obs}}$ , ppm			$\delta_{\text{obs}}$ , ppm	
		18°C	25°C	33°C	25°C	
Trp(21)B2	N <sub>p</sub> H	†	†	†	†	
	C <sub>α</sub> H	†	†	†	†	
	C <sub>β1</sub> H	†	†	†	†	
	C <sub>β2</sub> H	†	†	†	†	
	C <sub>δ1</sub> H (2H)	7.40	7.38	7.38	†	7.55
	N <sub>ε1</sub> H (1H)	10.38	10.32	10.31	†	10.66
	C <sub>ε3</sub> H (4H)	†	†	†	†	7.71
	C <sub>ζ2</sub> H (7H)	8.23	8.18	8.13	†	7.51
	C <sub>ζ3</sub> H (5H)	†	†	†	†	7.18
	C <sub>η2</sub> H (6H)	†	†	†	†	7.24
Tyr (29)B10	N <sub>p</sub> H	†	8.54	8.48	B10 <sub>δ</sub>	†
	C <sub>α</sub> H	†	4.30	4.18	†	†
	C <sub>β1</sub> H	†	3.43	3.40	B10 <sub>δ</sub>	†
	C <sub>β2</sub> H	†	3.63	3.61	B10N <sub>p</sub> H	†
	C <sub>δ</sub> H	8.32	8.22	8.17	B10N <sub>p</sub> H	†
	C <sub>ε</sub> H	11.83	11.60	11.38	B10N <sub>ε</sub> H	†
	O <sub>η</sub> H	†	31.00	30.09	†	†
Val(39)C4	N <sub>p</sub> H	†	6.72	6.78	†	6.72
	C <sub>α</sub> H	†	2.61	2.71	†	2.52
	C <sub>β</sub> H	†	2.00	2.05	†	1.92
	C <sub>γ1</sub> H <sub>3</sub>	†	-0.30	-0.18	4-V	-0.22
	C <sub>γ2</sub> H <sub>3</sub>	†	-0.18	-0.05	4-V	-0.54
Phe (43)CD1	N <sub>p</sub> H	†	†	†	†	†
	C <sub>α</sub> H	†	†	†	†	†
	C <sub>β1</sub> H	†	†	†	†	†
	C <sub>β2</sub> H	†	†	†	†	†
	C <sub>δ</sub> H	†	6.60	6.63	†	6.40
	C <sub>ε</sub> H	†	6.52	6.50	†	6.20
	C <sub>ζ</sub> H	†	†	†	†	7.26
Gln (64)E7	N <sub>p</sub> H	8.63	8.59	8.58	E8N <sub>p</sub> H	8.93
	C <sub>α</sub> H	4.00	3.98	4.02	E8N <sub>p</sub> H, E7 <sub>γ2</sub>	4.62
	C <sub>β1</sub> H	2.99	2.90	2.88	E8N <sub>p</sub> H, E7 <sub>γ2</sub>	3.03
	C <sub>β2</sub> H	2.66	2.60	2.59	E8N <sub>p</sub> H, E7 <sub>γ2</sub>	3.28
	C <sub>γ1</sub> H	6.66	6.46	6.26	E7 <sub>γ1</sub>	7.61
	C <sub>γ2</sub> H	4.46	4.31	4.18	E8 <sub>αs</sub> , E11 <sub>δ</sub> , B10 <sub>ε</sub> , E7 <sub>γ2</sub>	4.96
	N <sub>ε1</sub> H	†	10.66	10.35	E7 <sub>γ1</sub> , E7 <sub>ε2</sub>	14.05
	N <sub>ε2</sub> H	†	-3.27	-2.96	E7 <sub>γ</sub> 's, E7 <sub>ε</sub> 1, 6H <sub>β</sub> 's, 7H <sub>α</sub> 's	-1.39

**Table 3.9 (Continued)**

Residue	rHbICN PheB10Tyr				Major NOEs	rHbICN
	Protons	$\delta_{\text{obs}}$ , ppm				$\delta_{\text{obs}}$ , ppm
		18°C	25°C	33°C		25°C
Ala (65)E8	N <sub>p</sub> H	9.92	9.87	9.83	E9N <sub>p</sub> H, E8N <sub>p</sub> H, E8 <sub>α</sub> , E7 <sub>α</sub> , E7 <sub>β</sub> 's	10.18
	C <sub>α</sub> H	6.31	6.25	6.20	E11N <sub>p</sub> H, E9N <sub>p</sub> H, B10 <sub>ε</sub>	6.65
	C <sub>β</sub> H <sub>3</sub>	2.41	2.35	2.35	‡	2.54
Gln (66)E9	N <sub>p</sub> H	8.31	8.28	8.29	E8N <sub>p</sub> H, E8 <sub>α</sub>	‡
	C <sub>α</sub> H	4.46	4.45	4.48	‡	‡
	C <sub>β1</sub> H	‡	2.30	2.28	‡	‡
	C <sub>β2</sub> H	‡	2.40	2.38	‡	‡
	C <sub>γ1</sub> H	‡	‡	‡	‡	‡
	C <sub>γ2</sub> H	‡	‡	‡	‡	‡
	N <sub>ε1</sub> H	‡	‡	‡	‡	‡
	N <sub>ε2</sub> H	‡	‡	‡	‡	‡
Ser (67)E10	N <sub>p</sub> H	‡	8.04	8.06	E11N <sub>p</sub> H	8.58
	C <sub>α</sub> H	‡	3.41	3.48	E11N <sub>p</sub> H	3.59
	C <sub>β1</sub> H	‡	1.72	1.88	E11N <sub>p</sub> H	2.16
	C <sub>β2</sub> H	‡	2.90	2.97	E11N <sub>p</sub> H, E10N <sub>p</sub> H	3.45
	O <sub>γ</sub> H	‡	‡	‡	‡	‡
Phe (68)E11	N <sub>p</sub> H	9.15	9.09	9.08	E8 <sub>α</sub> , B10O <sub>η</sub> H	9.89
	C <sub>α</sub> H	‡	3.18	3.22	1-Me	3.81
	C <sub>β1</sub> H	5.40	5.33	5.25	E11 <sub>δ</sub> , E12N <sub>p</sub> H, B10O <sub>η</sub> H	9.05
	C <sub>β2</sub> H	‡	7.36	7.20	E11 <sub>δ</sub> , E12N <sub>p</sub> H	6.40
	C <sub>δ</sub> H	‡	11.75	11.53	E15 <sub>γ2</sub> , E7 <sub>γ1</sub> , E11 <sub>β</sub> 's	7.47
	C <sub>ε</sub> H	‡	9.26	9.16	E15 <sub>γ2</sub>	7.53
	C <sub>ζ</sub> H	‡	7.53	7.52	E15 <sub>γ2</sub>	7.87
Lys (69)E12	N <sub>p</sub> H	‡	8.49	8.47	E11 <sub>β</sub> 's, E11 <sub>δ</sub> , E13N <sub>p</sub> H	8.83
	C <sub>α</sub> H	‡	3.85	3.85	E15 <sub>γ</sub> 's	3.97
	C <sub>β1</sub> H	‡	1.57	1.59	E13N <sub>p</sub> H	‡
	C <sub>β2</sub> H	‡	1.95	1.93	E13N <sub>p</sub> H	‡
	C <sub>γ1</sub> H	‡	‡	‡	‡	‡
	C <sub>γ2</sub> H	‡	‡	‡	‡	‡
	C <sub>δ1</sub> H	‡	‡	‡	‡	‡
	C <sub>δ2</sub> H	‡	‡	‡	‡	‡
	C <sub>ε1</sub> H	‡	‡	‡	‡	‡
	C <sub>ε2</sub> H	‡	‡	‡	‡	‡
	N <sub>ζ</sub> H <sub>3</sub>	‡	‡	‡	‡	‡

**Table 3.9 (Continued)**

rHbICN PheB10Tyr					rHbICN	
Residue	Protons	$\delta_{\text{obs}}$ , ppm			Major NOEs	$\delta_{\text{obs}}$ , ppm
		18°C	25°C	33°C		25°C
Gly (70)E13	N <sub>p</sub> H	‡	7.82	7.87	‡	7.97
	C <sub><math>\alpha</math>1</sub> H	‡	3.45	3.50	‡	3.43
	C <sub><math>\alpha</math>2</sub> H	‡	3.35	3.42	‡	3.49
Leu (71)E14	N <sub>p</sub> H	‡	6.10	6.20	‡	6.03
	C <sub><math>\alpha</math></sub> H	3.03	3.09	3.15	‡	3.04
	C <sub><math>\beta</math>1</sub> H	-0.58	-0.50	-0.38	‡	-0.86
	C <sub><math>\beta</math>2</sub> H	-----	-0.67	-0.55	‡	-0.69
	C <sub><math>\gamma</math></sub> H	-1.82	-1.78	-1.69	‡	-2.01
	C <sub><math>\delta</math>1</sub> H <sub>3</sub>	-----	-0.73	-0.68	‡	-2.36
	C <sub><math>\delta</math>2</sub> H <sub>3</sub>	-2.02	-1.93	-1.80	1-Me	-0.83
Val (72)E15	N <sub>p</sub> H	‡	7.05	7.09	‡	6.87
	C <sub><math>\alpha</math></sub> H	‡	2.82	2.80	‡	2.77
	C <sub><math>\beta</math></sub> H	‡	1.06	1.05	‡	1.10
	C <sub><math>\gamma</math>1</sub> H <sub>3</sub>	‡	-0.61	0.01	E12a	0.02
	C <sub><math>\gamma</math>2</sub> H <sub>3</sub>	‡	0.02	-0.62	E11 <sub><math>\zeta</math></sub> , 1-Me, E11 <sub><math>\epsilon</math></sub>	-0.65
Phe (92)F4	N <sub>p</sub> H	‡	7.91	7.92	‡	7.89
	C <sub><math>\alpha</math></sub> H	5.95	5.95	5.98	‡	5.98
	C <sub><math>\beta</math>1</sub> H	3.55	3.52	3.53	‡	3.54
	C <sub><math>\beta</math>2</sub> H	3.17	3.16	3.19	‡	3.04
	C <sub><math>\delta</math></sub> H	‡	6.88	6.89	F5	6.74 (pH7.7,D <sub>2</sub> O,25°C)
	C <sub><math>\epsilon</math></sub> H	‡	‡	‡	‡	7.21 (pH7.7,D <sub>2</sub> O,25°C)
	C <sub><math>\zeta</math></sub> H	‡	‡	‡	‡	6.82 (pH7.7,D <sub>2</sub> O,25°C)
Ala (93)F5	N <sub>p</sub> H	9.60	9.54	9.49	F6	9.64
	C <sub><math>\alpha</math></sub> H	5.43	5.32	5.25	‡	5.60
	C <sub><math>\beta</math></sub> H <sub>3</sub>	2.20	2.15	2.16	F6, F7	2.31
Ala (94)F6	N <sub>p</sub> H	9.02	8.98	8.95	F7	9.05
	C <sub><math>\alpha</math></sub> H	5.02	4.97	4.97		5.10
	C <sub><math>\beta</math></sub> H <sub>3</sub>	‡	2.19	2.18	F5	2.26
Asn (95)F7	N <sub>p</sub> H	10.06	9.97	‡	F8	10.04
	C <sub><math>\alpha</math></sub> H	6.00	5.93	-----	‡	6.01
	C <sub><math>\beta</math>1</sub> H	‡	‡	‡	‡	5.72
	C <sub><math>\beta</math>2</sub> H	‡	‡	‡	‡	5.07
	N <sub><math>\delta</math>1</sub> H	7.68	7.62	-----	‡	
	N <sub><math>\delta</math>2</sub> H	6.91	6.90	-----	‡	‡

**Table 3.9 (Continued)**

Residue	rHbICN PheB10Tyr				Major NOEs	rHbICN
	Protons	$\delta_{\text{obs}}$ , ppm				$\delta_{\text{obs}}$ , ppm
		18°C	25°C	33°C		25°C
His (96)F8	N <sub>p</sub> H	12.30	12.10	11.90	F9	12.53
	C <sub>α</sub> H	10.43	10.17	9.88	‡	10.86
	C <sub>β1</sub> H	10.91	10.60	10.25	‡	11.34
	C <sub>β2</sub> H	8.09	7.84	7.67	‡	9.14
	N <sub>δ1</sub> H	15.10	14.86	14.59	‡	15.94
	C <sub>δ2</sub> H	‡	12.50	‡	‡	18.79
	C <sub>ε1</sub> H	‡	-5.86	‡	‡	-6.14
	N <sub>ε2</sub> H-bound with Fe-	‡	‡	‡	‡	‡
Lys (97)F9	N <sub>p</sub> H	12.05	11.91	11.78	F8	12.21
	C <sub>α</sub> H	5.23	5.20	5.19	‡	5.46
	C <sub>β1</sub> H	2.94	2.90	2.88	‡	3.33
	C <sub>β2</sub> H	3.20	3.12	3.09	‡	3.09
	C <sub>γ1</sub> H	‡	‡	‡	‡	2.48
	C <sub>γ2</sub> H	‡	‡	‡	‡	2.19
	C <sub>δ1</sub> H	‡	‡	‡	‡	3.42
	C <sub>δ2</sub> H	‡	‡	‡	‡	‡
	C <sub>ε1</sub> H	‡	‡	‡	‡	‡
	C <sub>ε2</sub> H	‡	‡	‡	‡	‡
	N <sub>ζ</sub> H <sub>3</sub>	‡	‡	‡	‡	‡
Ala (98)F10	N <sub>p</sub> H	9.08	8.85	8.82	F9	9.02
	C <sub>α</sub> H	‡	4.86	4.84	F7	4.97
	C <sub>β</sub> H <sub>3</sub>	2.41	2.35	2.35	‡	2.45
Leu (106)G5	N <sub>p</sub> H	‡	‡	‡	‡	‡
	C <sub>α</sub> H	1.92	2.02	2.17	‡	
	C <sub>β1</sub> H	1.75	1.75	1.79	‡	CxH = 1.35
	C <sub>β2</sub> H	0.54	0.57	0.63	‡	CxH' = 0.80
	C <sub>γ</sub> H	1.22	1.22	1.27	‡	1.67
	C <sub>δ1</sub> H <sub>3</sub>	-1.62	-1.53	-1.43	3-Me, 2-V	‡
	C <sub>δ2</sub> H <sub>3</sub>	1.00	0.98	0.96	‡	‡
	N <sub>p</sub> H	‡	6.88	6.93	‡	6.84
Ala (109)G8	C <sub>α</sub> H	‡	3.72	3.78	‡	3.61
	C <sub>β</sub> H <sub>3</sub>	‡	0.46	0.55	‡	0.23

‡ not assigned

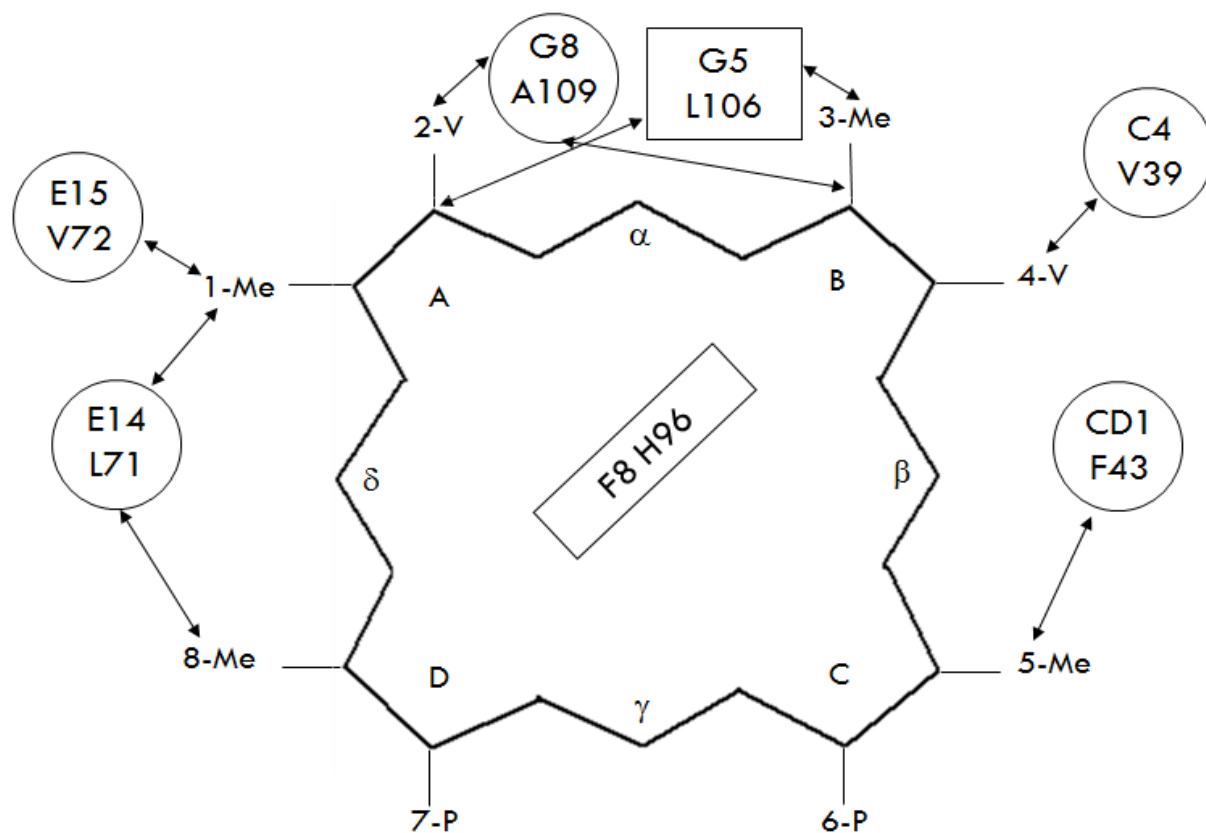


**Figure 3.19:** Schematic representation of the heme pocket structure of rHbI PheB10Tyr with face-on view from the proximal side illustrating the dipolar contacts of the conserved amino acid residues. The distal amino acid residues are labeled helix and one-letter code, C4 (V39), CD1 (F43), E14 (L71), E15 (V72), G8 (A109), and the proximal residue G5 (L106). The circles (  $\circ$  ) represent the distal residues and the square (  $\square$  ) represent the proximal residue. The solid, dashed and dashed-dots arrows represent strong, moderate and weak inter-residue and residue-heme dipolar contacts, respectively.

### 3.5 Determination of NH/OH hydrogen exchange relaxation protons and broad hyperfine shifted for the rHbI and rHbI PheB10Tyr CN complex.

#### 3.5.1 Deuterium isotopic labeling ( $^2\text{H}_2\text{O}$ ) data

A comprehensive isotopic experimental methodology was designed to confirm side chains of distal amino acids including the conservative HisF8. Detecting NH/OH solvent exchangeable protons required special efforts to avoid water resonance through the use of a selective pulse. The isotopic solvent exchangeable study performed allows identifying strongly relaxed signals and labile protons in the protein. Figure 3.20 compares the  $^1\text{H}$ -NMR spectra of the rHbICN PheB10Tyr mutant in  $^1\text{H}_2\text{O}$  (1A) and  $^2\text{H}_2\text{O}$  (1B). Comparison of these spectra reveals the presence of three strongly relaxed labile proton at 14.86, 31.00, and 3.27 ppm to the axial proximal residue HisF8  $\text{N}_{\delta_1}\text{H}$ , and distal residues TyrB10OH $_{\eta}$  and GlnE7N $_{\epsilon_2}\text{H}$ , respectively. The assignments were based on the presence or absence of the isotopic proton and by comparing the values of the axial conserved residue as reported here and in the literature [Nguyen et al. 1998, La Mar et al., 2000, Ramos-Santana et al., 2012].

Overall, Table 3.10 summarizes the  $^1\text{H}$ -NMR results obtained for rHbICN PheB10Tyr showing the distal residues rearrangement when compared to the wtHbICN complex. The significant changes in hyperfine chemical shifts, such as the 10.66ppm for GlnE7N $_{\epsilon_1}\text{H}$  and -3.27 ppm for GlnE7N $_{\epsilon_2}\text{H}$  in the rHbICN PheB10Tyr mutant compared to the 14.05 ppm for GlnE7N $_{\epsilon_1}\text{H}$  and -1.39 ppm for GlnE7N $_{\epsilon_2}\text{H}$  in the wtHbICN complex, reveal that a conformational effect results when Phe is substituted by Tyr in the B10 position. For example, the side chain GlnE7NH $_2$ -CO is shifted ( $\Delta\delta = \delta_{\text{wild type}} - \delta_{\text{mutant}}$ ) upfield with  $\Delta\delta = 3.39$  and  $\Delta\delta = 1.88$  ppm near to the 6-propionate form its native structural position.

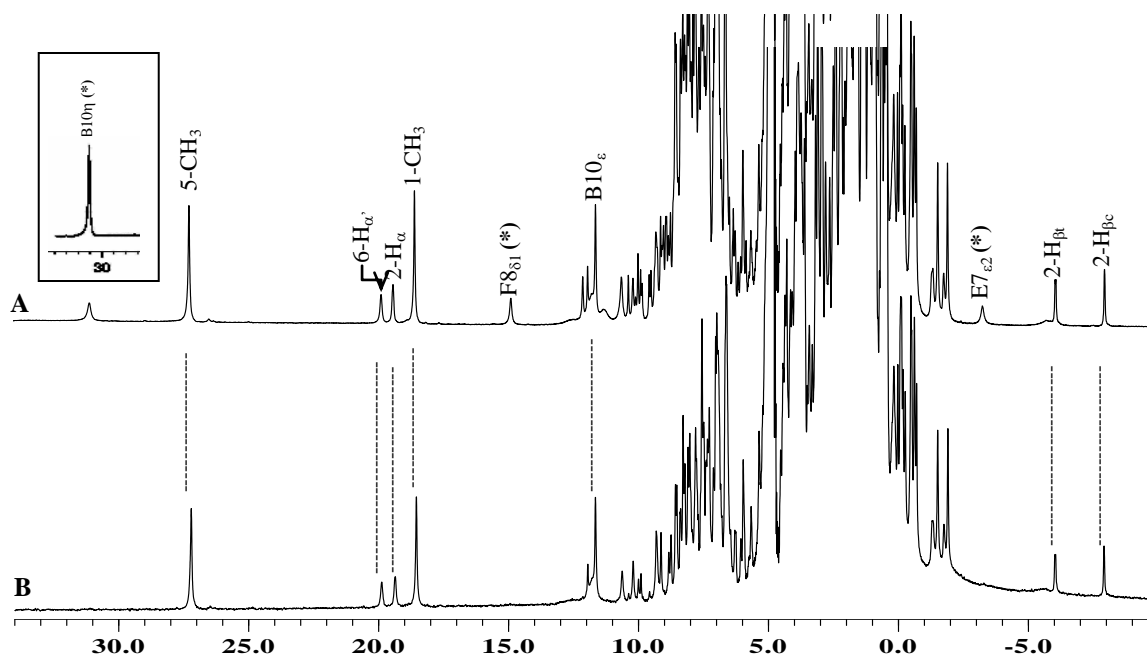


**Figure 3.20: 500 MHz  $^1\text{H}$ -NMR spectra of the rHbICN PheB10Tyr at 25°C and pH 7.00. (A)  $^1\text{H}_2\text{O}$  with frequency at 31.00 ppm in the inset. (B)  $^2\text{H}_2\text{O}$  solvent. Labeled signals include heme signals in Fisher Notation (i.e. 1-CH<sub>3</sub>, 6H<sub>α'</sub>) and amino acid signals in the helix position (i.e. B10<sub>η</sub> = Tyr29 ring OH<sub>η</sub>; B10<sub>ε</sub> = Tyr29 ring C<sub>ε</sub>H; E7<sub>ε2</sub> = Gln64 N<sub>ε2</sub>H; F8<sub>δ1</sub> = His96 imidazole N<sub>δ1</sub>H). Labile protons signals are identified with an asterisk(\*). [Ramos et al., 2012]**

**Table 3.10: Comparison of <sup>1</sup>H-NMR chemical shifts of the B10, E7 and E11 distal amino acid residues in rHbICN PheB10 mutant and wtHbICN from *Lucina pectinata*.**

Residues	Protons	Chemical Shifts (ppm) <sup>a</sup>	
		rHbICN Phe(B10)Tyr	wtHbICN <sup>b, (c)</sup>
Tyr <sup>29</sup> (B10)	N <sub>p</sub> H	8.54	-
	C <sub>α</sub> H	4.30	-
	C <sub>β1</sub> H	3.43	-
	C <sub>β2</sub> H	3.63	-
	C <sub>δ</sub> Hs	8.22	8.70
	C <sub>ε</sub> Hs	11.60	13.07
	C <sub>ζ</sub> H	-	18.77
	<b>O<sub>η</sub>H</b>	<b>31.00</b>	<b>-</b>
Gln <sup>64</sup> (E7)	N <sub>p</sub> H	8.59	8.93
	C <sub>α</sub> H	3.98	4.62
	C <sub>β1</sub> H	2.90	3.03
	C <sub>β2</sub> H	2.60	3.29
	C <sub>γ1</sub> H	6.46	7.63 (7.47)
	C <sub>γ2</sub> H	4.31	4.97 (4.90)
	<b>N<sub>ε1</sub>H</b>	<b>10.66</b>	<b>14.05 (13.80)</b>
	<b>N<sub>ε2</sub>H</b>	<b>-3.27</b>	<b>-1.39 (-1.40)</b>
Phe <sup>68</sup> (E11)	N <sub>p</sub> H	9.09	9.89
	C <sub>α</sub> H	3.18	3.81
	<b>C<sub>β1</sub>H</b>	<b>5.33</b>	<b>9.05</b>
	C <sub>β2</sub> H	7.36	6.40
	<b>C<sub>δ</sub>Hs</b>	<b>11.75</b>	<b>7.47</b>
	<b>C<sub>ε</sub>Hs</b>	<b>9.26</b>	<b>7.53</b>
	C <sub>ζ</sub> H	7.53	7.87

–not observed.

<sup>a</sup>Chemical shifts in ppm at 25°C, pH 7.0 (rHbICN PheB10Tyr) and pH 7.2 (wtHbICN).

<sup>b</sup>data from Nguyen, B.D., et.al. 1998.

<sup>(c)</sup>data from Ramos, B., 2003 at 28°C, pH 7.5.

### 3.6 Characterization of rHbI in the hydrogen sulfide complex

This section shows the NMR spectroscopy results that contribute to understand how relevant is the iron oxidation state in the hemoglobin of invertebrate species such as *L. pectinata* and others hemoproteins for their vital role in globins systems. The following results show a structural characterization of the heme group and distal site of the rHbI in the hydrogen sulfide complex. These are valuable to reveal a magnetic field mapping around the iron center in the rHbI, particularly in the heme reduction process.

#### 3.6.1 *rHbIH<sub>2</sub>S* complex formation and stabilization analysis data

The principal challenge in the hydrogen sulfide <sup>1</sup>H-NMR studies was to preparing the rHbIH<sub>2</sub>S complex in solution. The rHbIH<sub>2</sub>S complex formation involved the development to titration procedure to monitor the UV-Vis bands characteristic to the complex. Figure 3.21 shows the comparison of the UV-Vis spectra obtained upon titration of rHbI with the H<sub>2</sub>S buffer solution at pH 6.5. Formation of the rHbIH<sub>2</sub>S derivative is clearly-demonstrated by the presence of the characteristic hydrogen sulfide Soret band at 426 nm and Q bands maxima at 544 and 574 nm, as previously reported [Wittenberg et al., 1990]. Titration of rHbI with increment of H<sub>2</sub>S by a factor of 2 μl induced formation of the hydrogen sulfide complex. However, the results demonstrated an opposite effect at 6 μl of H<sub>2</sub>S buffer solution, in which distinctive bands at 412, 540, 576, and 633 nm were observed that noticeably indicates the possible existence of two species.

Figure 3.22 shows UV-Vis spectra maximum absorbance during a period of 2½ days after preparation of the sulfide complex. It is observed that after 4 hours of sulfide complex preparation, the UV-Vis spectra of rHbIH<sub>2</sub>S showed a tendency toward formation of metaquo complex, as judged by the 426 to 408nm displacement of the Soret band, as well the presence of

Q band at 633 nm. The results suggest that a transition from H<sub>2</sub>S to metaquo ferric species exists in a mixture after long time of exposition to the environment. However, it is questionable if some any other processes may be responsible of this mixture.

Figure 3.23 shows the UV-Vis spectrum of the rHbIH<sub>2</sub>O complex. This complex was important to understand the structural changes as a function of the different ligands at the binding site, and the effect in the iron spin and oxidation state. The spectra indicated a Soret band at 407 nm and Q bands at 502 and 633 nm, typically expected for the metaquo complex. Water ligand binds in ferric form with the heme iron as well as hydrogen sulfide to form rHbIH<sub>2</sub>O and rHbIH<sub>2</sub>S complexes. Comparative UV-Vis spectra analysis between rHbIH<sub>2</sub>O and rHbIH<sub>2</sub>S spectra suggested that titration over a 6 µl of the H<sub>2</sub>S buffer solution promotes a detectable changes in the formation of the complex as observed in the Figure 3.21. This result demonstrated dependable concentration of the H<sub>2</sub>S in solution to form the rHbIH<sub>2</sub>S derivative. Overall, the UV-Vis results showed that the best conditions to form the H<sub>2</sub>S derivative for a 3.0 mM protein concentration was prepared the rHbI with a maximum of 4 µl of the H<sub>2</sub>S buffer solution and perform the rHbIH<sub>2</sub>S NMR studies in a maximum period of two hours to maintain the integrity of the sample.

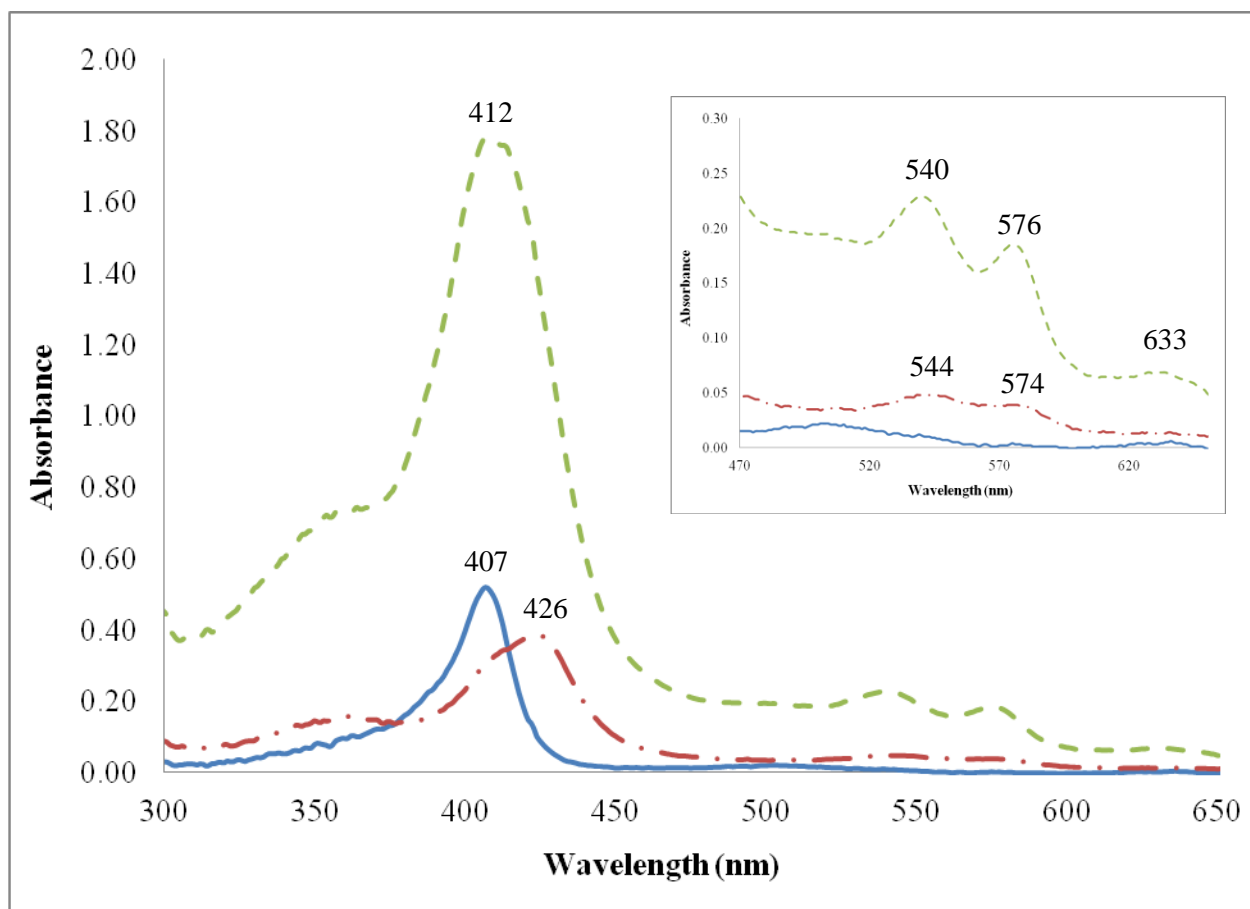


**Figure 3.21: UV-Vis spectra obtained upon titration of rHbI with the H<sub>2</sub>S buffer solution at 0 μL (blue solid line), 4 μL (red dash-dot line), and 6 μL (green dash line) in pH 6.5. The inset shows the Q bands in the spectra.**

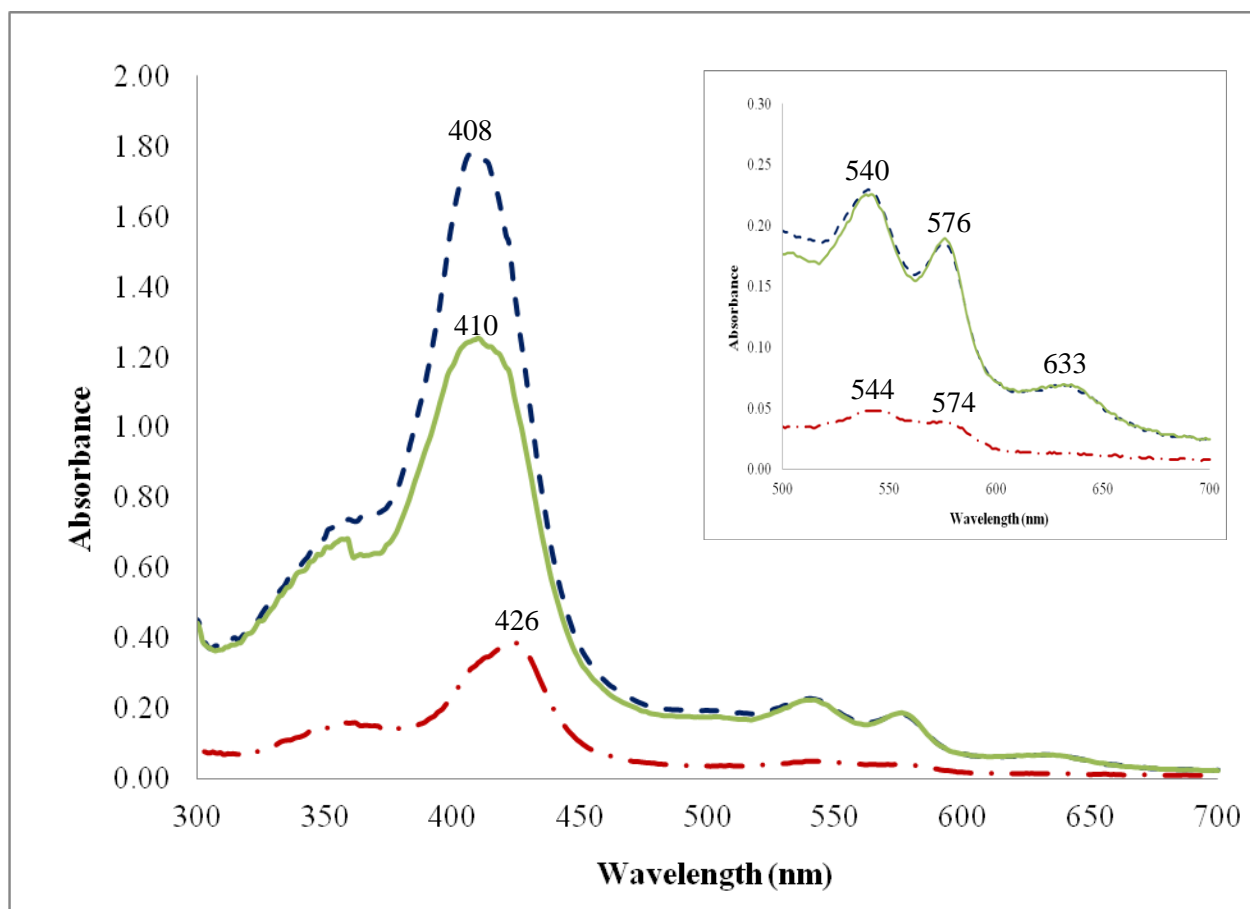


**Figure 3.22: UV-Vis spectra of rHbIH<sub>2</sub>S during two and half (2½) days after preparation at initial time (red dash-dot line), 4 hrs (green solid line), and 2 days 14 hrs (blue dash line). The inset shows the Q bands in the spectra.**

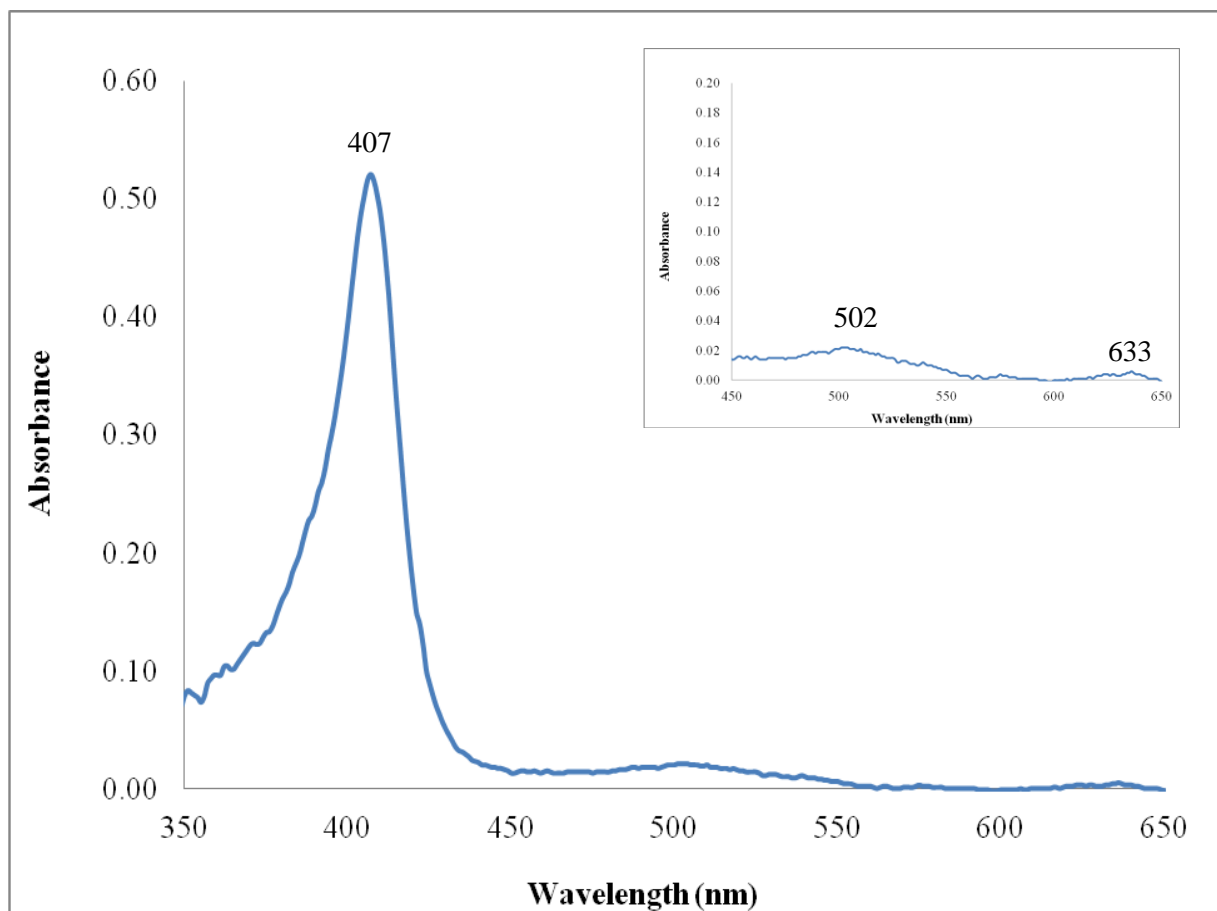


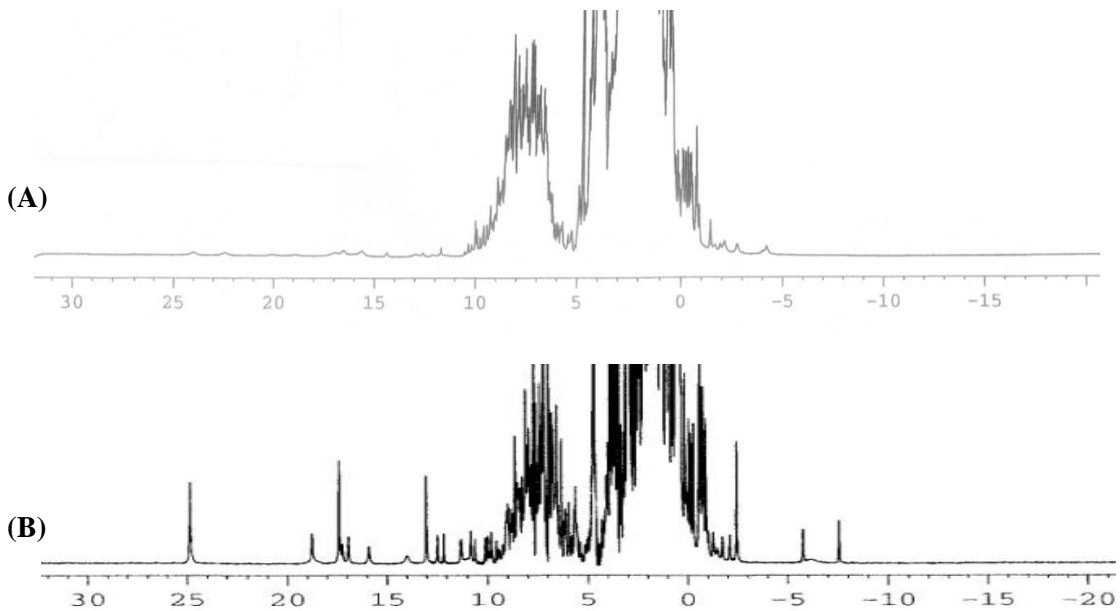
**Figure 3.23: UV-Vis spectrum of the rHbIH<sub>2</sub>O derivative. The inset shows the Q bands in the spectra. The optical spectra illustrated the characteristic UV-Vis bands for metaquo form at 407 nm for maximum absorption and Q bands at 502 and 633 nm showed in the inset.**

### 3.6.2 One dimensional (1D) Pulse Sequences: $^1\text{H-NMR}$ Experiments

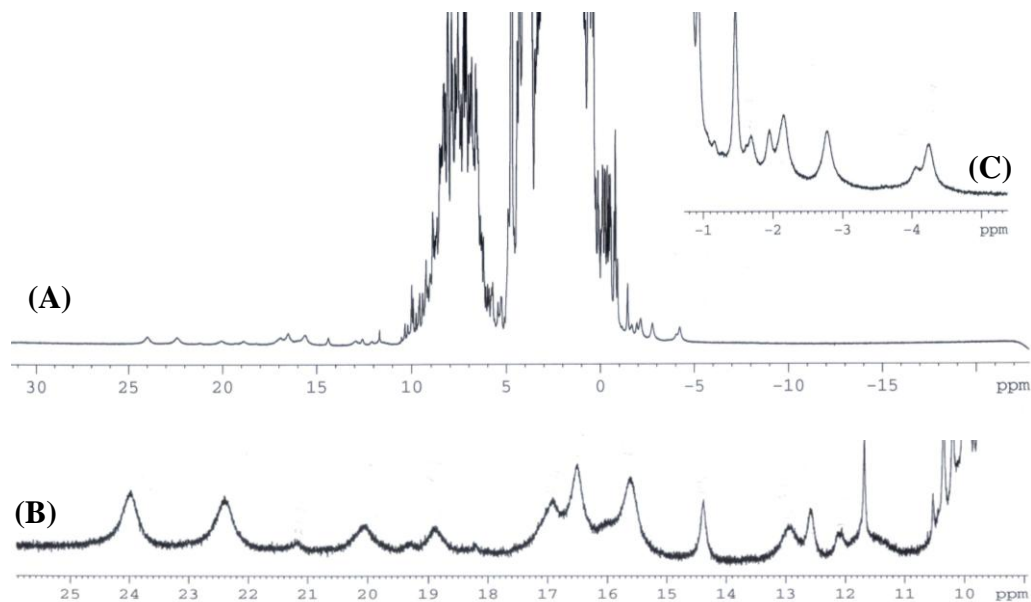
#### 3.6.2.1 Water Solvent Suppression Data

Figure 3.24 show  $^1\text{H-NMR}$  spectra of the ferric HbI derivatives, rHbICN and rHbIH<sub>2</sub>S, that suggests differences in the anisotropic magnetic field distribution from the heme group according the reactivity of H<sub>2</sub>S in the active site of the rHbI. Both cyanide and hydrogen sulfide derivative have the property to bind the ligand in the ferric state of the protein expecting similar electronic and magnetic properties of heme iron. While cyanide is considered a strong-field ligand that result in low spin (LS) ( $S= 1/2$ ) state, results of the  $^1\text{H-NMR}$  from rHbIH<sub>2</sub>S have provided a large questionable understanding about the H<sub>2</sub>S magnetic field strength.

Figure 3.25 (A) shows  $^1\text{H-NMR}$  spectrum of rHbIH<sub>2</sub>S in  $^1\text{H}_2\text{O}$  at 25 °C and pH 7.36. It is observed an iron paramagnetic influence of the heme group with hyperfine resonance lines in the downfield region (10.00 to 25.00 ppm) and upfield region (-1.00 to -5.00 ppm) as similar to cyanide derivative. Also, an intense diamagnetic envelope is observed between 10.00 to -1.00 ppm from the outside protons in the globin. Figure 3.25 (B) shows an expansion of the downfield region illustrating strong resonance lines at 23.99, 22.41, 16.50, 15.62, 14.38, 11.68 ppm. Figure 3.25 (C) shows an expansion of the upfield region illustrating strong resonance lines at -1.46, -2.16, -2.78, and -4.24 ppm. However, the strong resonance lines complexity results in the H<sub>2</sub>S spectrum which lead to a high spin (HS) ( $S=5/2$ ) ↔ low spin (LS) ( $S =1/2$ ) mixture characteristic for intermediate-field ligands. This behavior may be modulated by the sixth (6<sup>th</sup>) to fifth (5<sup>th</sup>) coordination of the heme group when the heme reduction process take place in the H<sub>2</sub>S dissociation. The water suppression data along with the isotopic analysis and variable temperature also suggest that H<sub>2</sub>S can be produced sulfhydroxyl (SH) ligand species that can modify the H<sub>2</sub>S stability.



**Figure 3.24: 500 and 600 MHz  $^1\text{H}$ -NMR reference spectra of the hyperfine shifted regions of (A) rHbIH<sub>2</sub>S (pH 7.36) and (B) rHbICN (pH 7.00) complexes in  $^1\text{H}_2\text{O}$  at 25 °C.**

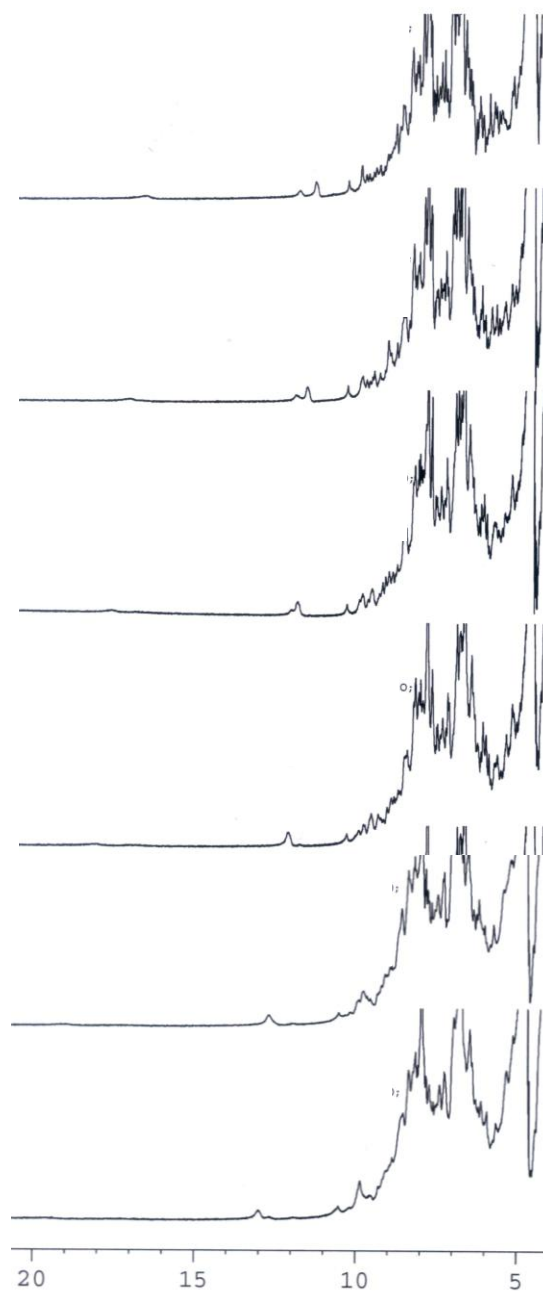


**Figure 3.25:** 500 MHz <sup>1</sup>H-NMR spectrum of the hyperfine shifted regions of rHbIH<sub>2</sub>S complex in <sup>1</sup>H<sub>2</sub>O at 25 °C and pH 7.36: (A) reference spectrum, (B) downfield region at 10.00 to 25.00 ppm, and (C) the inset show the upfield region at -1.00 to -5.00 ppm.

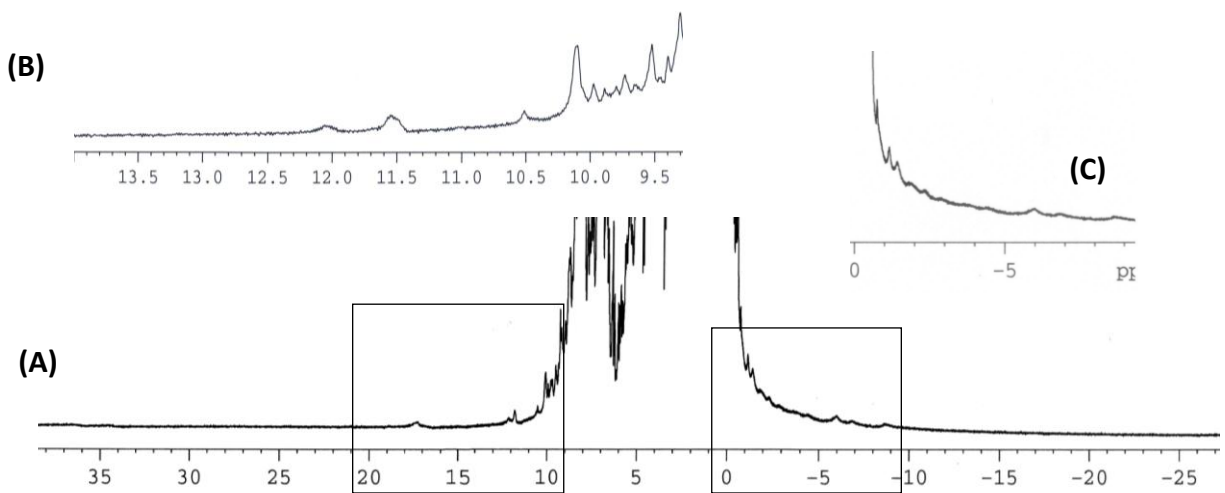
### 3.6.2.2 Variable Temperature (VT) spectra and Deuterium isotopic labeling ( $^2\text{H}_2\text{O}$ )

Figure 3.26 shows the downfield signals at 5.00 to 20.00 ppm between 5 to 30 °C variable temperatures for rHbIH<sub>2</sub>S in  $^2\text{H}_2\text{O}$  at pH 6.50. The spectrum shows a displacement of the resonance lines to the diamagnetic envelop. New broadband with low intensity resonance lines are detected exhibiting significant proton chemical shifts as temperature increase from 15 °C to 30 °C. The chemical shifts are observed in the spectra at 16.83, 12.033, and 11.54 ppm. These resonance signals are characterized using NH/OH exchangeable proton as well the variable temperature studies. As opposed to CN binding, there is not a direct correlation between dipolar contact indicative of electrostatic interactions in the heme pocket of the H<sub>2</sub>S derivative suggesting that its behavior may also be governed by an reduction ( $\text{Fe}^{(\text{III})} \rightarrow \text{Fe}^{(\text{II})}$ ) of the iron center.

Detecting NH/OH solvent exchangeable protons required special efforts to avoid water resonance through the use of a selective pulse. The isotopic solvent exchangeable study performed allows identifying strongly relaxed signals and labile protons in the protein. Figure 3.27 shows the  $^1\text{H}$ -NMR spectrum of rHbIH<sub>2</sub>S in  $^2\text{H}_2\text{O}$  at pH 6.50. The analysis of this spectrum portions in combination with the variable temperature reveals the presence of several non-labile protons especially in the downfield region. The question is where are the paramagnetic resonance lines observed in the  $^1\text{H}$ -NMR under water conditions. Based on this, a comparative study with the metaquo rHbI complex was developed obtaining the results as shown in the Figure 3.28. It is observed that a mixture between two species predominate in the downfield region of the spectra similar to rHbIH<sub>2</sub>S and rHbIH<sub>2</sub>O.



**Figure 3.26: 500 MHz <sup>1</sup>H-NMR spectra portion of the variable temperature spectral window (5.00 to 20.00 ppm), of rHbIH<sub>2</sub>S in <sup>2</sup>H<sub>2</sub>O at pH 6.50. The temperature dependence spectra were observed in the range of 5-30 °C with increments of 5 °C between each spectrum. Arrows indicate the overlapping signals in the spectra.**



**Figure 3.27: (A) 500 MHz <sup>1</sup>H-NMR reference spectrum of the hyperfine shifted regions of rHbIH<sub>2</sub>S complex in <sup>2</sup>H<sub>2</sub>O at 25 °C and pH 6.50: (B) downfield region (9.00 to 20.00 ppm) at 30 °C and (C) upfield region (0.00 to -9.00 ppm).**

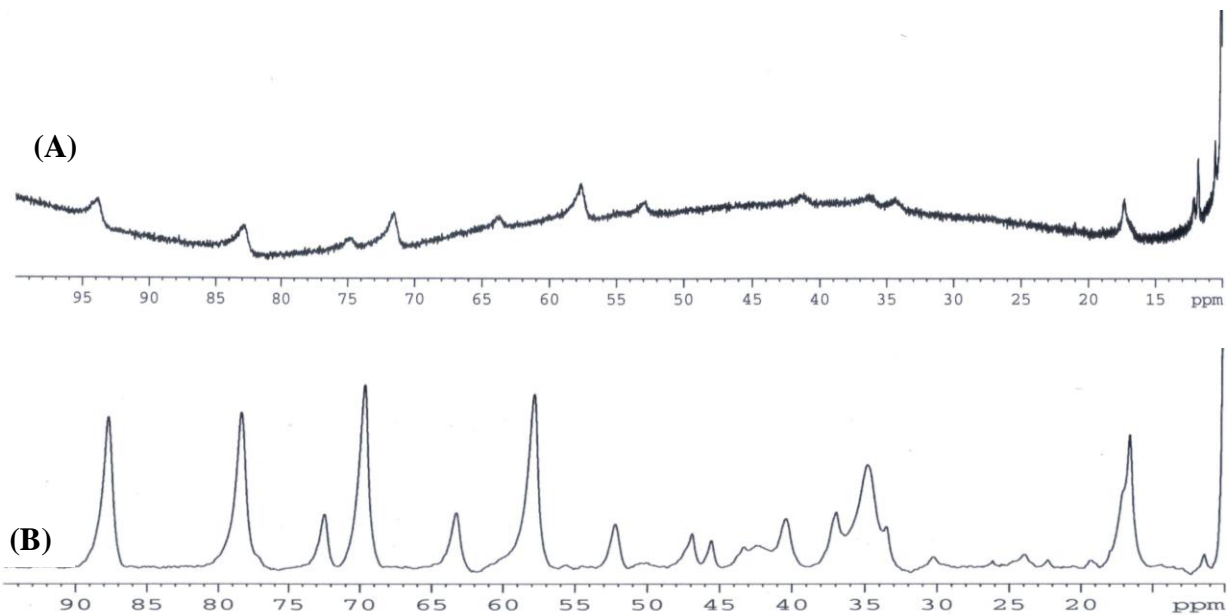


**Figure 3.28: 500 and 600 MHz  $^1\text{H}$ -NMR downfield region, (15.00 to 95.00 ppm) in  $^2\text{H}_2\text{O}$  at 25 °C and pH 6.50 for (A) rHbIH $_2$ S and (B) rHbIH $_2$ O PheB10Tyr complexes.**

### 3.7 Nuclear Magnetic Resonance structural model construction for the rHbIPheB10Tyr mutant in the CN heme pocket.

#### 3.7.1 Nuclear magnetic axes coordinate system

The iron-centered reference coordinates system,  $x',y',z'$  ( $R',\theta',\Omega'$ ) was derived from the HbICN X-Ray crystal coordinates (PDB ID: 1BOB, Bolognesi et al., 1999) for the very close structural homolog to rHbICN PheB10Tyr mutant from *Lucina pectinata*. Figure 3.29 shows the most convenient molecular heme reference frame,  $x',y',z'$ , with the axes including the N-Fe-N vectors. The magnetic axes,  $x^*,y^*,z^*$ , were described relative to the reference axes,  $x',y',z'$  in terms of the Euler angles for globins  $(\alpha,\beta,\gamma)$ ,  $(x^*,y^*,z^*) = (x',y',z')\Gamma(\alpha,\beta,\gamma)$  as previously published [La Mar et al., 2000] where;  $\beta$  is the tilt of  $z^*$  axis from the heme normal (Figure 3.29B),  $\alpha$  is the angle between the projection of the  $z^*$  axis on the heme ( $x',y'$ ) plane and the  $x'$  axis, and  $\kappa$  is the angle with the  $x', y'$  pair of axes obtained from the orientation of the new  $x^*, z^*$  pair axes projected on the heme ( $x',y'$ ) plane as given by  $\kappa \sim \alpha + \gamma$ . The major magnetic axis were determined by the strongest field-ligand relating the magnetic rhombic ( $x^*,y^*$ ) axes to the orientation of nonaxially symmetric cyanide ligand, and the  $\phi$  defines the orientation of the axial HisF8 plane relative to the  $x'$  axis as proposed by  $-\kappa = \phi$  that relates the electronic and magnetic coordinate systems. The magnetic axes determination used the observed dipolar shifts for all protons from residues that occupy unique positions relative to the iron, as defined by the coordinates of *L. pectinata* wtHbICN crystal structure. These protons are assignable using their conservative and fixed positions as instead HisF8, LeuE14, and LeuG5.

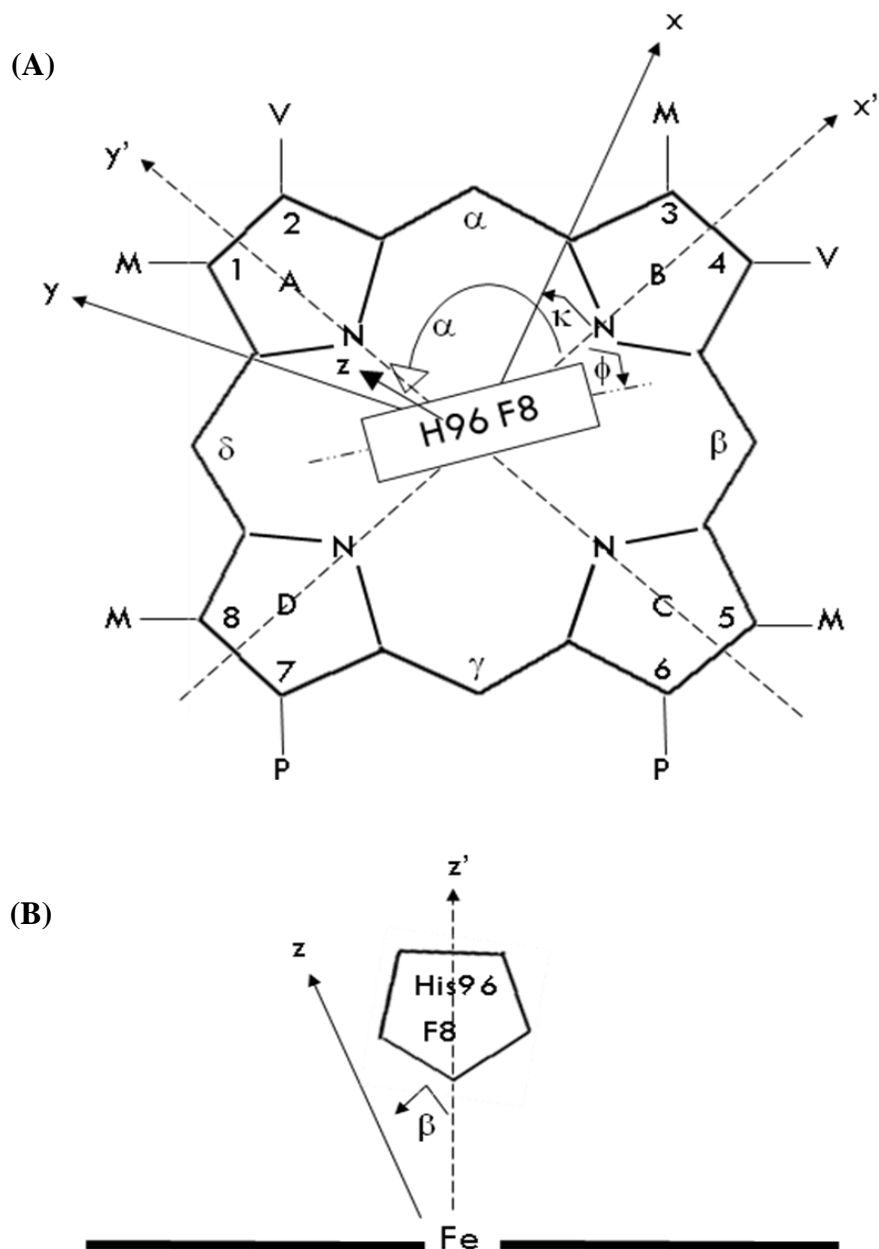


**Figure 3.29:** Illustration of the iron-centered reference coordinate system,  $x',y',z'$  ( $R',\theta',\Omega'$ ), for a porphyrin, the electronic coordinate system,  $x,y,z$  where  $d_{xz}$ ,  $d_{yz}$  are each eigen functions, and the magnetic coordinate system,  $x^*,y^*,z^*$  ( $R,\theta^*,\Omega^*$ ), in which  $\chi$  is diagonal from (A) distal and (B) proximal views. The heme is labeled with the Fisher notation, and the substituent's are labeled M(methyl), V(vinyl), and P(propionate).

### 3.7.2 Hyperfine ( $\delta_{\text{hf}}$ ) and Dipolar ( $\delta_{\text{dip}}$ ) chemical shift validation

Paramagnetic hemoproteins require the determination of the net paramagnetic hyperfine shift due to the unpaired electron spin(s) on the iron ( $\delta_{\text{hf}}$ ) using the shifts for a diamagnetic structural analog, that is, wtHbICN for the rHbICN PheB10Tyr mutant. The  $\delta_{\text{hf}}$  has two contributions, a scalar or contact contribution,  $\delta_{\text{con}}$ , and a dipolar or through-space contribution,  $\delta_{\text{dip}}$ , as given by equation 2.15. The  $\delta_{\text{con}}$  arises from unpaired spin delocalization onto nuclei on the ligand in the heme pocket. The quantitative determination of the magnetic axes in the temperature range 18-33 °C provides the  $\delta_{\text{dip(cal)}}$  that allows determination of  $\delta_{\text{con}}$  by equation 2.16. The resulting  $\delta_{\text{obs}}$ ,  $\delta_{\text{sec}}$ ,  $\delta_{\text{rc}}$ ,  $\delta_{\text{dia}}$ ,  $\delta_{\text{dip(obs)}}$ ,  $\delta_{\text{dip(cal)}}$ ,  $\delta_{\text{hf}}$ , and  $\delta_{\text{con}}$  at 25 °C for HisF8, GlnE7, TyrB10 and PheE11 distal amino acids are listed in Table 3.11.

The dipolar chemical shift plot ( $\delta_{\text{dip(obs)}}$  versus  $\delta_{\text{dip(calc)}}$ ) was used as the principal validation parameter after each manual inspection of the proton resonance signals assignment to the porphyrin system and amino acid sequence in the rHbICN PheB10Tyr mutant. The results of the least-square search for the Euler angles using the  $\delta_{\text{dip(obs)}}$  for residues whose heme-residue and inter-residue NOESY contact indicate conserved structures relative to rHbICN PheB10Tyr, using optimized anisotropies  $\Delta\chi_{\text{ax}} = 2.48 \times 10^{-9} \text{ m}^3/\text{mol}$  and  $\Delta\chi_{\text{rh}} = -0.58 \times 10^{-9} \text{ m}^3/\text{mol}$ , lead to  $\alpha = 0.10 \pm 10^\circ$ ,  $\beta = 0.10 \pm 1.0^\circ$  and  $\kappa = -1.69 \pm 10^\circ$  with a resultant excellent correlation between  $\delta_{\text{dip(obs)}}$  and  $\delta_{\text{dip(calc)}}$ , as shown in Figure 3.30. Table 3.12 details the magnetic axes parameters calculated by a 3-parameter program [Emerson, 1990] for the rHbI PheB10Tyr mutant in the CN complex. These parameters were used to refine the dipolar chemical shift plot an F/n value of 0.16 at 29 protons initial input set data and F/n value of 0.27 at 40 input set data. The rhombic axes for 40 protons input set data are defined by  $\kappa = -1.69 \pm 10^\circ$ , and are correlated to the

**Table 3.11: Chemical shifts contributions for HisF8, GlnE7, TyrB10 and PheE11 distal amino acids in the rHbICN PheB10Tyr mutant**

Residues	Protons	$\delta_{\text{obs}}^{\text{a}}$	$\delta_{\text{sec}}^{\text{b}}$	$\delta_{\text{rc}}^{\text{c}}$	$\delta_{\text{dia}}^{\text{d}}$	$\delta_{\text{dip (obs)}}^{\text{e}}$	$\delta_{\text{dip (calc)}}^{\text{f}}$	$\delta_{\text{hf}}^{\text{g}}$	$\delta_{\text{con}}^{\text{h}}$
His (96)F8	N <sub>p</sub> H	12.10	7.9000	-1.5281	6.3719	5.7281	6.0222	5.7281	-0.2941
	C <sub><math>\alpha</math></sub> H	10.17	4.2000	-1.8245	2.3755	7.7945	7.1168	7.7945	0.6777
	C <sub><math>\beta</math>1</sub> H	10.60	2.6900	-2.0705	0.6195	9.9805	7.0470	9.9805	2.9335
	C <sub><math>\beta</math>2</sub> H	7.84	2.6900	-2.2383	0.4517	7.3883	7.9828	7.3883	-0.5945
	N <sub><math>\delta</math>1</sub> H	14.84	10.3600	-3.1992	7.1608	7.6992	14.6284	7.6992	-6.9292
	C <sub><math>\delta</math>2</sub> H	12.50	7.1100	-7.1818	-0.0718	12.5718	15.0856	12.5718	-2.5138
	C <sub><math>\epsilon</math>1</sub> H	-5.86	8.0700	-6.9342	1.1358	-6.9958	23.5169	-6.9958	-30.5127
Gln (64)E7	N <sub>p</sub> H	8.59	8.1100	-0.3945	7.7155	0.8745	1.2343	0.8745	-0.3598
	C <sub><math>\alpha</math></sub> H	3.98	4.0200	-0.6807	3.3393	0.6407	2.2068	0.6407	-1.5661
	C <sub><math>\beta</math>1</sub> H	2.90	2.1000	-1.5035	0.5965	2.3035	3.6635	2.3035	-1.3600
	C <sub><math>\beta</math>2</sub> H	2.60	2.1000	-0.8277	1.2723	1.3277	2.3898	1.3277	-1.0621
	C <sub><math>\gamma</math>1</sub> H	6.46	2.3800	-2.3817	-0.0017	6.4617	10.4142	6.4617	-3.9525
	C <sub><math>\gamma</math>2</sub> H	4.31	2.3800	-1.4985	0.8815	3.4285	5.8131	3.4285	-2.3846
	N <sub><math>\epsilon</math>1</sub> H	10.66	6.9500	-2.1808	4.7692	5.8908	5.9538	5.8908	-0.0630
	N <sub><math>\epsilon</math>2</sub> H	-3.27	6.9500	-0.3806	6.5694	-9.8394	-1.4117	-9.8394	-8.4277
Tyr(29)B10	N <sub>p</sub> H	8.54	8.0400	-0.8273	7.2127	1.3273	1.2228	1.3273	0.1045
	C <sub><math>\alpha</math></sub> H	4.30	4.1500	-1.5799	2.5701	1.7299	1.5008	1.7299	0.2291
	C <sub><math>\beta</math>1</sub> H	3.43	2.9800	-1.4665	1.5135	1.9165	1.7183	1.9165	0.1982
	C <sub><math>\beta</math>2</sub> H	3.63	2.9800	-0.8938	2.0862	1.5438	1.6200	1.5438	-0.0762
	C <sub><math>\delta</math></sub> H	8.24	7.1500	-1.2120	5.9380	2.3020	2.7638	2.3020	-0.4618
	C <sub><math>\epsilon</math></sub> H	11.60	6.8600	-1.5991	5.2609	6.3391	7.4344	6.3391	-1.0953
	O <sub><math>\eta</math></sub> H	31.00	9.2800	-2.2941	6.9859	24.0141	17.7013	24.0141	6.3128
Phe(68)E11	N <sub>p</sub> H	9.09	8.1900	-0.4966	7.6934	1.3966	1.8863	1.3966	-0.4897
	C <sub><math>\alpha</math></sub> H	3.18	4.1600	0.1071	4.2671	-1.0871	-1.2356	-1.0871	0.1485
	C <sub><math>\beta</math>1</sub> H	5.33	3.0800	-0.0283	3.0517	2.2783	2.6372	2.2783	-0.3589
	C <sub><math>\beta</math>2</sub> H	7.36	3.0800	-1.2725	1.8075	5.5525	7.0157	5.5525	-1.4632
	C <sub><math>\delta</math></sub> H	11.75	7.3000	-1.0980	6.2021	5.5480	5.2196	5.5480	0.3284
	C <sub><math>\epsilon</math></sub> H	9.26	7.3900	-0.0247	7.3654	1.8947	0.1121	1.8947	1.7825
	C <sub><math>\zeta</math></sub> H	7.53	7.3400	-0.0342	7.3058	0.2242	0.0065	0.2242	0.2177

<sup>a</sup> Chemical shift in ppm in H<sub>2</sub>O at pH 7.0 and 25 °C.

<sup>b</sup> Secondary structure chemical shifts in ppm as structural analog [Wishart et al., 1991].

<sup>c</sup> Ring current chemical shift in ppm using ring current program-unix shell system.

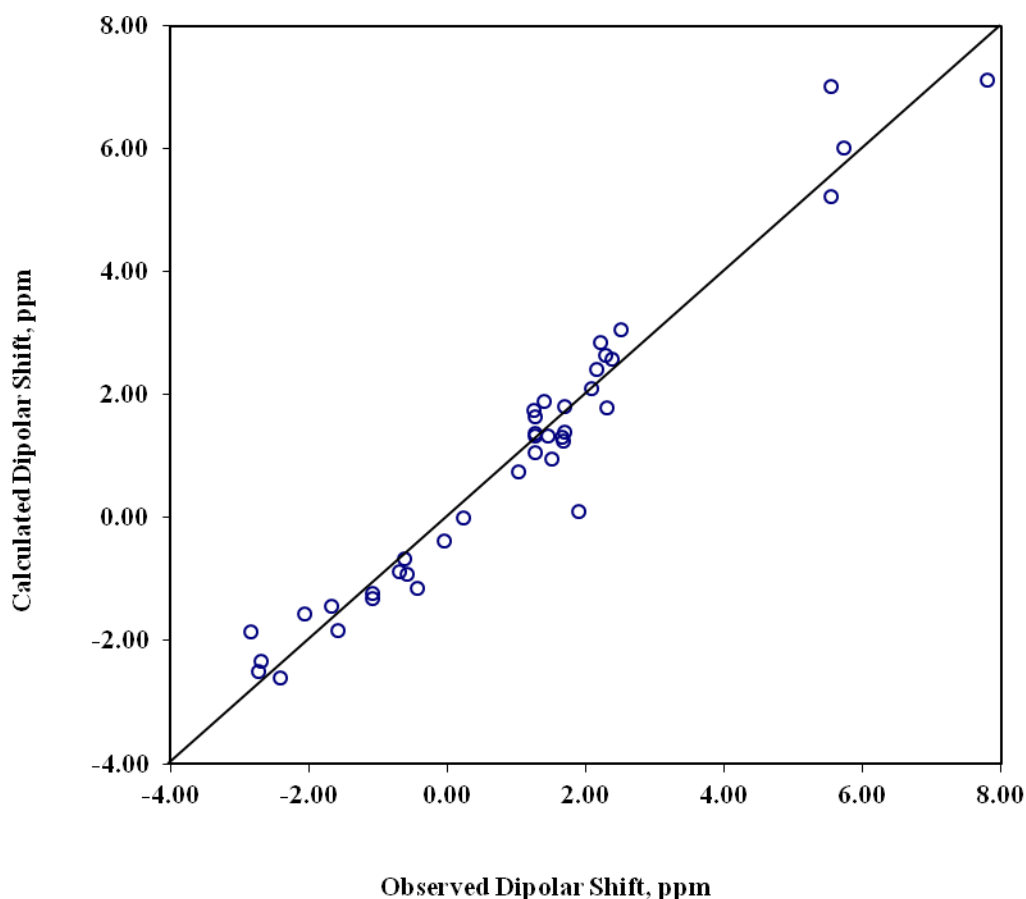
<sup>d</sup> Chemical shift of a diamagnetic structural analog calculated using  $\delta_{\text{sec}} + \delta_{\text{rc}}$ .

<sup>e</sup> Dipolar shifts in ppm at 25 °C as calculated from  $\delta_{\text{obs}} - \delta_{\text{sec}} - \delta_{\text{rc}}$ .

<sup>f</sup> Dipolar shift in ppm calculated from 3 parameters program-  $\alpha=0.10$ ,  $\beta=0.10$ ,  $\kappa=-1.69$ ,  $\Delta\chi_{\text{ax}}=2.48$ ,  $\Delta\chi_{\text{rh}}=-0.58$ , Input Set-40 protons. [Emerson et al., 1990].

<sup>g</sup> Hyperfine shifts in ppm at 25 °C, defined as  $\delta_{\text{con}} + \delta_{\text{dip}}$ .

<sup>h</sup> Contact shifts in ppm at 25 °C obtained from  $\delta_{\text{obs}} - \delta_{\text{dia}} - \delta_{\text{dip (calc)}}$ .



**Input Set:**

**Distal:** Val(39)C4  $\alpha$ ,  $\beta$ ,  $\gamma$ 1,  $\gamma$ 2; Ala(65)E8 NpH,  $\alpha$ ,  $\beta$ ; Ser(67)E10  $\alpha$ ;  
Phe(68)E11 NpH,  $\alpha$ ,  $\beta$ 1,  $\beta$ 2,  $\delta$ 1,  $\epsilon$ 1,  $\zeta$ ; Leu(71)E14  $\alpha$ ,  $\beta$ 2; Val(72)E15  $\alpha$ ,  $\beta$ .

**Proximal:** Phe(92)F4  $\alpha$ ; Ala(93)F5 NpH,  $\alpha$ ,  $\beta$ ; Ala(94)F6 NpH,  $\alpha$ ,  $\beta$ ;  
Asn(95)F7 NpH,  $\alpha$ ; His(96)F8 NpH,  $\alpha$ ; Lys(97)F9  $\alpha$ ,  $\beta$ 1,  $\beta$ 2;  
Ala(98)F10 NpH,  $\alpha$ ,  $\beta$ ; Leu(106)G5  $\alpha$ ; Ala(109)G8 NpH,  $\alpha$ ,  $\beta$ .

**Figure 3.30:** Plot of the  $\delta_{\text{dip}}$  (cal) versus  $\delta_{\text{dip}}$  (obs) for 40 amino acids input data set in *Lucina pectinata* rHb1CN PheB10Tyr at 25°C obtained from the optimized magnetic axes with  $\Delta\chi_{\text{ax}} = 2.48 \times 10^{-9} \text{ m}^3/\text{mol}$ ,  $\Delta\chi_{\text{rh}} = -0.58 \times 10^{-9} \text{ m}^3/\text{mol}$ ,  $\alpha = 0.10^\circ$ ,  $\beta = 0.10^\circ$  and  $\kappa = -1.69^\circ$ . The open circles represent the 40 protons data used as input to determine the magnetic axes. The points for the GlnE7 and TyrB10 spin system protons were not used as input. The solid line represents unit slope for a perfect fit.

**Table 3.12: Euler angles and magnetic anisotropies parameters for the cyanide complex in the rHbI PheB10Tyr mutant.**

<b>Data</b>	<b>CN (pH 7.0, 25°C, <sup>1</sup>H<sub>2</sub>O)</b>	
<i>amino acids input set (N)</i>	29	40
$\alpha$ (°)	0.10	0.10
$\beta$ (°)	1.18	0.10
$\kappa$ (°)	-2.30	-1.69
$\Delta\chi_{ax}$ ( $\times 10^{-9}$ m <sup>3</sup> /mol)	2.48	2.48
$\Delta\chi_{rh}$ ( $\times 10^{-9}$ m <sup>3</sup> /mol)	-0.58	-0.58
<b>Refinement</b>		
<i>Gln(64)E7 angles (°)</i>		
C <sub><math>\alpha</math></sub> -C <sub><math>\beta</math></sub>	-159.91	-146.61
C <sub><math>\beta</math></sub> -C <sub><math>\gamma</math></sub>	56.52	49.30
C <sub><math>\gamma</math></sub> -C <sub><math>\delta</math></sub>	-140.03	81.91
<i>Tyr(29)B10 angle (°)</i>		
C <sub><math>\zeta</math></sub> -OH <sub><math>\eta</math></sub>	-125.01	-71.03
<b>F/n</b>	0.16	0.27

orientation of proximal HisF8 imidazole orientation. The magnetic axes of rHbICN PheB10Tyr predict smaller by ~5-10 ppm upfield or downfield dipolar shifts for the axial HisF8 C<sub>ε</sub>H at -5.86 ppm and C<sub>δ</sub>H at 12.50 ppm than in wtHbICN (C<sub>ε</sub>H at -6.14 ppm and C<sub>δ</sub>H at 18.79 ppm) and accounts the fact of these two broad and strongly relaxed peaks. This plot predicted the favorable amino acid side chain orientations based on the magnetic axes (x\*,y\*,z\*) and anisotropies (χ<sub>ax</sub>, χ<sub>rh</sub>) calculated for the iron-centered reference coordinate system, and the minimum of the global error function, F/n (Δχ<sub>ax</sub>, Δχ<sub>rh</sub>, α, β, γ) in the paramagnetic and diamagnetic complex amino acid sequence.

The analysis of the dipolar shift pattern for individual residues consider the magnitude and direction of the dipolar shifts near the nodal surface for the axial dipolar shift allowing mapping of their orientations in the heme pocket. Based on the wtHbICN crystal coordinates with the original angles, predicted δ<sub>dip</sub> values for the TyrB10 C<sub>ε</sub>H-OH<sub>η</sub> ring at -125.01 ° and GlnE7 C<sub>α</sub>-C<sub>β</sub> at -159.91 °, C<sub>β</sub>-C<sub>γ</sub> at 56.52 °, C<sub>γ</sub>-C<sub>δ</sub> at -140.03 ° side chain protons are illustrated in Figure 3.31. Table 3.12 summaries the refinement data for the original and new angles of the amino acid residues. It is observed that the uniquely placed protons on the GlnE7 result in shifts that are well predicted from original to the new angles, indicating that this residue in rHbI PheB10Tyr shifts close to the propionate groups as Phe was changed by Tyr at B10 position. The GlnE7 N<sub>ε2</sub>H labile proton position is consistent with an upfield shift direction at -3.27 ppm to the crowded aliphatic envelope. In the case of TyrB10, the dipolar shifts are very well predicted for the ring. The TyrB10 OH<sub>η</sub> labile proton position is consistent with a downfield shift direction at 31.00 ppm towards the paramagnetic region. The placement of the TyrB10 OH<sub>η</sub> is calculated as a function of rotation of the dihedral angle between the H-O-C and ring planes leads us to obtain a uniquely spatially located of the labile proton OH<sub>η</sub> in the rHbICN

PheB10Tyr. Figure 3.32 show the dipolar shifts for residues TyrB10 and GlnE7vwith the orientation determined by paramagnetic relaxation, dipolar shifts, and dipolar contacts for *Lucina pectinata* rHbICN PheB10Tyr mutant at 25°C obtained from the optimized magnetic axes with  $\Delta\chi_{ax} = 2.48 \times 10^{-9} \text{ m}^3/\text{mol}$ ,  $\Delta\chi_{rh} = -0.58 \times 10^{-9} \text{ m}^3/\text{mol}$ ,  $\alpha = 0.10^\circ$ ,  $\beta = 0.10^\circ$  and  $\kappa = -1.69^\circ$ . The plot of the  $\delta_{\text{dip}}$  (cal) versus  $\delta_{\text{dip}}$  (obs) illustrated The GlnE7 new angles are  $C_\alpha\text{-}C_\beta = -146.61^\circ$ ,  $C_\beta\text{-}C_\gamma = 49.30^\circ$ ,  $C_\gamma\text{-}C_\delta = 81.91^\circ$ . The TyrB10 new angle is  $C_\zeta\text{H-OH}_\eta = -71.03^\circ$ .

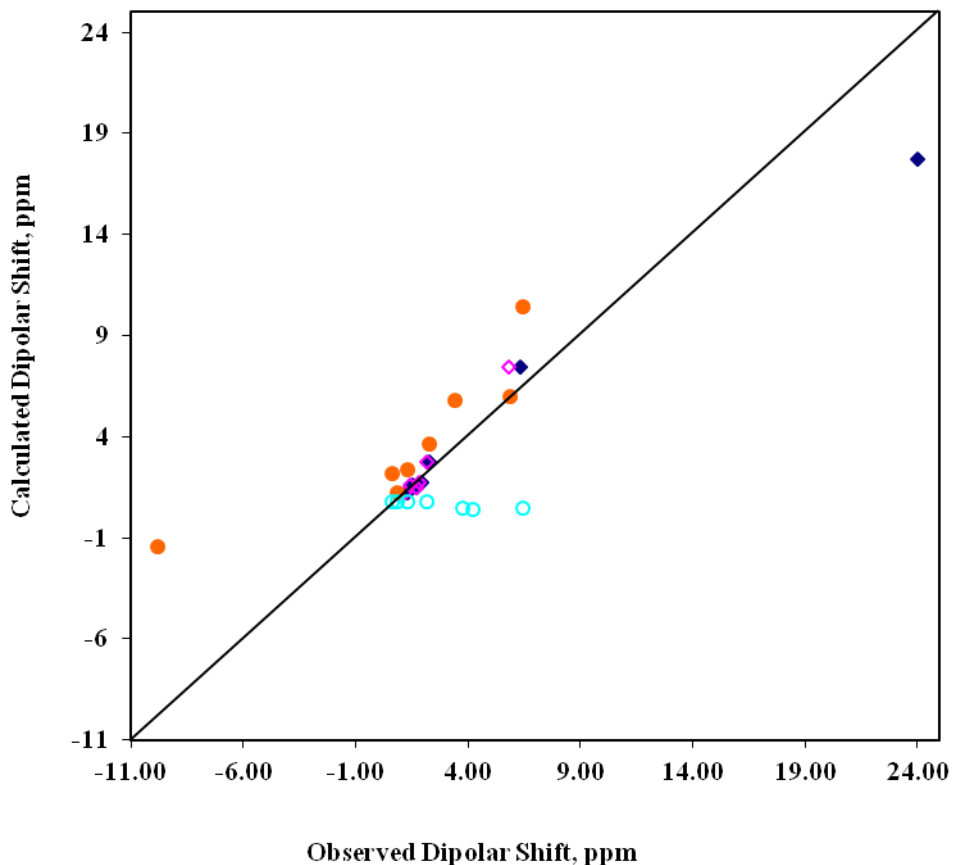


**Figure 3.31:** Plot of the  $\delta_{\text{dip}}$  (cal) versus  $\delta_{\text{dip}}$  (obs) for GlnE7 and TyrB10 distal residues in *Lucina pectinata* rHbICN PheB10Tyr at 25°C obtained from the optimized magnetic axes with  $\Delta\chi_{\text{ax}} = 2.48 \times 10^{-9} \text{ m}^3/\text{mol}$ ,  $\Delta\chi_{\text{rh}} = -0.58 \times 10^{-9} \text{ m}^3/\text{mol}$ ,  $\alpha = 0.10^\circ$ ,  $\beta = 0.10^\circ$  and  $\kappa = -1.69^\circ$ . The aqua open circle ( $\circ$ ) represent the GlnE7 original angles at  $C_\alpha\text{-}C_\beta = -159.91^\circ$ ,  $C_\beta\text{-}C_\gamma = 56.52^\circ$ ,  $C_\gamma\text{-}C_\delta = -140.03^\circ$ . The pink open diamond ( $\diamond$ ) represent the TyrB10 original angles at  $C_\zeta\text{H-OH}_\eta = -125.01^\circ$ . The orange close circle ( $\bullet$ ) represent the GlnE7 new angles at  $C_\alpha\text{-}C_\beta = -146.61^\circ$ ,  $C_\beta\text{-}C_\gamma = 49.30^\circ$ ,  $C_\gamma\text{-}C_\delta = 81.91^\circ$ . The navy blue close diamond ( $\blacklozenge$ ) represent the TyrB10 new angles at  $C_\zeta\text{H-OH}_\eta = -71.03^\circ$ . The solid line represents unit slope for a perfect fit.

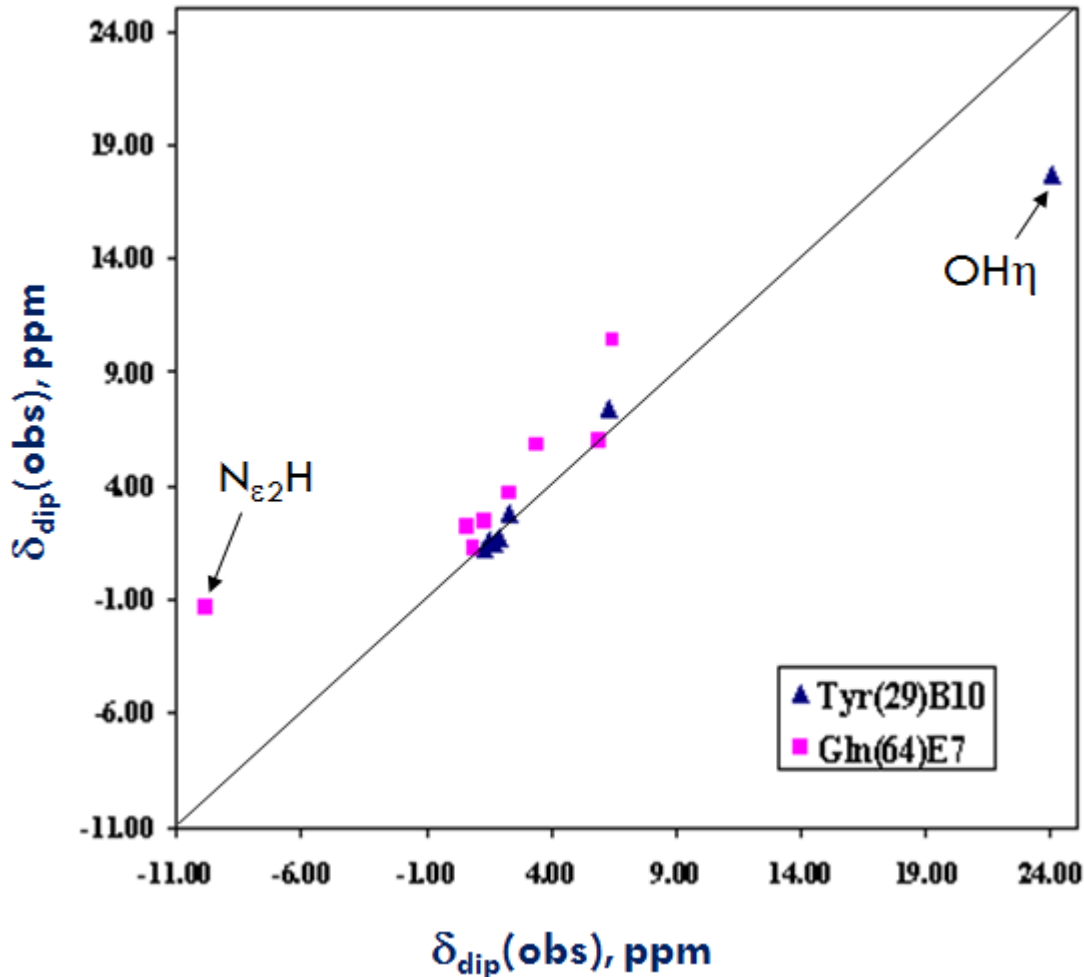


Figure 3.32: Plot of the  $\delta_{\text{dip}}(\text{cal})$  versus  $\delta_{\text{dip}}(\text{obs})$  for GlnE7 and TyrB10 distal residues in *Lucina pectinata* rHbICN PheB10Tyr at 25°C obtained from the optimized magnetic axes with  $\Delta\chi_{\text{ax}} = 2.48 \times 10^{-9} \text{ m}^3/\text{mol}$ ,  $\Delta\chi_{\text{rh}} = -0.58 \times 10^{-9} \text{ m}^3/\text{mol}$ ,  $\alpha = 0.10^\circ$ ,  $\beta = 0.10^\circ$  and  $\kappa = -1.69^\circ$ . The plot illustrated the dipolar shifts for residues TyrB10 (▲) and GlnE7 (■) with the orientation determined by paramagnetic relaxation, dipolar shifts, and dipolar contacts. The GlnE7 new angles are  $C_{\alpha}-C_{\beta} = -146.61^\circ$ ,  $C_{\beta}-C_{\gamma} = 49.30^\circ$ ,  $C_{\gamma}-C_{\delta} = 81.91^\circ$ . The TyrB10 new angle is  $C_{\zeta}H-OH_{\eta} = -71.03^\circ$ . The solid line represents unit slope for a perfect fit.

## CHAPTER 4: DISCUSSION

The Nuclear Magnetic Resonance spectroscopic studies presented herein establish structural details of how aspects of the local structure in the recombinant hemoglobin I heme pocket from *Lucina pectinana* modulate ligand binding. Specifically, the structural mapping of rHbICN, rHbICN PheB10Tyr single point mutation, and rHbIH<sub>2</sub>S elucidate (a) the constraints related to the heme pocket conformation as consequence of PheB10Tyr mutation, (b) the distal amino acids orientations in the heme pocket, (c) the role of propionate heme groups in the ligand binding, (d) the interactions that control the stabilization of the bound ligand in the active center, (e) the effect of the ligand reactivity in the heme group oxidative state, and (f) the structure-activity relationship in the functionality of the heme protein.

### **4.1 Recombinant PheB10Tyr mutant *Lucina pectinana* HbI expression and purification**

The development of site-directed mutant as PheB10Tyr in the recombinant hemoglobin I (rHbI) from *Lucina pectinana* allowed to build a detailed knowledge about the structural determinants that regulate ligand binding in the active site of the protein [Leon, et.al., 2004]. The successful expression in large quantities of the rHbI PheB10Tyr is a first step toward the spectroscopic approaches. Recombinant HbI PheB10Tyr mutant was expressed in large quantities using an improved fermentation process [Ramos et al., 2010]. The expression of rHbI PheB10Tyr mutant in a 5 L bioreactor yielded the protein by transforming rHbI PheB10Tyr cDNA into the *Escherichia coli* BLi5 cells, inducing and supplementing the culture with 1 mM IPTG, 30.0 µg/mL hemin chloride and 1% glucose. The results indicated that controlling the growth conditions of the *Escherichia coli* cells is the key to obtaining high culture density of the

recombinant and mutant HbI from *L. pectinata*. Furthermore, an affinity, desalting, and size-exclusion combined chromatography techniques improved the quality of NMR spectrum avoiding large accumulation of ionic residues (e.i. imidazole and salts) that can otherwise be extremely sensitive to the magnetic fields. The results indicated that the purification process provided a complete stable purified protein ready to concentrate and use for NMR spectroscopic studies. The UV-Vis spectroscopy results confirmed a functional recombinant protein.

## 4.2 Heme propionate hydrogen bonding network loop in the cyanide moiety

The  $^1\text{H}$ -NMR spectrum of rHbICN PheB10Tyr confirms a strong downfield shift for the 6- $\text{H}_\alpha/\text{H}_\alpha'$  propionate with peaks at 7.23 and 19.90 ppm. Saturation transfer between amide,  $\text{N}_\epsilon\text{H}$ , in the glutamine E7 distal residue in rHbICN PheB10Tyr reveals strong and moderate NOEs connections with the 6-propionate  $\text{C}_\beta\text{H}/\text{C}_\beta'\text{H}$ , respectively. The structural behavior of the distal residues and the heme group in the active center was established by the NOESY cross-peak and NOE patterns including the paramagnetic relaxation properties, distinctive of the heme iron with 6<sup>th</sup> coordinate cyanide axial ligand [La Mar et al., 2000]. The interactions that involve the peripheral groups in the heme via NOE showed a stable contribution in the rHbICN PheB10Tyr moiety. Regarding this, structural changes are revealed throughout major NOEs connections of the TyrB10-OH $_\eta$  at 31.00 ppm with GlnE7-C $_{\gamma 1}\text{H}/\text{C}_{\gamma 2}\text{H}$  at 6.46/4.31 ppm and PheE11-C $_{\beta 1}\text{H}/\text{C}_{\beta 2}\text{H}$  at 5.33/7.36 ppm. Figure 4.1 shows a schematic that describes the heme cavity in *Lucina pectinata* rHbICN PheB10Tyr mutant with the distal residues in contact with the heme, using iron-centered reference coordinate system ( $x'$ ,  $y'$ ,  $z'$ ) for a porphyrin and defines the orientation of the axial His plane by the position of helices relative to the  $x'$ -axis [La Mar et al., 2000].

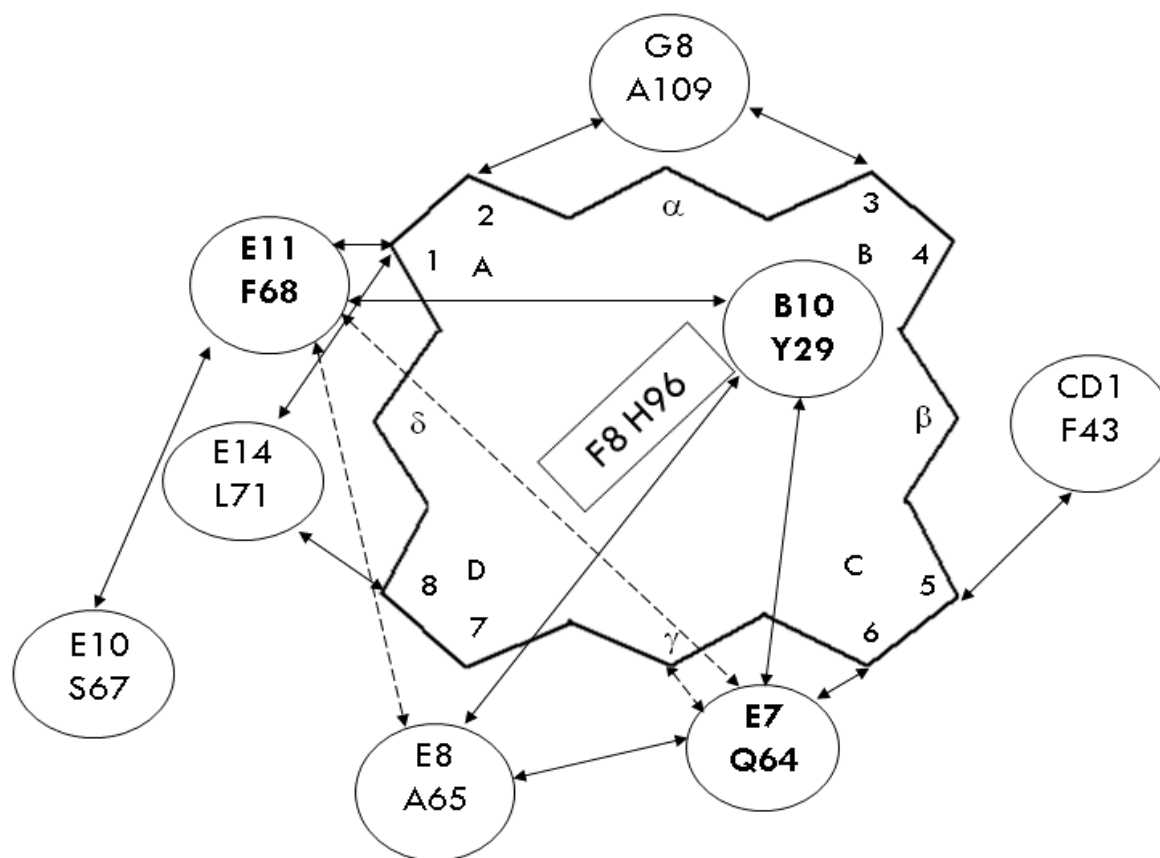


**Figure 4.1:** Schematic representation of the distal heme pocket of rHbICN PheB10Tyr mutant showing major NOE dipolar contacts between distal residues (circles) and heme group. The NOEs connectivities are illustrated using double arrows where dashed (---) and solid (-) lines enclose the moderate and strong dipolar contacts, respectively. The heme group is located face-on view from the proximal side HisF8. The amino acids are labeled using the one-letter code, helix and sequence position. [Ramos et al., 2012]

The dipolar contacts are shown using double arrows where dashed and solid lines enclose the moderate and strong dipolar contacts, respectively. As illustrated, the single PheB10Tyr mutation promotes a constrained heme pocket through structural conformational changes that include significant movements of the key distal side chains residues GlnE7 and PheE11 in the active center. A change in orientation is observed for GlnE7 as well as the 6-propionate group, which allows dipole interactions. Rotation of the heme 6-propionate group has also been observed in the photosynthetic cytochrome C6 Q51V variant from *Phormidium laminosum*, which showed that the axial Met ligand was stabilized through polar interactions with the imidazole and heme 6-propionate. The latter was possible owing to a 180 ° rotation of both heme propionates upon imidazole binding [Rajagopal et al., 2011].

The detection of strong NOESY cross peaks between the C<sub>δ</sub>H and the adjacent C<sub>ε</sub>H on the PheE11 aromatic ring at 11.75 and 9.26 ppm reveals strong displacement of the ring with respect to its native structure that have ring signals at 7.47 and 7.53 ppm [Nguyen et al., 1998]. Based on this, we suggest that the side chain of phenylalanine E11 swing 3.91 Å close to the ligand in the heme pocket compared to the native HbICN complex as consequence of PheB10 substitution. Conserved residues such as PheCD1, AlaE8, LeuE14, AlaG8 and SerE10 are shown as probe for the sequence specific assignment through the NOE connectivities. These dipolar interactions in the distal cavity determine the geometry and properties of the active heme center for the rHbICN PheB10Tyr variant. Moreover, the X-ray crystal structure of the HbII-HbIII cyanide complex from *Lucina pectinata*, which has the same active center as rHbICN PheB10Tyr, shows that the 6-propionate and the GlnE7 residue have H-bonding orientation with distances between the 6-propionate C<sub>β</sub> and the GlnE7N<sub>ε2</sub> of 4.37 Å in HbII chain A and 4.32 Å in HbIII chain B and between the 6-propionate C<sub>β</sub> and GlnE7O<sub>ε1</sub> of 3.49 Å in HbII chain A and 3.58 Å in HbIII chain

B (data unpublished). Taken together, the results suggest that the dipolar contacts between the GlnE7 distal residue and the 6-propionate group are due to the tyrosine at the B10 position and that this residue is responsible for the new electrostatic interactions. Thus, a hydrogen bonding network is established in the distal region between the GlnE7 and 6-propionate group in rHbICN PheB10Tyr relative to the axial His plane, due to the electron withdrawing character of the hydrogen bonding, which contribute significantly to the modulation the heme iron electron density. This hydrogen bonding network loop between propionate, heme ligand and nearby amino acids support the fact that the heme reduction potentials are in part controlled by the interaction of the propionates and the nearby electronic environments [Warren et al., 2011]. Figure 4.2 shows a stereo diagram of the distal active site heme pocket illustrating the orientation of the GlnE7, TyrB10 and propionate 6-H as determined by NMR.

Analyses of the resonance Raman spectra of deoxyHbI, metcyano, carbonmonoxy, and oxy HbI derivatives have suggested the presence of moderate hydrogen bonding between Arg-99 and the heme-7-propionate. However, <sup>1</sup>H-NMR indicated that hydrogen bonding between the heme-6-propionate and amino acid residues is absent [Silfa et al. 1997]. The flexibility of the heme-6-propionate observed in the rHbICN PheB10Tyr variant suggest that hemeproteins with the same electrostatic environment have the ability to induce a hydrogen bonding network loop between GlnE7, TyrB10, 6-propionate group, and the heme ligand. We suggest that for these systems the hydrogen bonding network may help to create a driving force that may modify the oxygen-heme reactivity, activate the heme chemical environment, and regulates the iron electron density of the heme, facilitating in turn oxygen metabolism. Hence, for *L. pectinata* HbII and HbIII as well as other truncated hemoglobins (trHbs) this network might activate O<sub>2</sub> delivery and chemistry. Indeed, the X-ray crystal structure of the trHb from the green algae *Chlamydomonas*

*eugametos* with cyanide as ligand (trHbC-CN<sup>-</sup>) (PDB: 1DLY) strongly suggest H-bonding networks between GlnE7, TyrB10, 6-propionate group, and the bound ligand, which can modulate O<sub>2</sub> metabolism [Egawa et al., 2005]. Analysis of the structure indicates distances for polar contacts between the 6-propionate C<sub>β</sub> and the GlnE7N<sub>ε2</sub> at 4.87 Å, the 6-propionate C<sub>β</sub> and GlnE7O<sub>ε1</sub> at 4.15 Å, TyrB10OH<sub>η</sub> and GlnE7C<sub>γ</sub> at 3.44 Å, and TyrB10OH<sub>η</sub> and CN<sup>-</sup> at 2.36 Å [Pesce et al., 2000]. Similarly, a sperm whale myoglobin mutant having GlnE7 and TyrB10 (PDB: 1F63) and the hemoglobin from *Ascaris suum* (PDB: 1ASH), which naturally bears these two residues at the distal site show distances between the heme 6-propionate and nearby residues that can induce the H-bonding network mentioned above [Zhang et al., 1997]. For instance, in the Mb mutant, designated to mimic the distal pocket of oxy-*Ascaris suum* Hb, possible hydrogen bonding interactions between 6-propionate C<sub>β</sub> and the GlnE7N<sub>ε2</sub>, 6-propionate C<sub>β</sub> and GlnE7O<sub>ε1</sub>, and TyrB10OH<sub>η</sub> and GlnE7C<sub>γ</sub> are observed with X-ray distance of 4.54, 3.63, and 4.10 Å, respectively [Brunori et al., 1999; Yang et al., 1995]. It is important to mention that the reactivity and affinity of these proteins for O<sub>2</sub> have been attributed to the H-bonding network between the TyrB10/GlnE7 pair. However, as we have shown, interactions of this pair with flexible propionates groups should also be taken into account when analyzing the metabolism of O<sub>2</sub> with these proteins.

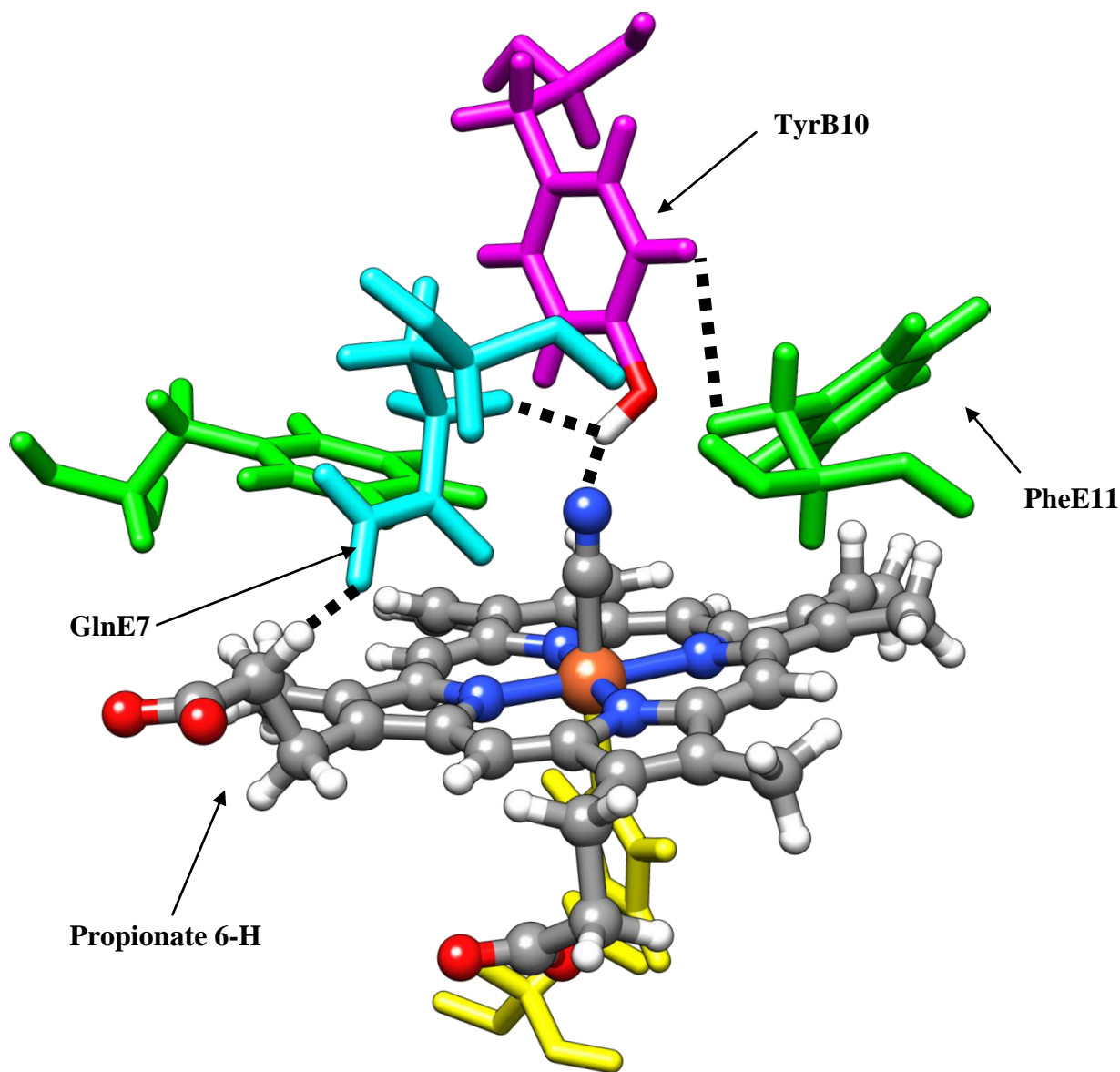


**Figure 4.2:** Model of the distal heme pocket of rHbICN PheB10Tyr mutant showing the representation of the TyrB10 mutated residue and GlnE7 as elucidated by NMR spectroscopy. The amino acids are labeled using the one-letter code, helix and sequence position. The dashed lines represent the hydrogen bonding network inter-residue and residue-heme interactions.

### 4.3 Distinctive magnetic field of the H<sub>2</sub>S influences distal structural geometry in hemeproteins.

The <sup>1</sup>H-NMR results obtained with the ferric rHbI derivatives, which are illustrated in figure 3.24, show that ligand binding magnetic properties provokes differences in the molecular and electronic heme pocket structure. These properties influence directly or indirectly the extent of interaction of CN<sup>-</sup> and H<sub>2</sub>S with the ferric iron center. The spectral interpretation reveal that hydrogen sulfide derivative have a weak low spin paramagnetic behavior relative to the strong field cyanide ligand. The common features of the hydrogen sulfide binding properties of the rHbI are Fe<sup>III</sup>-H<sub>2</sub>S polar bond, H from the H<sub>2</sub>S serving as an H-bond donor, and H<sub>2</sub>S has a magnetic spin value of the  $S = \frac{1}{2}$ . The studies of these magnetic properties of H<sub>2</sub>S molecule are applied to the study of those parameters that determine an observed NMR signal: the magnetizability, the nuclear shielding, and the indirect spin-spin coupling constants.

The electronic contact upon H<sub>2</sub>S binding is observed when anisotropic effect was generated by the electron density of the iron in the heme and the phenyl ring current of the “Phe cage” characteristic in the rHbI hemepocket. The hyperfine shifts suggested that the C<sub>6</sub>H is oriented close enough to be in contact with the bound H<sub>2</sub>S ligand. The presence of the electronic interaction of the phenyl ring with the ligand suggested an increase H<sub>2</sub>S affinity through multipolar interaction in the heme pocket. As a result, an alternate conformation mechanism is observed between H<sub>2</sub>S and CN<sup>-</sup> ligand where the GlnE7 has the ability to change its geometrical orientation relative to the heme normal as function of the bound ligand [Ramos-Santana, 2003]. Figure 4.3 show a stereo diagram of the heme pocket of the HbIH<sub>2</sub>S and HbICN illustrating the characteristic of GlnE7 as a proton acceptor or donator group.

#### 4.4 H<sub>2</sub>S interaction with ferric rHbI derivative

Comparative <sup>1</sup>H-NMR structural analysis of rHbIH<sub>2</sub>S and HbIH<sub>2</sub>O achieves insight about the conformation that it is adopted in the distal heme pocket. Saturation of the rHbI with H<sub>2</sub>S confirms the dependable concentration of the hydrogen sulfide as a ligand. Figure 3.25 shows the isotopic effect in rHbIH<sub>2</sub>S and rHbIH<sub>2</sub>O derivatives in <sup>2</sup>H<sub>2</sub>O. These complexes differ from HbICN in that they decreased resolution for the heme signals at the higher field due to Curie relaxation. Two possible electron configurations with unpaired spin into both  $\sigma$  and  $\pi$  bonding orbitals, and hence contact shifts are expected to reflect some combinations of  $\sigma$  and  $\pi$  spin delocalization. The presence of high spin (HS) iron(II) exhibits strong downfield chemical shifts signals between 20 to 100 ppm, poor resonance lines resolution and heme methyl with T<sub>1</sub>s ~50 ms. Then, it will be suggested that a mixture between two species, high spin (HS) and low spin (LS) predominate according to the similar behavior observed in the spectra of the rHbIH<sub>2</sub>S and rHbIH<sub>2</sub>O. As opposed to CN binding, there is not a direct correlation between dipolar contact indicative of electrostatic interactions in the heme pocket of the H<sub>2</sub>S derivative suggesting that its behavior may also be governed by an reduction ( $\text{Fe}^{(\text{III})} \rightarrow \text{Fe}^{(\text{II})}$ ) of the iron center. In this regard, the hypothesized reactions of H<sub>2</sub>S with hemoproteins suggested by Pietri and coworkers, in where the electron transfer process is greatly enhanced at high H<sub>2</sub>S concentrations and in those variants having proton acceptor groups near the bound H<sub>2</sub>S will be dominated in the system.

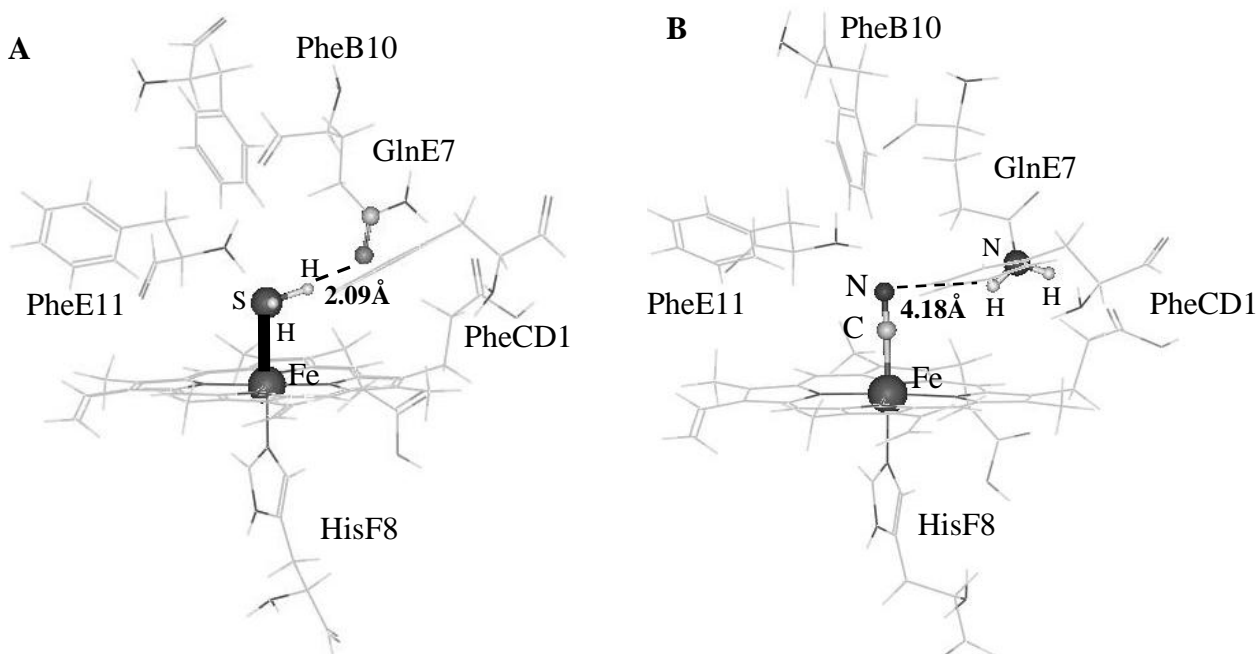


**Figure 4.3: Stereo diagram of the heme pocket of the A) HbISH<sub>2</sub> and B) HbICN showing the position of the ligand and orientation of distal GlnE7. Structure A illustrate the distal H-bond, with a GlnC=O···HSH distance at 2.09Å. Structure B shows the non-hydrogen bonding GlnNH CN···distance at 4.18Å. The amino acids are labeled using the one-letter code, helix and sequence position.**

## CHAPTER 5: CONCLUSIONS AND OUTLOOK

The characterization of key residues such as TyrB10, GlnE7, HisF8, PheCD1, PheE11 in the distal site, the heme pocket resonances signals, and the interaction sites between them by using direct and transferred NMR-based approach described above rapidly provide information on possible: (a) targeting of peripheral groups, 6-H and 7-H propionate group, as a threshold in hemeproteins reactivity, and (b) stimulating electron transfer in the iron reduction process under physiological conditions. Detailed magnetic axes calculations of the spin distribution in the low-spin ferric heme have shown the dipolar correlation to spin density on the heme periphery and distal site orientation. Current research effort was focused on determining a fine structure that evidences the structural determinants in hemoglobins like a hydrogen bonding network. The combination of bioinformatics, sequences analysis, X-Ray Structures, and NMR spectroscopy in one and two dimension generated a number of answers for our questions, but at the same time pop-up other questions about the structure-function relationship in hemoproteins. Overall, NMR spectroscopy has been playing a significant role in the structural elucidation of hemoproteins, especially in the determination of the heme cavity structure of hemoglobin I from *Lucina pectinata* in solution.

Some futures works that will be performed are:

- (1) The electron transfer process inside of the heme pocket from *L. pectinata* can be analyzed by Electron Paramagnetic Resonance (EPR) technique. These studies will be performed on based to the HbI capability to react with hydrogen sulfide under solution conditions in presence and absent of oxygen environment.
- (2) For recombinant proteins that can be obtained from bacterial expression systems (mainly *E. coli*), enrichment of protein samples with  $^{15}\text{N}$  and  $^{13}\text{C}$  nuclei (labeling proteins) to explore the

magnetization transfer between neighboring  $^1\text{H}$ ,  $^{15}\text{N}$  and  $^{13}\text{C}$  nuclei in heme protein moiety, and after the assignments for most hydrogen resonances applied 3D or 4D version of the 2D [ $^1\text{H}$ - $^1\text{H}$ ] NOESY experiment to minimize the problem of resonance overlapping in the heme protein. Also, triple resonance techniques generally require  $^1\text{H}$ ,  $^{13}\text{C}$  and  $^{15}\text{N}$  chemical shift assignment in a proton.

## BIBLIOGRAPHY

- Alyakrinskaya, I. O. Tissue Hemoglobins in Bivalvia (Mollusca). *Biol. Bull.* **2003**, 6, 735-746.
- Antommattei-Pérez, F.M.; Rosado-Ruiz, T.; Cadilla, C. L.; López-Garriga, J. The cDNA-Derived Amino Acid Sequence of Hemoglobin I from *Lucina pectinata*. *J. Protein Chem.* **1999**, 18(8), 831-836.
- Bolognesi, M.; Rosano, C.; Romeo, L.; Borráis, A.; Rizzi, M.; Wittenberg, J.B. Bofii, A.; Ascenzi, P. Cyanide Binding to *Lucina pectinata* Hemoglobin I and to Sperm Whale Myoglobin: An X-ray Crystallographic Study. *Biophys. J.* **1999**, 77, 1093-1099.
- Brunori, M.; Cutruzzola, F.; Savino, C.; Travaglini-Allocatelli, C.; Vallone, B.; Gibson, Q. H. Crystal structure of deoxy sperm whale myoglobin mutant Y(B10)Q(E7)R(E10). *Biophys. J.* **1999**, 76, 1259-1269.
- Cerda-Colón, J. F.; Silfa, E.; López-Garriga, J. Unusual Rocking Freedom of the Heme in the Hydrogen Sulfide-Binding Hemoglobin from *Lucina pectinata*. *J. Am. Chem. Soc.* **1998**, 120, 9312-9317.
- Collazo, E.; Pietri, R.; De Jesús, W.; Ramos, C.; Del Toro, A.; León, R.G.; Cadilla, C. L.; López-Garriga, J. Functional Characterization of the Purified Holo Form of Hemoglobin I from *Lucina pectinata* Overexpressed in *Escherichia coli*. *J. Protein.* **2004**, 23, 239-245.
- Collman, J. P.; Ghosh, S.; Dey, A.; Decréau, R. A. Using a functional enzyme model to understand the chemistry behind hydrogen sulfide induced hibernation. *PNAS* **2009**, 106(52), 22090-22095.
- Egawa, T.; Yeh, Syun-Ru. Structural and functional properties of hemoglobins from unicellular organisms as revealed by resonance Raman spectroscopy. *J. Inorg. Biochem.* **2005**, 99, 72-96.
- Emerson, S. D.; La Mar, G. N. NMR determination of the orientation of the magnetic susceptibility tensor in cyano met-myoglobin: a new probe of steric tilt of bound ligand. *Biochemistry* **1990**, 29, 1556-1566.
- Emerson, S. D., La Mar, G.N. Solution Structural Characterization of Cyanometmyoglobin: Resonance Assignment of Heme Cavity Residues by Two-Dimensional NMR. *Biochemistry* **1990**, 29(6), 1545-1556.

Freeman, R. Handbook of Nuclear Magnetic Resonance. Review by: Dybowski, C. Delaware, United State, **1987**; Vol. 60, No. 22.

Frenkiel, L.; Gros, O.; Moueza, M. Storage tissue and reproductive strategy in *Lucina pectinata* (Gmelin), a tropical lucinid bivalve adapted to a reducing sulfur-rich, mangrove environment. *Invertebr. Reprod. Dev.* **1997**, 31:1-3, 1992-210.

Friebolin, H. *Basic One- and Two- Dimensional NMR Spectroscopy*, Third Revised Edition; Wiley-VCH: Federal Republic of Germany, **1998**.

Gao, Y.; El- Mashtoly, S. F.; Pal, B.; Hayashi, T.; Harada, K.; Kitagawa, T. Pathway of Information Transmission from Heme to Protein upon Ligand Binding/Dissociation in Myoglobin Revealed by UV Resonance Raman Spectroscopy. *J. Biol. Chem.* **2006**, 281, 24637-24646.

Gavira, J. A.; Camara- Artigas, A.; De Jesús- Bonilla, W.; López- Garriga, J.; Lewis, A.; Pietri, R.; Yeh, S-R.; Cadilla, C. L.; García- Ruiz, J. M. Structure and Ligand Selection of Hemoglobin II from *Lucina pectinata*. *J. Biol. Chem.* **2008**, 283, 9414-9423.

Guallar, V.; Olsen, B. The role of the heme propionates in heme biochemistry. *J. Inorg. Biochem.* **2006**, 100, 755-760.

Guo, W.; Kan, J-t.; Cheng, Z-y.; Chen, J-f.; Shen, Y-q. Xu, J.; Wu, D.; Zhu, Y-z. Hydrogen Sulfide as an Endogenous Modulator in Mitochondria and Mitochondria Dysfunction. *Oxid. Med. Cell. Longev.* **2012**, 1-9.

Hayashi, T.; Harada, K.; Sakurai, K.; Shimada, H.; Hirota, S. A Role of the Heme-7-Propionate Side Chain in Cytochrome P450cam as a Gate for Regulating the Access of Water Molecules to the Substrate-Binding Site. *J. Am. Chem Soc.* **2009**, 131(4), 1398-1400.

Hayashi, T.; Matsuo, T.; Hitomi, Y.; Okawa, K.; Suzuki, A.; Shiro, Y.; Iizuka, T.; Hisaeda, Y.; Ogoshi, H. Contribution of heme-propionate side chains to structure and function of myoglobin: chemical approach by artificially created prosthetic groups. *J. Inorg. Biochem.* **2002**, 91, 94-100.

Hockenhull-Johnson, J.D.; Stern, M.S.; Martin, P.; Dass, C.; Desiderio, D.M.; Wittenberg, J.B.; Vinogradov, S.N.; Walz, D.A. The amino acid sequence of hemoglobin II from the symbiont-harboring clam *Lucina pectinata*. *J Protein Chem.* **1991**, 10(6), 609-22.

Hockenhull-Johnson, J.D.; Stern, M.S.; Wittenberg, J.B.; Vinogradov, S.N.; Kapp, O.H.; Walz, D.A. The amino acid sequence of hemoglobin III from the symbiont-harboring clam *Lucina pectinata*. *J Protein Chem.*, **1993**, 12(3), 261-77.

Hus, J-C.; Prompers, J. J.; Brüschweiler, R. Assignment Strategy for Proteins with known Structure. *J. Magn. Reson.* **2002**, 157, 119-123.

Keifer, P. A. Pulse Width Calibrations: How to Read a Pulse Width Array. *Concepts in Magnetic Resonance* **1998**, 11(3) 165-180.

Kraus, D. W.; Wittenberg, J. B. Hemoglobins of the *Lucina pectinata*/Bacteria Symbiosis: I. Molecular Properties, kinetics and Equilibria of Reactions with Ligands. *J. Biol. Chem.* **1990**, 265(27), 16043-16053.

Kraus, D. W.; Wittenberg, J. B. Hemoglobins of the *Lucina pectinata*/Bacteria Symbiosis: II. An Electron Paramagnetic Resonance and Optical Spectral Study of the Ferric Proteins. *J. Biol. Chem.* **1990**, 265(27), 16054-16059.

La Mar, G. N.; Satterlee, J. D.; De ropp, J. S. Nuclear Magnetic Resonance of Hemoproteins. The Porphyrin Handbook; Kadish, K. M., Smith, K. M.; Guillard, R. (Eds): Academic Press **2000**; Chapter 37, Vol. 5. pp. 185-296.

León, R. G.; Munier- Lehmann, H.; Barzu, O.; Baudin- Creuza, V.; Pietri, R.; López- Garriga, J.; Cadilla, C. L. High- level production of recombinant sulfide- reactive hemoglobin I from *Lucina pectinata* in *Escherichia coli* High yields of fully functional holoprotein synthesis in the BLi5 *E. coli* strain. *Protein Expr. Purif.* **2004**, 38(2), 184-195.

Lu, C.; Egawa, T.; Wainwright, L. M.; Poole, R. K.; Yeh, S-R. Structural and Functional Properties of a Truncated Hemoglobin from a Food-Borne Pathogen *Campylobacter*. *J. Biol. Chem.* 2007, 282(18), 13627-13636.

Nguyen, B. D.; Zhao, X.; Vyas, K.; La Mar, G. N.; Lile R. A.; Brucker, E. A.; Phillips, G. N.; Olson, J.H.; Wittenberg, J. Solution and Crystal Structures of a Sperm Whale Myoglobin Triple Mutant that Mimics the Sulfide- binding Hemoglobin from *Lucina pectinata*. *J. Biol. Chem.* **1998**, 273, 9517-9526.

Olson, K. Hydrogen sulfide: both feet on the gas and none on the brake?. *Physiol.* **2013**, 4, 1-3.

Ouellet, H., Juszczak, L., Dantsker, D., Samuni, U., Ouellet, Y.H., Savard, P., Wittenberg, J.B., Wittenberg, B.A., Friedman, J.M., and Guertin, M. Reactions of *Mycobacterium tuberculosis* truncated hemoglobin O with ligands reveal a novel ligand- inclusive hydrogen bond network. *Biochemistry* **2003**, 42, 5764-5774.

Ouellet, H., Ouellet, Y.H., Richard, C., Labarre, M., Wittenberg, B.A., Wittenberg, J.B., and Guertin, M. Truncated hemoglobin HbN protects *Mycobacterium bovis* from nitric oxide. *Proc. Natl. Acad. Sci.* **2002**, 99, 5902-5907.

Pellecchia, M. Solution Nuclear Magnetic Resonance Spectroscopy Techniques for Probing Intermolecular Interactions. *Chem. Biol.* **2005**, 12, 961-971.

Pesce, A.; Couture, S.; Dewilde, S.; Guertin, M.; Yamauchi, K.; Ascenzi, P.; Moens, L.; Bolognesi, M. X-Ray crystal structure of hemoglobin from the green unicellular alga *Chlamydomonas eugametos*. *EMBO J.* **2000**, 19, 2424- 2434.

Peterson, E. S.; Huang, S.; Wang, J.; Miller, L. M.; Vidugiris, G.; Kloek, A. P.; Goldberg, D. E.; Chance, M. R.; Wittenberg, J. B.; Friedman, J. M. A Comparison of Functional and Structural Consequences of the Tyrosine B10 and Glutamine E7 Motifs in Two Invertebrate Hemoglobins (*Ascaris suum* and *Lucina pectinata*). *Biochemistry* **1997**, 36, 13110-13121.

Pietri, R.; Granell, L.; Cruz, A.; De Jesús, W.; Lewis, A.; León, R.; Cadilla, C. L.; López-Garriga, J. Tyrosine B10 and heme-ligand interactions of *Lucina pectinata* hemoglobin II: control of heme reactivity. *Biochim. Biophys. Acta.* **2005**, 1747, 195-203.

Pietri, R.; León, R. G.; Kiger, L.; Marden, M. C.; Granell, L. B.; Cadilla, C. L.; López- Garriga, J. Hemoglobin I from *Lucina pectinata*: A model for distal heme-ligand control. *Biochim. Biophys. Acta.* **2006**, 1764, 758-765.

Pietri, R.; Lewis, A.; León, R. G.; Casabona, G.; Kiger, L.; Yeh, S-R.; Fernández-Alberti, S.; Marden, M. C.; Cadilla, C. L.; López- Garriga, J. Factors Controlling the Reactivity of Hydrogen Sulfide with Hemeproteins. *Biochemistry* **2009**, 48(22), 4881-94.

Pietri, R.; Román-Morales, E.; López-Garriga, J. Hydrogen Sulfide and Hemeproteins: knowledge and Mysteries. *Antioxid. Redox Sign.* **2011**, 15, 393-404.

Predmore, B. L.; Lefer, D. J.; Gojon, G. Hydrogen Sulfide in Biochemistry and Medicine. *Antioxid. Redox Sign.* **2012**, 119-140.

Rajagopal, B. S.; Wilson, D. S.; Bendall, C. J.; Worrall, J. A. R. Structural and kinetic studies of imidazole binding to two members of the *cytochrome c6* family reveal an important role for a conserved heme pocket residue. *J. Biol. Inorg. Chem.* **2011**, 577-588.

Ramírez, E.; Cruz, A.; Rodríguez, D.; Uchima, L.; Pietri, R.; Santana, A.; López-Garriga, J.; López, G. E. Effects of active site mutations in haemoglobin I from *Lucina pectinata*: a molecular dynamic study. *Mol. Simul.* **2008**, 34, 715-725.

Ramos, C.; Pietri, R.; Lorenzo, W.; Román, E.; Granell, L. B.; Cadilla, C. L.; López-Garriga, J. Recombinant Hemoglobin II from *Lucina pectinata*: A Large-Scale Methods for Hemeprotein Expression in *E. coli*. *Protein J.* **2010**, 29(2), 143-151.

Ramos- Santana, B. J. A Nuclear Magnetic Resonance Investigation of the Influence of Distal Glutamine on Structural Properties of *Lucina pectinata* Hemoglobin I. M. S. Thesis, University of Puerto Rico Mayagüez Campus, May **2003**.

Ramos-Santana, B. J.; López- Garriga, J. Tyrosine B10 triggers a heme propionate hydrogen bonding network loop with glutamine E7 mioety. *Biochem. Biophys. Res. Commun.* **2012**.

Read, K. R. H. The Hemoglobin of the Bivalve Mollusc *Phacoides pectinatus* Gmelin. *Bio. Bull.* **1962**, 123, 605-617.

Rizzi, M.; Wittenberg, J. B.; Coda, A.; Fasano, M.; Ascenzi, P.; Bolognesi, M. Structure of the Sulfide-reactive Hemoglobin I from the Clam *Lucina pectinata*. *J. Mol. Biol.* **1994**, 244, 86-99.

Rizzi, M.; Wittenberg, J. B.; Coda, A.; Fasano, M.; Ascenzi, P.; Bolognesi, M. Structure Bases of sulfide Recognition in *Lucina pectinata* Hemoglobin I. *J. Mol. Biol.* **1996**, 258,1-5.

Román-Morales, E.; Pietri, R.; Ramos-Santana, B.; Vinogradov, S. N.; Lewis- Ballester, A.; López- Garriga, J. Structural determinants for the formation of sulfhemeprotein complexes. *Biochem. Biophys. Res. Commun.* **2010**, 400, 489-492.

Rule, G.; Hitchens, T. K. Practical Aspects of Acquiring NMR Spectra. Fundamentals of Protein NMR Spectroscopy. Springer: Netherlands, **2006**; Chapter 2, Vol. 5, pp.29-64.

Rule, G.; Hitchens, T. K. Practical Aspects of N-Dimensional Data Acquisition and Processing. Fundamentals of Protein NMR Spectroscopy. Springer: Netherlands, **2006**; Chapter 15, Vol. 5, pp.313-351.

Rule, G.; Hitchens, T. K. Resonance assignments: Homonuclear Methods. Fundamentals of Protein NMR Spectroscopy. Springer: Netherlands, **2006**; Chapter 13, Vol. 5, pp.251-275.

Schneider, S.; Marles-Wright, J.; Sharp, K.H.; Paoli, M. Diversity and conservation of interactions for binding heme. *Nat. Prod. Rep.* **2007**, 24(3), 621-30.

Silfa, E.; Almeida, M.; Cerda, J.; Wu, S.; López- Garriga, J. Structural characterization and dynamics events in hemoglobin I from *Lucina pectinata*: Unusual conformation of propionates and vinyl's heme peripheral groups. *Spectrosc.. Biol. Mol. Trends* **1997**, 79-80.

Silfa, E.; Almeida, M.; Cerda, J.; Wu, S.; López- Garriga, J. Orientation of the Heme Vinyl Groups in the Hydrogen Sulfide-Binding Hemoglobin I from *Lucina pectinata*. *Biospectroscopy* **1998**, 4, 311-326.

Torres-Mercado, E.; Renta, J. Y.; Rodríguez, Y.; López- Garriga, J.; Cadilla, C. L. The cDNA-Derived Amino Acid Sequence of Hemoglobin II from *Lucina pectinata*. *J. Protein Chem.* **2003**, 22, 683-690.

Wang, R. Toxic Gas, Lifesaver: Hydrogen sulfide, a lethal gas best know for smelling like rotten eggs, turns out to play key roles in the body- a finding that could lead to new treatments for heart attack victims and others. *Sci. Am.* **2010**, 67-71.

Warren, J. J.; Mayer, J. M. Proton-coupled electron transfer reactions at a heme-propionate in an iron-protoporphyrin-IX. *J. Am. Chem. Soc.* **2011**, 133, 8544-8551.

Weber, R. E.; Vinogradow, S. N. Nonvertebrate Hemoglobins: Functions and Molecular Adaptations. *Physiol. Rev.* **2001**, 81, 569-628.

Wishart, D. S.; Sykes, B. D.; Richards F. M. Relationship between Nuclear Magnetic Resonance Chemical Shift and Protein Secondary Structure. *J. Mol. Biol.* **1991**, 222,311-333.

Wishart, D. S.; Sykes, B. D.; Richards F. M. The Chemical Shift Index: A fast and Simple Method for the Assignment of Protein Secondary Structure through NMR Spectroscopy. *Biochemistry* **1992**, 31, 1647-1651.

Wittenberg, J-B.; Bolognesi, M.; Wittenberg, B-A.; Michel Guertin. Truncated Hemoglon=bins: A New Family of Hemoglobins widely distributed in ABcteria, unicellular Eucaryotes and Plantas. *J. Biol. Chem.* **2002**, 277(2), 871-874.

Wüthrick, K. Sequential Assignment Strategies in Protein. NMR of Protein and Nucleic Acids. Wiley, **1986**; Vol. 3.

Xia, Z.; Zhang, W.; Nguyen, B. S.; La Mar, G. N. H NMR Investigation of the Distal Hydrogen Bonding Network and Ligands Tilt in the Cyanomet Complex of Oxygen-avid *Ascaris suum* Hemoglobin. *J. Biol. Chem.* **1999**, 274(45), 31819-31826.

Yang, J.; Kloek, A. P.; Goldberg, D. E.; Mathews, F. S. The structure of *Ascaris* hemoglobin domain I at 2.2 Å resolution: molecular features of oxygen avidity. *Proc. Natl. Acad. Sci. USA* **1995**, 92, 4224-4228.

Zhang, W.; Cutruzzola, F.; Travaglini-Allocatelli, C.; Brunori, M.; La Mar, G. N. A myoglobin mutant designed to mimic the oxygen-avid *Ascaris suum* hemoglobin: elucidation of the distal hydrogen bonding network by solution NMR. *Biophys. J.* **1997**, 73, 1019-1030.